

*Russian Original Vol. 53, No. 5, November, 1982*

---

May, 1983

11

SATEAZ 53(5) 747-806 (1982)

# SOVIET ATOMIC ENERGY

АТОМНАЯ ЭНЕРГИЯ  
(ATOMNAYA ÉNERGIYA)

TRANSLATED FROM RUSSIAN



CONSULTANTS BUREAU, NEW YORK

# SOVIET ATOMIC ENERGY

*Soviet Atomic Energy* is abstracted or indexed in *Chemical Abstracts*, *Chemical Titles*, *Pollution Abstracts*, *Science Research Abstracts*, *Parts A and B*, *Safety Science Abstracts Journal*, *Current Contents*, *Energy Research Abstracts*, and *Engineering Index*.

*Soviet Atomic Energy* is a translation of *Atomnaya Energiya*, a publication of the Academy of Sciences of the USSR.

An agreement with the Copyright Agency of the USSR (VAAP) makes available both advance copies of the Russian journal and original glossy photographs and artwork. This serves to decrease the necessary time lag between publication of the original and publication of the translation and helps to improve the quality of the latter. The translation began with the first issue of the Russian journal.

## Editorial Board of *Atomnaya Energiya*:

**Editor:** O. D. Kazachkovskii.

**Associate Editors:** N. A. Vlasov and N. N. Ponomarev-Stepnoi

**Secretary:** A. I. Artemov

I. N. Golovin  
V. I. Il'ichev  
V. F. Kalinin  
P. L. Kirillov  
Yu. I. Koryakin  
E. V. Kulov  
B. N. Laskorin

V. V. Matveev  
I. D. Morokhov  
A. A. Naumov  
A. S. Nikiforov  
A. S. Shtan  
B. A. Sidorenko  
M. F. Troyanov

E. I. Vorob'ev

Copyright © 1983, Plenum Publishing Corporation. *Soviet Atomic Energy* participates in the program of Copyright Clearance Center, Inc. The appearance of a code line at the bottom of the first page of an article in this journal indicates the copyright owner's consent that copies of the article may be made for personal or internal use. However, this consent is given on the condition that the copier pay the stated per-copy fee through the Copyright Clearance Center, Inc. for all copying not explicitly permitted by Sections 107 or 108 of the U.S. Copyright Law. It does not extend to other kinds of copying, such as copying for general distribution, for advertising or promotional purposes, for creating new collective works, or for resale, nor to the reprinting of figures, tables, and text excerpts.

Consultants Bureau journals appear about six months after the publication of the original Russian issue. For bibliographic accuracy, the English issue published by Consultants Bureau carries the same number and date as the original Russian from which it was translated. For example, a Russian issue published in December will appear in a Consultants Bureau English translation about the following June, but the translation issue will carry the December date. When ordering any volume or particular issue of a Consultants Bureau journal, please specify the date and, where applicable, the volume and issue numbers of the original Russian. The material you will receive will be a translation of that Russian volume or issue.

Subscription (2 volumes per year)

Vols. 52 & 53: \$440 (domestic); \$489 (foreign)

Single Issue: \$100

Vols. 54 & 55: \$500 (domestic); \$555 (foreign)

Single Article: \$7.50

Mailed in the USA by Publications Expediting, Inc., 200 Meacham Avenue, Elmont, NY 11003.

**POSTMASTER:** Send address changes to *Soviet Atomic Energy*, Plenum Publishing Corporation, 233 Spring Street, New York, NY 10013.

## CONSULTANTS BUREAU, NEW YORK AND LONDON



233 Spring Street  
New York, New York 10013

Published monthly. Second-class postage paid at Jamaica, New York 11431.

# SOVIET ATOMIC ENERGY

A translation of *Atomnaya Énergiya*

May, 1983

Volume 53, Number 5

November, 1982

## CONTENTS

Engl./Russ.

### ARTICLES

- Synthesis of a System of Local Automatic Regulators for Power Reactors  
 — I. Ya. Emel'yanov, L. N. Podlazov, A. N. Aleksakov,  
 E. V. Nikolaev, V. M. Panin, and V. D. Rogova. . . . . 747 301
- Corrosion of St.3 and 12Kh18N10T Steels and NP-1 Nickel in High-Level  
 Wastes from Gas-Fluoride Reprocessing of Fast-Reactor Rods  
 — A. P. Kirillovich, R. K. Gazizov, V. S. Bushkovskii,  
 V. N. Golovanov, Yu. G. Lavrinovich, V. S. Belokopytov,  
 and V. K. Shamardin. . . . . 753 305
- Interaction of  $^4\text{He}^+$  Ions with Polycrystalline and Single-Crystal Metals  
 — N. P. Katrich and A. T. Budnikov . . . . . 758 309
- Thermoradiation Decomposition of Carbon Dioxide — B. G. Dzantiev,  
 A. N. Ermakov, V. M. Zhitomirskii, and V. N. Popov . . . . . 764 314
- Increase of the Electron-Beam Irradiation Efficiency of Cylindrical  
 Objects by Means of Magnetic Systems — L. L. Akrachkova,  
 N. K. Kuksanov, R. A. Salimov, Yu. N. Timko, and É. É. Finkel' . . . . . 768 317

### LETTERS TO THE EDITOR

- Distribution of Gas in a Reactor with Spherical Fuel Elements  
 — A. S. Pushnov, I. I. Gel'perin, and A. M. Kagan. . . . . 773 320
- A Nondestructive Method of Determining the Pu/U Ratio in Fast Reactor  
 Fuel Elements, Based on X-Ray Spectrometry — A. V. Bushuev,  
 V. I. Galkov, A. V. Zbonarev, A. F. Zolotov, A. A. Kutuzov,  
 N. A. Mel'nichenko, V. N. Ozerkov, and V. V. Chachin . . . . . 776 322
- Calculation of Energy Liberation in the Loop Channels by the Monte  
 Carlo Method — V. A. Antonov, F. M. Arinkin, G. A. Batyrbekov,  
 A. A. Blyskavka, V. V. Sinyavskii, and Yu. A. Sobolev. . . . . 778 323
- Investigation of the Structure of Kh18N10T Stainless Steel, Irradiated  
 with Fast Neutrons at a Temperature of 300°C — Sh. Sh. Ibragimov,  
 V. F. Reutov, S. P. Vagin, and B. D. Utkelbaev . . . . . 781 324
- New Class of Boundary Integral Equations of Neutron-Transport Theory  
 — B. D. Abramov. . . . . 783 325
- Influence of Radiation History on the Swelling of Steel  
 — N. A. Demin and Yu. V. Konobeev. . . . . 785 327
- Determining the Relaxation Length of a Flux of Moderated and Thermal  
 Neutrons on the Basis of the  $P_2$  Approximation — I. A. Kozachok  
 and V. V. Kulik. . . . . 787 328
- Accommodation Length of Helium in the Gap between the Fuel and the Shell  
 — Yu. M. Golovchenko, V. M. Makhin, V. A. Neverov,  
 B. V. Samsonov, A. P. Sych, V. A. Tsykanov, and V. P. Sheshunov. . . . . 791 330
- A Scintillation Gamma Spectrometer for the Investigation of Ultra-Deep  
 Boreholes — E. M. Arm, A. A. Il'inskii, B. É. Metzger,  
 and V. I. Pyatakhin. . . . . 794 332

**CONTENTS**

(continued)

Engl./Russ.

Remote Control Measurements of Ionizing Radiation Fields in Boreholes, Based on a Fiber-Optics Cable — V. A. Andronov, V. I. Balaev, E. M. Dianov, A. A. Il'inskii, E. V. Karus, O. L. Kuznetsov, E. V. Mishin, L. G. Petrosyan, A. M. Prokhorov, and V. I. Pyatakhin.	797	333
Applying Summator Operators to the Computer Solution of the Integrodifferential Equation of Radiation Transfer — V. I. Bilenko . . . . .	800	335
Durability of ZTL Piezoceramic Under the Action of Reactor Radiation — V. M. Baranov, S. P. Martynenko, and A. I. Sharapa . . . . .	803	337
Radioactive Aerosols in Ventilation Systems of the Chernobyl'sk Nuclear Power Plant — S. S. Chernyi and V. P. Grigorov . . . . .	805	338

The Russian press date (podpisano k pechatu) of this issue was 10/25/1982.  
Publication therefore did not occur prior to this date, but must be assumed  
to have taken place reasonably soon thereafter.

SYNTHESIS OF A SYSTEM OF LOCAL AUTOMATIC REGULATORS  
FOR POWER REACTORS

I. Ya. Emel'yanov, L. N. Podlazov,  
A. N. Aleksakov, E. V. Nikolaev,  
V. M. Panin, and V. D. Rogova

UDC 621.039.515

The reliability of operation of the reactors of powerful nuclear power plant units has been determined to a significant extent by successes in the solutions of a number of new problems of controlling such reactors in connection with three-dimensional dynamic instability of the energy distribution in the active zone volume which is characteristic of them [1]. An important practical step in the solution of these problems is the creation and introduction of an automatic system for control of reactor power which is capable of simultaneously suppressing the most rapid distortions in the energy distribution. The main stages in the realization of such a system, which is called a system of local automatic regulators (LAR), have been described in [2]. An engineering procedure is proposed in this paper for the synthesis of such systems. The procedure is comprised of a process of computational justification of the LAR system and is a self-consistent and important result of the research, together with the practical realization and introduction of this system in nuclear power plants with high-power water-cooled channel reactors (RBMK).

The principle of zonal regulation [3, 4] has been adopted as the basis in connection with the creation of an LAR system. It consists of an arbitrary division of the entire active zone of the reactor into a certain number of sections, each of them being equipped with detectors which measure the power of the section, and of the suppression of deviations of the instantaneous value of its power from a specified value due to displacement of a rod in the section in question. It is evident that this principle determines the overall approach to the construction of an LAR, but it does not permit adopting rational specific engineering solutions.

Taking account of the high requirements on response speed and reliability which are imposed on a system for control of the total power and primary stabilization of the field, one can formulate the problem of an engineering synthesis of such a system in general form as follows: It is necessary to create a system with a specified effectiveness using only the minimum necessary number of elements. The following meaning is included in the concept of specified effectiveness:

1. When operating a reactor at a steady power level and with slow planned variations of it under conditions of actual external perturbations, it is necessary to suppress, practically without dynamic errors, zeroth-order deviations of the amplitudes of a specified set of the lowest harmonics of the energy distribution. This set contains the proper number of first harmonics so that the characteristic values of the rise time of the amplitude of the "residual" motion, whose suppression does not enter into the system functions, is no less than several hours. One can satisfy this requirement only approximately in an actual LAR system with a limited number of rods and detectors, but as has been shown above, to an accuracy adequate for practical purposes.

2. With the help of compensating rods a system should provide for automatic urgent, power reduction according to a specified program and stabilize the operating conditions at a new specified level during at least several minutes without operator participation in all situations specified in what has been enumerated.

The procedure under discussion for the synthesis of an LAR system includes two main stages. In the first stage the operation of LAR has been discussed in a steady regime from the standpoint of the quality of the suppression of perturbations of arbitrary form, and the characteristic time of the natural, motion of the energy distribution with an operating LAR

---

Translated from *Atomnaya Énergiya*, Vol. 53, No. 5, pp. 301-305, November, 1982. Original article submitted December 12, 1981.

system and the most unfavorable combinations of reactivity coefficients has been determined. The second stage is associated with providing the necessary effectiveness of this system under conditions of an urgent power reduction.

A linearized model of the three-dimensional dynamics of an RBMK is sufficient for the first stage:

$$[(M^2\Delta^2 + \kappa_0^2)/\beta - W_c(s)] \varphi(\mathbf{r}, s) + \Phi_0(\mathbf{r}) [W_{p.f.l.}(s) \varphi(\mathbf{r}, s) + k_r(\mathbf{r}, s) + k_p(\mathbf{r}, s)] = 0,$$

where, in addition to the generally adopted notation,  $W_c(s)$  is an operator which describes the dynamics of the yield of delayed neutrons;  $W_{p.f.l.}(s)$ , power feedback loop operator;  $k_r(\mathbf{r}, s)$ , regulating influence; and  $k_p(\mathbf{r}, s)$ , perturbation.

This equation has been solved for a two-dimensional circular reactor in the form of a Galerkin series [5]. For the LAR system under discussion, a realistic algorithm of the operation of the LAR loops with relay regulators has been taken into account in the calculations:

$$k_r(\mathbf{r}, t) = \sum_{k=1}^p \rho_k l_k(t) \delta(\mathbf{r} - \mathbf{r}_k);$$

$$dl_k(t)/dt = U_k(t) V_k;$$

$$U_k(t) = \begin{cases} 1 & \text{when } \sum_{l=1}^m C_{lk} \varphi(\mathbf{r}_{lk}, t) < -\varepsilon; \\ 0 & \text{when } -\varepsilon \leq id \leq \varepsilon; \\ -1 & \text{when } id > \varepsilon, \end{cases}$$

where  $\rho_k$ ;  $l_k(t)$ ;  $\mathbf{r}_k$ ;  $V_k$  are the "weight," submersion depth, location, and displacement rate of the  $k$ -th rod, respectively;  $C_{lk}$ , "weight" coefficients; and  $\varepsilon$ , width of the insensitivity zone.

A measure of the deformation of the energy distribution is the dispersion

$$D(t) = \int_S \varphi^2(\mathbf{r}, t) d\mathbf{r} = \sum_{i=1}^n \int_S [\Phi_i(t) \psi_i(\mathbf{r})]^2 d\mathbf{r} = \sum_{i=1}^n \Phi_i^2(t),$$

where  $\psi_i(\mathbf{r})$  are orthonormalized and orthogonal coordinate functions and  $\Phi_i(t)$  are their amplitudes.

The chief problem of the first stage of synthesis of an LAR system is the investigation of the reaction of the system to a perturbation of universal form:

$$k_p(\mathbf{r}, t) = \sum_{i=1}^n \psi_i(\mathbf{r}) 1(t),$$

i.e., a stepwise perturbation in time with unit amplitude of all the harmonics which participate in the solution. Along with the dispersion it is taken into account how strongly, for

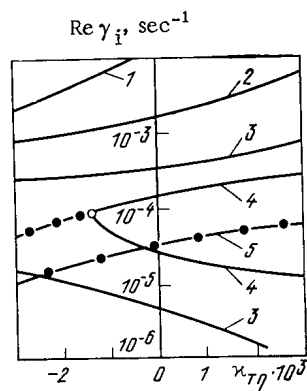


Fig. 1. Dependence of the real part of the roots of the characteristic equation on the total "rapid" effect of the reactivity  $\kappa_{T\eta}$  (the reactivity coefficient with respect to the graphite temperature is  $\kappa_{gr} = 0.012$ ); —) real root; ●) real part of the complex root; ○) multiple root; 1) fundamental harmonic; 2, 3, 5) first, second, and third azimuthal harmonics, respectively; and 4) first radial harmonic.

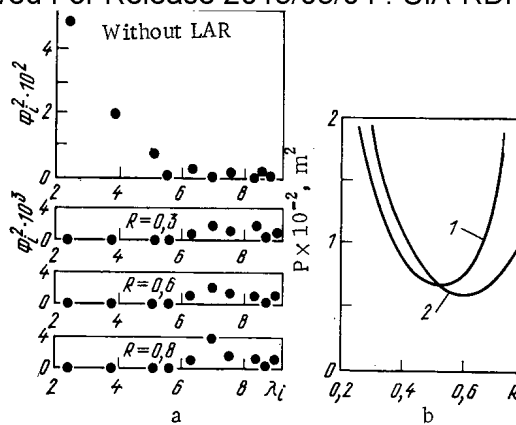


Fig. 2. Optimization of the placement of LAR rods: a) "spectra" of the amplitudes of harmonics arranged in order of increasing eigenvalues without and with an LAR system for various placement radii of the peripheral LAR rods; b) dependence of the measure  $P$  on placement radii of the peripheral LAR rods upon variation of  $R_1$ : 1)  $R_1 = 0.5$ ; 2)  $R_1 = 0.7$ .

a specified amplitude, it is necessary to shift the rods for its suppression. The measure

$$P(t) = \sum_{k=1}^p \Delta l_k^2(t)$$

is introduced as a quantitative characteristic of the rod displacements.

The initial instant for LAR synthesis is a known position, which indicates that for practically instantaneous suppression of the deviations specified by some fixed number of lowest harmonics it is necessary to have an equal number of rods. The number of lowest harmonics subject to suppression has been determined from an analysis of the three-dimensional dynamics of an RBMK performed by the harmonic method. The basis for this choice are the dependences of the roots of the characteristic equation for several first harmonics on the reactivity coefficients with respect to fuel temperature, vapor content, and graphite temperature, which have the strongest effect on the three-dimensional dynamics of an RBMK [6]. A portion of these dependences is given in Fig. 1. It is sufficient, in practice, to increase the development period of the "residual" distortion to several hours ( $1/\text{Re} \gamma_1 \geq 10^4$  sec). With this taken into account it follows from Fig. 1 that it is necessary to stabilize the first seven harmonics in an RBMK, i.e., to include no less than seven rods in the LAR system. Taking into account the "geometry" of the first seven harmonics, one should distribute these rods centrally and symmetrically — one in the center and six around the periphery of the reactor. It is further necessary to determine the most effective radius for the placement of the detector placement, since variations in their placement affect the result, and the problem of simultaneous determination of the optimal position of both the rods and the detectors is a cumbersome one. The first position adopted as the initial one in the synthesis of LAR avoiding these difficulties: The LAR should maintain the amplitudes of the first seven harmonics equal to zero practically instantaneously without dynamic error. To do this it is sufficient to "secure" the field determined by superposition of the first seven harmonics at seven points of the plan view of the reactor. This is formally expressed in a change in the

method of formation of the imbalance signal, namely, instead of  $\sum_{l=1}^m C_{lh} \varphi(r_{lh}, t)$  we adopt

$$\sum_{i=1}^r \Phi_i(t) \psi_i(r_k) \text{ for each LAR.}$$

A perturbation which is stepwise in the time is introduced in the calculations. The reading of  $D$  and  $P$  for determination of the optimal placement radius of the peripheral rods

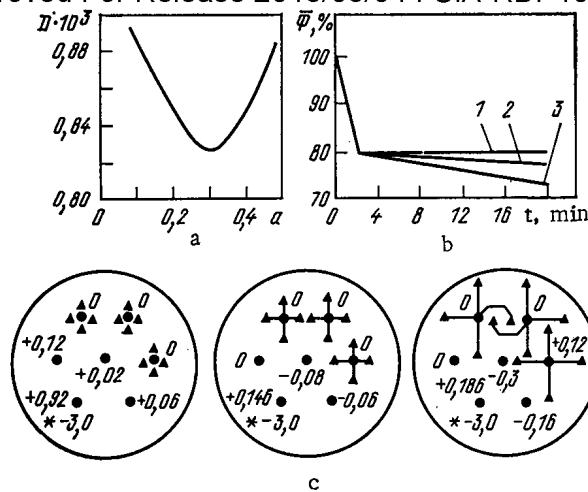


Fig. 3. Optimization of placement of the LAR detectors: a) dependence of the dispersion on the distance of the detectors from the rods; b) transitional processes upon a changeover of the neutron power of the reactor ( $\bar{\phi}$ ) from 100 to 80% by an LAR system: 1)  $\alpha > 0.2R_0$ ; 2)  $\alpha = 0.15R_0$ ; 3)  $\alpha = 0.075R_0$ ; c) suppression of a perturbation caused by shifting a manual regulation rod; the shifts (m) of the perturbing rod and the LAR rods in suppressing the perturbation are indicated by numbers; (\*) place at which the perturbation is introduced; (●) LAR rod, (▲) LAR detector).

starts at the time at which the last of the LAR imbalances enter the limits of the insensitivity zone ( $\epsilon = 0.01$ ) and the relay LAR, having suppressed the initial perturbation in one insertion, enter the grazing regime. The results of calculations for different placement radii of the peripheral LAR rods ( $R$ ) and plateau zone radii ( $R_1$ ) are given in Fig. 2. It follows from Fig. 2a, in which are illustrated the "spectra" of the harmonic amplitudes ( $\Phi_1^2$ ) arranged in order of increasing eigenvalues ( $\lambda_1$ ), upon an initial perturbation and after its suppression by the LAR system, that the amplitudes of the first seven harmonics practically vanish for wide variations of  $R$ . The differences in the dispersion for different  $R$  are associated with deformations of the field in the higher harmonics, which are not suppressed and can even increase upon suppression of the perturbation by the LAR rods. The more significant this amplification is, the greater is the necessity to shift the rods in connection with suppression of the perturbations. In addition, for relay LAR the rod displacement and the time to suppress a perturbation are proportionally related. According to these ideas, the condition  $\min P$  has been taken as the basis of optimization of  $R$ . The  $P(R)$  dependence is given in Fig. 2b, from which it follows that the optimal  $R$  depends on the dimensions of the plateau zone. In practice  $R_1 \approx (0.7-0.8)R_0$  ( $R_0$  is the extrapolated reactor radius); therefore, the rods of peripheral LAR should be located at radius  $R \approx 0.6R_0$ .

The question of the optimal placement of LAR detectors has been solved by varying the distance from the detectors to the LAR rod; it has been assumed that all the detectors are located on the same radius. In particular, it has been assumed that four detectors are used in each LAR in an RBMK, mounted in a square with side  $a$  at whose center is located an LAR rod. The computational results are given in Fig. 3. 3a, from which it follows that the optimal value is  $a \approx (0.25-0.3)R_0$ , i.e., 6-7 lattice steps of the reactor channels. The physical causes for the presence of an extremum are illustrated in Figs. 3b and c. Thus, with power variations and too small a value of there remain imbalances in the LAR channels within the limits of the insensitivity zone after shutdown of the detector, but the energy yield continues to vary in the intervals between the LAR. The reactor power also varies. Starting approximately from  $a = 1$  m, this phenomenon is practically eliminated, and a further removal of the detectors from the rods has no effect on the power. The inadequacies of excessive remoteness of the detectors from the rods is illustrated in Fig. 3c, in which are given the computational results of the suppression of a per-

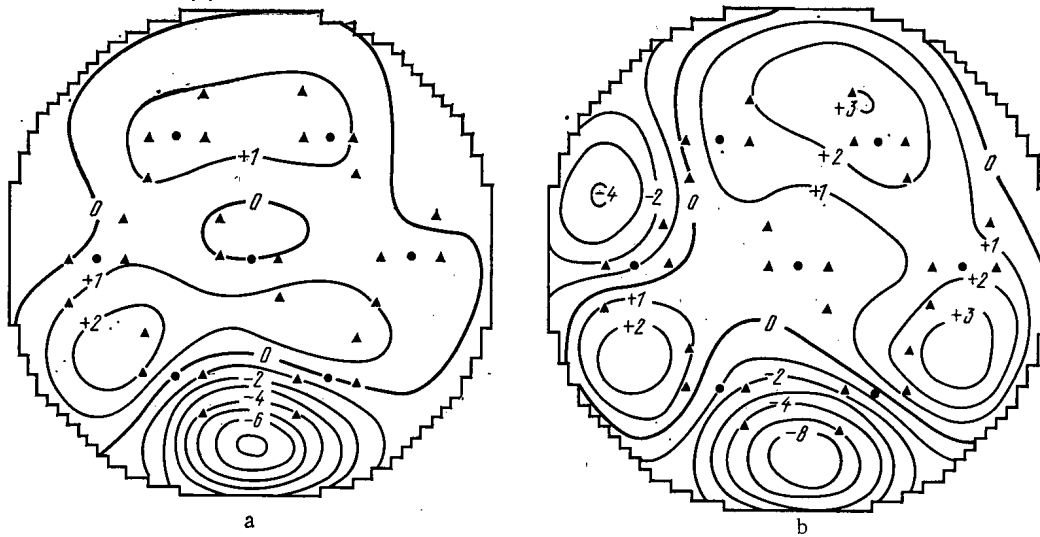


Fig. 4. Three-dimensional shape of the natural motion of the energy distribution in a reactor equipped with a seven-zone LAR system; a) calculation; b) experiment; ● LAR rod; ▲ LAR detector; +1) line of equal deviation from the original state, %.

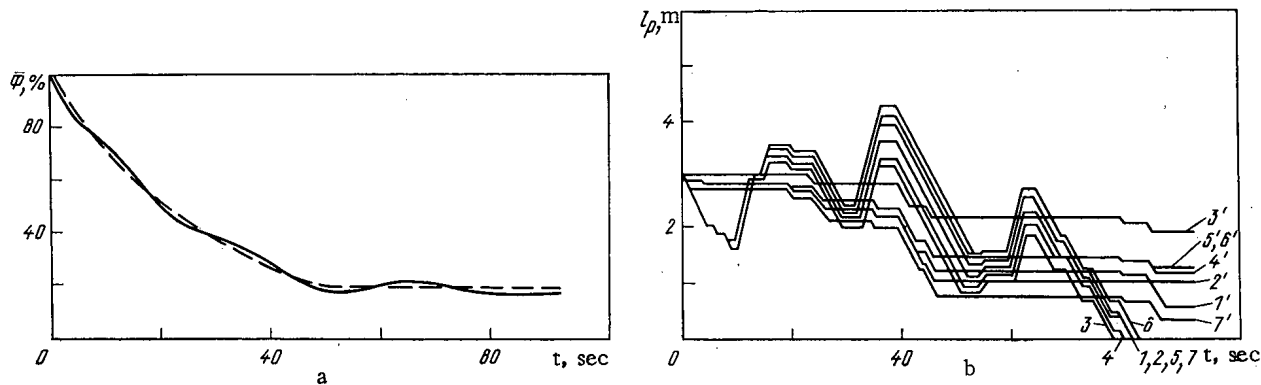


Fig. 5. Transitional processes in the regime of urgent power reduction by the LAR system: a) behavior of the neutron power ( $\Phi$ ); of the reactor: —)  $\Phi$ ; ---) setting; b) position of the LAR and RC rods ( $l_p$ ): 1, 2, ..., 7) LAR rods; 1', 2', ..., 7') RC rods.

turbation introduced by a rod in the region of one of the LAR. If the detectors are placed near the rod ( $\alpha \approx 0.5$  m), then the LAR nearest to the perturbation site suppresses the perturbation only partially, and therefore the adjacent LAR channels are involved. With optimal remoteness of the detectors, the perturbation is practically suppressed by just the nearest LAR. If the detectors are located too far away, adjacent LAR are again brought into play, but they are shifted in the very same direction as is the "perturbing" rod.

Investigations of the natural motion of the field in a reactor equipped with an LAR system have also been included in the synthesis procedure. To this end, a detailed three-dimensional dynamic model has been used with which a regime of prolonged maintenance of a steady power level by an LAR system is reproduced in the absence of any other kind of control influences, similar to what has been done on operating RBMK reactors during experiments. The results of this calculation for a seven-zone LAR system operating in the first and second units of the LNPP are given in Fig. 4a. The experimental results are given in Fig. 4b. A comparison of Figs. 4a and b indicates good agreement of calculation with experiment [2].

The second stage of LAR synthesis is associated with providing for regimes of urgent power reduction. The main problem of this stage is the choice of the number, position, and algorithm for operation of the compensating rods which are connected to assist the LAR. It

has proven possible to solve most correctly and effectively the complex of problems arising here by virtue of a rational sorting out of the alternatives, comparing them with regard to the quality of the transitional processes. It is necessary for such calculations to use a nonlinear three-dimensional dynamic digital model of the reactor, which permits reproducing the actual operating regimes of the operation of the power assembly. The choice of acceptable alternatives for placement of the recompensation rods (RC) was determined by the following obvious considerations: The RC rods should be distributed as uniformly as possible in the plan view of the reactor to avoid misalignments of the energy distribution during operation of the RC; and the RC rods belonging to each of the LAR should be located in that section of the reactor which is serviced by the LAR in question.

The computational results of the most difficult of the regimes of urgent power reduction with disconnection of the unit from the grid and a transition to providing for its intrinsic needs are given in Fig. 5. It follows from Fig. 5 that the adopted algorithm for the operation of LAR with groups of RC rods provides for a power changeover in accordance with specification and a stabilization of the regime at an established level during a sufficiently extended time without operator participation or participation of the higher-level systems of the hierarchy of reactor control.

The experiment to design, test, and introduce LAR systems for the power units of nuclear power plants has shown that the main problems with a practical synthesis of such systems are the choice of the number of LAR which provide for a specified level of stabilization of the energy distribution, and the maintenance of a specified effectiveness of the LAR system in all operating regimes, including regimes of urgent emergency power reduction.

Thus, a practical synthesis of an LAR system on these criteria can be successfully accomplished on the basis of the complex use of harmonic and nonlinear nodal three-dimensional temporal models. Complicated experimental investigations of a mock-up and then tests of a regular model of an LAR system at the LNPP have confirmed the effectiveness of the proposed procedure for synthesis of LAR.

#### LITERATURE CITED

1. N. A. Dollezhal' and I. Ya. Emel'yanov, A Channel Nuclear Power Reactor [in Russian], Atomizdat, Moscow (1980).
2. I. Ya. Emel'yanov et al., At. Énerg., 49, No. 6, 357 (1980).
3. A. Hitchcock, The Stability of Nuclear Reactors [Russian translation], Gosatomizdat, Moscow (1963).
4. I. Ya. Emel'yanov et al., Vopr. Atomnoi Nauk. Tekh., Ser. Fiz. Tekh. Yadernykh Reaktorov, No. 1 (5), 3 (1979).
5. L. É. El'sgol'ts, Differential Equations and Variational Calculus [in Russian], Nauka, Moscow (1969).
6. A. N. Aleksakov et al., At. Énerg., 46, No. 4, 227 (1979).

CORROSION OF St.3 AND 12Kh18N10T STEELS AND NP-1  
NICKEL IN HIGH-LEVEL WASTES FROM GAS-FLUORIDE  
REPROCESSING OF FAST-REACTOR RODS

A. P. Kirillovich, R. K. Gazizov,  
V. S. Bushkovskii, V. N. Golovanov,  
Yu. G. Lavrinovich, V. S. Belokopytov,\*  
and V. K. Shamardin

UDC 621.039.546

Reliability is decisive in selecting of storing high-level wastes (HLW) formed by reprocessing nuclear fuel. One of the main factors governing reliability is the corrosion resistance of the materials in the storage vessels. Reliability requires constant monitoring of the state of these, together with a knowledge of the laws of corrosion in the HLW medium [1-3].

Carbon and stainless steels are used throughout the world in vessels for storing liquid HLW [4, 5], but preference is given to stainless steels of types 12Kh18N10T, 304-L, and 310-L. Some experimental evidence is already available on the corrosion of materials in liquid HLW. However, there is virtually no information for the solid HLW from gas-fluoride reprocessing, which is considered to be one of the promising methods for rods from fast reactors.

The corrosion was examined on flat specimens of size  $25 \times 20 \times 2.5$  mm made of St.3 carbon steel, 12Kh18N10T austenitic steel, and NP-1 nickel. Table 1 gives the chemical compositions of the materials, which were chosen for examination because of their extensive use in the production of uranium fluoride, and also on technological and cost grounds. The corrosion rate was estimated by the methods of [6]. The phase composition of the deposits was determined by electron diffraction with an ER-100 camera. The specimens were examined in transmission and reflection. On some of the specimens, the chemical compositions of the corrosion products were examined by layerwise analysis.

The wastes from gas-fluoride reprocessing represent a mixture of complex chemical and radionuclide compositions with high specific radioactivity and heat production (up to 500 W/kg). Table 2 gives the characteristics of the wastes, which are described in more detail in [2].

Below we give the chemical compositions of the fluorination wastes in mass %:<sup>†</sup>

F	Fe	Al	Ni	Ca	Na	Cr
37.5±1	30-50	>0.1	>0.1	>0.1	0.1	0.1
Si	U	Pu	H <sub>2</sub> O			
0.1	0.36±0.03	0.004	1.7and0.03	‡		

The corrosion in fluoride wastes is more rapid on account of the high oxidation capacity of the medium, and also because of the radiation, which stimulates chemical reactions, including the release of fluorine and hydrogen fluoride [2], in addition to the heating due to the high specific radioactivity. Therefore, in optimizing the storage conditions one has to consider factors such as temperature, time, radiation level, and waste composition.

Tables 3 and 4 give the results from corrosion tests made in media of various compositions and activity levels containing the wastes from fluorination together with NaF solvents for various temperatures and times.

\*Deceased.

<sup>†</sup>The specific radioactivity was  $7.3 \times 10^5$  Bq/kg and corresponds to low-activity wastes.

<sup>‡</sup>The H<sub>2</sub>O content of 1.7 mass % corresponds to moist wastes, while 0.03 mass % corresponds to dry ones.

Translated from Atomnaya Energiya, Vol. 53, No. 5, pp. 305-309, November, 1982. Original article submitted December 7, 1981.

The corrosion rate increases exponentially in accordance with  $K = A \exp(-E/RT)$  as the temperature increases. At 400°C, St.3 and 12Kh18N10T were completely corroded away in the fluorination residues, while the rate of penetration of the corrosion into the nickel was 0.25 mm/yr. At the same temperature, the rate of penetration of the corrosion in the NaF solvent was lower than that in the fluorination residue.

The data of Table 4 show that the corrosion rates are largely dependent on the composition of the solvent, being maximal for a solvent containing hydrogen fluoride. Figure 1 shows the characteristic failure of a carbon-steel container on heating to 400°C in fluorination residues (water content 0.03%).

TABLE 1. Chemical Compositions of Constructional Materials

Material	Component contents, mass %												
	C	Si	Mn	S	P	Cr	Ni	Ti	Cu	Zn	Fe	Co	Mg
St. 3	0,18	0,011	0,48	0,029	0,020	—	—	—	—	—	Base	—	—
12Kh18N10T	0,10	0,61	1,9	—	—	17,5	9,5	0,5	—	—	Base	—	—
NP-1	0,01	0,002	0,001	0,001	0,001	—	99,93	—	0,02	0,001	0,01	0,005	0,001

TABLE 2. Characteristics of High-Level Fluoride Wastes Obtained in Experimental Gas-Fluoride Reprocessing of Fuel from the BOR-60 Reactor

Material	Specific activity, Bq/kg	Activities of radionuclides, Bq/kg								
		<sup>144</sup> Ce— <sup>144</sup> Pr	<sup>141</sup> Ce	<sup>106</sup> Ru— <sup>106</sup> Rh	<sup>103</sup> Ru	<sup>137</sup> Cs	<sup>134</sup> Cs	<sup>95</sup> Zr	<sup>95</sup> Nb	<sup>90</sup> Sr
NaF sorbent	222·10 <sup>10</sup>	1,26·10 <sup>10</sup>	—	69,2·10 <sup>10</sup>	22,2·10 <sup>3</sup>	22,2·10 <sup>10</sup>	4,88·10 <sup>10</sup>	—	—	3,59·10 <sup>10</sup>
Fluorination	333·10 <sup>12</sup>	77,7·10 <sup>12</sup>	7,77·10 <sup>2</sup>	250·10 <sup>18</sup>	14,1·10 <sup>4</sup>	296·10 <sup>10</sup>	92,5·10 <sup>10</sup>	5,33·10 <sup>10</sup>	5,6·10 <sup>1</sup>	5476·10 <sup>10</sup>
residues	2042·10 <sup>12</sup>	685·10 <sup>12</sup>	101,8·10 <sup>10</sup>	40,7·10 <sup>10</sup>	248·10 <sup>10</sup>	981·10 <sup>10</sup>	—	40,7·10 <sup>10</sup>	2128·10 <sup>10</sup>	—

TABLE 3. Rates of Penetration of Corrosion into Carbon and Austenitic Steels and into Nickel in Fluorination Wastes Containing Fission Products, mm/yr

Test conditions		St3			12Kh18N10T			Nickel		
time, h	tempera- ture, °C	high- level wastes	low-level wastes		high- level wastes	low-level wastes		high- level wastes	low-level wastes	
			dry	moist		dry	moist		dry	moist
300	100	0,37	0,025	0,050	0,025	0,0004	0,0005	0,0088	0,0005	0,0032
	200	0,67	0,150	0,364	0,145	0,0086	0,195	0,031	0,0016	0,0088
	300	2,03	1,90	2,00	0,49	0,367	0,699	0,087	0,016	0,010
	400	—	Failed		—	Failed		—	0,37	—
500	100	0,29	0,020	0,040	0,020	0,0003	0,0003	0,0074	0,0002	0,0015
	200	0,63	0,130	0,40	0,0191	0,0053	0,190	0,027	0,0009	0,0065
	300	1,78	1,63	1,75	0,40	0,329	0,500	0,069	0,013	0,0064
	400	—	Failed		—	Failed		—	0,26	—
1500	100	0,18	0,010	0,035	0,011	0,0002	0,0001	0,0051	0,0001	0,0009
	200	0,50	0,120	0,303	0,063	0,0024	0,184	0,020	0,0008	0,0058
	300	1,37	1,15	1,20	0,270	0,242	0,305	0,051	0,010	0,0060
	400	—	Failed		—	Failed		—	0,25	—
9170	140—60	0,21	—	—	0,00012	—	—	0,0012	—	—
8740	80—49	0,062	—	—	0,0018	—	—	0,0015	—	—

**Note:** The errors of the results in Tables 3 and 4 do not exceed  $\pm 5\%$  at the 0.95 probability level.



Fig. 1. External view of a container of diameter 100 mm made of carbon steel after corrosion tests in dry fluorination residues (0.03 mass % water) of activity  $7.3 \times 10^5$  Bq/kg at 400°C for 1513 h.

TABLE 4. Rates of Corrosion Penetration (mm/yr) in Carbon and Austenitic Steels and in Nickel in High-Level NaF Sorbent (Specific Activity  $222 \times 10^{10}$  Bq/kg) Containing Fission Products, in Pure NaF Sorbent, and in a Sorbent Containing 30% Hydrogen Fluoride

Test conditions		St3		12Kh18N10T		Nickel NP-1	
time, h	temperature, °C	high-level solvent	pure sorbent	high-level sorbent	pure sorbent	high-level sorbent	pure sorbent
300	100	—	0,007	—	0,00065	—	0,00028
	200	0,58	0,030	0,014	0,0034	0,019	0,00071
	300	1,0	0,076 (1,9)	0,027	0,0098 (0,7)	0,046	0,0013 (0,0015)
	400	—	7,15	—	0,032	—	0,024
500	100	—	0,0055	—	0,00053	—	0,00027
	200	0,53	0,024	0,011	0,0027	0,016	0,00065
	300	0,91	0,063 (1,3)	0,022	0,0076 (0,52)	0,037	0,0011 (0,0032)
	400	—	7,2	—	0,031	—	0,035
1500	100	0,096	0,0073	0,0031	0,00021	0,0039	0,0002
	200	0,33	0,029	0,0099	0,0011	0,0148	0,00048
	300	0,77	0,071 (0,52)	0,021	0,003 (0,2)	0,036	0,00085 (0,0025)
	400	—	3,2	—	0,012	—	0,026
10296	25	0,044	—	0,001	—	0,001	—

Note: In parentheses we give the rates of penetration of corrosion in the NaF solvent saturated with hydrogen fluoride (NaF·HF).

The effect of waste composition on the corrosion was considered from the viewpoint of possible changes during production. In particular, the water and fluorine contents may vary widely. The corrosion in the fluorination residues increases with temperature and as the water content rises from 0.03 to 1.7 mass %. The exact variation is different for each material. The maximum increase in corrosion rates occurs in the range 100–200°C, particularly for 12Kh18N10T steel, and to a smaller extent for nickel.

We examined the ratio of the corrosion rates  $K_2/K_1$  as a function of temperature for the constant radioactivity ratio  $Q_2/Q_1 \approx 10^{10}$  (Fig. 2), where  $K_2$  and  $K_1$  are the corrosion rates,

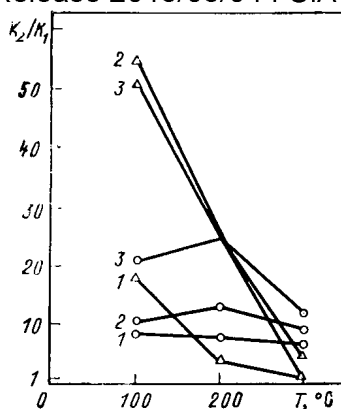


Fig. 2. Temperature dependence of corrosion in the fluoride media of various activity levels (○ in solvent, Δ in fluorination residues): 1) St.3; 2) 12Kh18N10T; 3) NP-1.

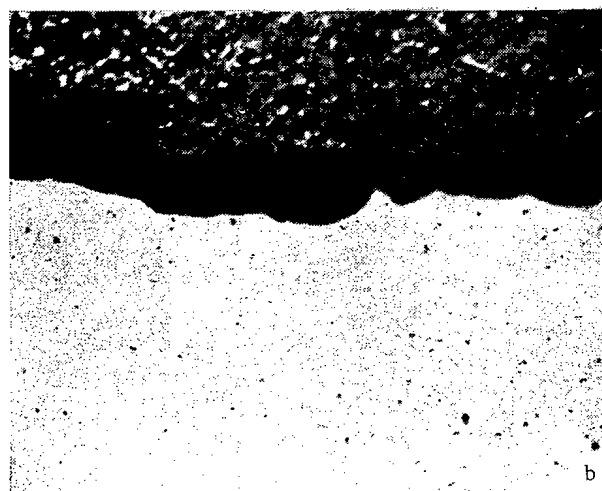
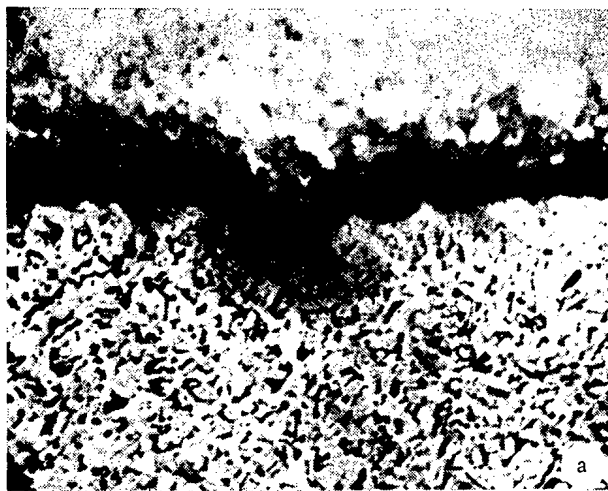


Fig. 3. Microstructure of the surface of St.3 after tests: a) in high-level sorbent for 8400 h, pit depth 0.03-0.07 mm, diameter 0.15-0.3 mm; b) in high-level fluorination residues for 9170 h,  $T = 140-60^{\circ}\text{C}$ , pit depth 0.05-0.07 mm, diameter 0.2-0.3 mm ( $\times 100$ ).

correspondingly, in high-level and low-level wastes similar in composition, and it is clear that the corrosion rate is increased for all the materials in the higher-level activity medium when the temperature is reduced to  $100^{\circ}\text{C}$ . The same relationship occurred, but much more weakly for NaF sorbent with nickel, 12Kh18N10T, and St.3. On raising the temperature to  $300^{\circ}\text{C}$ , there was a tendency for  $K_1$  and  $K_2$  to become the same, i.e., the contribution from the radioactivity was reduced.

There were two basic forms of corrosion — general frontal and local pitting (Fig. 3). Slight pitting corrosion (depth of pits up to 0.07 mm) was appreciable only for St.3 after testing in HLW.

The results from the three materials in various forms of waste indicate that the corrosion rates of St.3 and 12Kh18N10T are dependent on the capacity of the wastes to release gaseous fluorine and hydrogen fluoride. Wastes from gas-fluoride reprocessing fall in the following sequence of decreasing corrosion activity: moist wastes, dry ones, and NaF sorbent with radionuclides.

TABLE 5. Phase Composition of Corrosion Products

Test conditions	Material	Phase composition and lattice type
Fluorination residues 0.03 mass % $H_2O$ ; $7.3 \cdot 10^5$ Bq/kg 1500h; 300 °C	St.3	$\alpha$ - $Fe_2O_3$ (rhombohedral) $Fe_3O_4$ (spinel) traces $Fe_2O_3$ (monoclinic)
	12Kh18N10T	$\alpha$ - $Fe_2O_3$ (rhombohedral) $Fe_3O_4$ and $NiO \cdot Cr_2O_3$ (spinel)
Fluorination residues 1.7 mass % $H_2O$ ; $7.3 \cdot 10^5$ Bq/kg; 1500h, 300 °C	NP-1	$NiO$ (cubic)
	St.3	$Fe_2O_3$ (monoclinic) $\alpha$ - $Fe_2O_3$ (rhombohedral) and $Fe_3O_4$
Fluorination residues $2042 \times 10^{12}$ Bq/kg; 8400 h; 90—40 °C The same	12Kh18N10T	$\alpha$ - $Fe_2O_3$ (rhombohedral) and $Fe_2O_3$ (monoclinic) $NiO \cdot Cr_2O_3$ , $3Cr_2O_3 \cdot Fe_2O_3$ (spinel)
	NP-1	$NiO$ (cubic)
Sorbent NaF; $222 \times 10^{10}$ Bq/kg	St.3	$Fe_3O_4$ (spinel) and traces of $\alpha$ - $Fe_2O_3$
	12Kh18N10T	$\gamma$ - $Fe_2O_3$ ( $\gamma$ - $Fe_2O_3 \cdot H_2O$ ) (tetragonal), traces and $\alpha$ - $Fe_2O_3$ $Fe_3O_4$ (spinel)

The corrosion products consisted of oxides (Table 5); the higher resistance of nickel is probably due to the formation of a dense surface film of  $NiO$ , while the fall in the corrosion rate with the lapse of time (Tables 3 and 4) is due to a character of the products. The corrosion products contained up to 0.2 mass % fluoride, which indicates that this participates in the process.

These studies lead us to recommend that 12Kh18N10T stainless steel should be used as the main material for constructing vessels for storing fluoride HLW. Carbon steel can be used at low temperatures (not above 35–65°C) with appropriate protection from atmospheric corrosion. If the medium is more corrosive (fluorination residues with elevated water contents, traces of HF, etc.) and at higher temperatures it is preferable to use nickel. The vessels should be reliably sealed, e.g., by welding, to improve the reliability in long-term storage of HLW and to eliminate corrosion arising from water taken up by the waste. The corrosion resistance of NP-1 and 12Kh18N10T in high-level fluorination wastes and in NaF sorbent containing fission products is estimated in accordance with GOST 13819-68 up to 80–85°C as 1 point, while the resistance of St.3 under the same conditions is estimated as 3 or 4 points.

Therefore, these experiments have given the optimum temperature for using various materials to provide an acceptable corrosion rate of not more than 0.05 mm/yr. The values for fluorination residues are as follow: 35°C for St.3, 180°C for 12Kh18N10T, and 250°C for NP-1; similarly, for sodium fluorides: 65°C for St.3 and up to 300°C for 12Kh18N10T and NP-1.

## LITERATURE CITED

1. V. V. Kulichenko and Yu. P. Martynov, Paper ML/41, presented at: The Third COMECON Symposium on Research in Reprocessing Irradiated Fuel, March 24–26, 1974, Marianske Lazne, Czechoslovakia.
2. A. P. Kirillovich et al., At. Energ., 42, No. 2, 94 (1977).
3. A. I. Antipin, At. Tekh. Rubezhom, No. 4, 10 (1971).

4. Z. Dlougi [1], Paper ML 74/56.
5. W. G. Belter, Paper USA 28/P/869, presented at: The Third Geneva Conference, 1964.
6. V. V. Romanov, Methods of Examining Metal Corrosion [in Russian] Metallurgiya, Moscow (1965).

# INTERACTION OF ${}^4\text{He}^+$ IONS WITH POLYCRYSTALLINE AND SINGLE-CRYSTAL METALS

N. P. Katrich and A. T. Budnikov

UDC 548:539.12.04

There is extensive experimental evidence on the interactions of fast gas ions with metals, which indicates that the formation of blisters is preceded by the trapping of gas atoms by vacancies and the fusion of these complexes into gas bubbles. It has previously been shown [1] that this mechanism is present on bombardment with  $\text{H}^+$  ions even for metals with exothermic solubility if the hydrogen concentration exceeds the limit such that  $\text{H}/\text{M} = 1-2$ . However, the data on the interactions of  ${}^4\text{He}^+$  ions with metals are conflicting, and they are far from sufficient to resolve problems in radiation resistance [2, 3]. We have therefore examined the implantation of helium as well as the spontaneous and thermally activated desorption of the helium, along with blistering processes.

We used the apparatus of [4] with the chamber shown schematically in Fig. 1. Polycrystalline and single-crystal specimens of tungsten, aluminum, niobium, molybdenum, and other metals were bombarded with a beam of  ${}^4\text{He}^+$  ions at a current  $i = 10 \mu\text{A}$  ( $j = 50 \mu\text{A}\cdot\text{cm}^{-2}$ ),  $E = 30 \text{ keV}$ , temperature  $78-2000^\circ\text{K}$ , and initial background gas pressure  $p_0 \leq 1.3 \cdot 10^{-7} \text{ Pa}$ . The ion beam was generated by extracting the helium ions from the plasma of a high-frequency ion source. After electrostatic focusing, the ion beam was separated in a magnetic mass analyzer. In the chamber of this, the  ${}^4\text{He}^+$  ions were deflected through  $60^\circ$  and passed through a collimator system onto the target. The target had been mechanically polished and then chemically or electrolytically polished to remove contaminants, and it was set up in a hollow holder fitted with electrical leads. A given temperature at the target was provided by passing liquid nitrogen or water through the hollow holder or by heating thin targets electrically. The holder was mounted on a flange in the same block as the mass-spectrometer transducer and the IPD0-2 partial-pressure gauge, along with the thin-walled stainless-steel cylinder. The flange, the thin-walled cylinder, and the cylindrical cavity formed the chamber around the holder that communicated with the rest of the volume through a standardized hole. The design of the vacuum system and the multistage gas pumping provided high stability in the vacuum and adequate cleanness in the target. The method involving measurement of the helium partial pressure was used to examine the implantation and desorption in the chamber and outside it, using the mass-spectrometer transducer with dynamic pumping through the standardized hole. During the irradiation, the partial pressure in the chamber increased because of scattering of the  ${}^4\text{He}^+$  ions and release of the implanted helium. The partial pressure of helium outside the chamber altered only slightly. The implantation coefficient and the desorption rate  $dn/dt$  were calculated from the following formula [5, 6]:

$$\eta = 1 - \frac{n_0 q (p - p_0) w}{i}; \quad (1)$$

$$dn/dt = n_0 (p - p_0) w, \quad (2)$$

where  $w$  is the rate of pumping through the calibrated hole;  $\eta$ , implantation coefficient;  $n_0$ , number of helium atoms in  $1 \text{ cm}^3$  at a pressure of  $133 \text{ Pa}$  and normal temperature,  $\text{cm}^{-3}$ ;  $p$  and  $p_0$ , helium pressures in the target chamber and outside it,  $\text{Pa}$ ;  $i$ ,  ${}^4\text{He}^+$  beam current,  $\text{A}$ ; and  $q$ , charge of an ion,  $\text{C}$ .

All the mass-spectrometer transducers had previously been calibrated by measuring the dependence of the helium pressure in the chamber on the  ${}^4\text{He}^+$  current for thin tungsten

Translated from *Atomnaya Énergiya*, Vol. 53, No. 5, pp. 309-314, November, 1982. Original article submitted May 15, 1982.

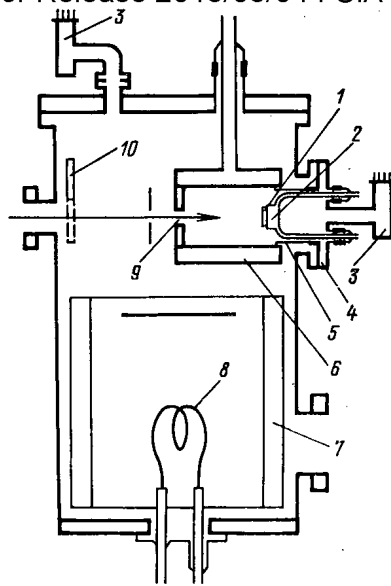


Fig. 1. Measurement chamber: 1) target; 2) target holder; 3) mass-spectrometer transducers; 4) flange; 5) thin-walled cylinder; 6) cylindrical cavity; 7) low-temperature titanium pump; 8) titanium evaporator; 9) standardized hole; 10) flap for covering ion beam.

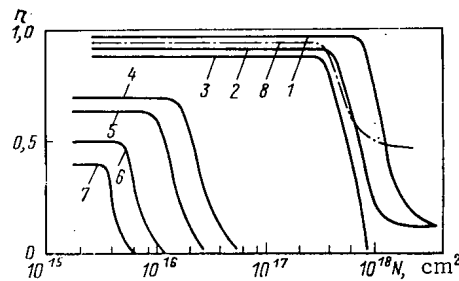


Fig. 2. Dependence of the  ${}^4\text{He}^+$  implantation coefficient  $\eta$  on implanted helium concentration  $N$ : 1, 2) W(100) and W(110), correspondingly,  $T = 78^\circ\text{K}$ ; 3-7) polycrystalline W,  $T = 78, 1000, 1500, 1700,$  and  $2000^\circ\text{K}$ , correspondingly; 8) polycrystalline Al,  $T = 78^\circ\text{K}$ .

targets at  $T = 2500^\circ\text{K}$ , when  $\eta = 0$ . To increase the sensitivity, the supply of helium was stopped before the desorption-rate measurements, and then the helium pressure outside the chamber was not more than  $1.3 \times 10^{-8}$  Pa. The blistering was examined by recording the fluctuations in helium pressure when the bubbles broke during and after the irradiation, which occurred against the background of spontaneous and thermally activated desorption. The size and shape of the blisters were determined with an MIM-8 optical microscope.

Figure 2 shows how  $\eta$  varies with the concentration  $N$  of implanted helium. These metals give  $\eta = \text{const}$ , no matter what the temperature  $T$ , in the range  $N < N_0$  ( $N_0$  is the concentration of implanted helium at which  $\eta$  begins to fall). As the temperature rises,  $N_0$  begins to fall, as does  $\eta$  in the range  $N < N_0$ ; for example, for tungsten at  $300^\circ\text{K}$ , the values of  $\eta$  and  $N_0$  are reduced by about 10% relative to  $78^\circ\text{K}$ . For  $N > N_0$ ,  $\eta$  for polycrystalline tungsten falls to zero at all  $T$ , while for single-crystal tungsten  $\eta$  at  $78^\circ\text{K}$  falls to a value close to zero.

The same  $\eta(N)$  relationship is observed for niobium, molybdenum, and other metals of high atomic mass. For metals of low atomic mass such as aluminum,  $\eta$  at 78°K falls to about 0.5 and then remains virtually unaltered at higher doses.

There is a resemblance to the results obtained with  $H^+$  on metals [7-9] in that this  $\eta(N)$  dependence occurs because the blisters are formed at a depth less than the mean range  $\lambda_m$  of the  $He^+$  ions in aluminum and other metals of low atomic mass, so most of the  $He^+$  penetrates through the tops of the blisters. Under these conditions, the implanted helium diffuses to the surface and also down into the target. The downward flux at high doses, and consequently the resulting minimum value of  $\eta$ , is probably determined by a potential barrier arising from the accumulation of radiation defects [10]. In tungsten, molybdenum, and niobium the blisters are formed at depths greater than  $\lambda_m$ . The  $He^+$  ions then do not penetrate through the tops of the blisters, the diffusion of the implanted helium into the target is locked by the blister layer, and all of the helium for  $N > N_0$  is released into the measurement volume no matter what the magnitude of the surface potential barrier.

The radiation-damage profile evidently determines the depth at which the blisters are produced for metals of low and high atomic mass, as in the case of bombardment with  $H^+$  [9, 11, 12]. Radiation defects are formed mainly in a layer  $\Delta L$  at a depth equal to  $\lambda_m$ . Here the recombination probability is the highest on account of the high defect density. Nearer the surface and deeper in the target, the density and the recombination probability are comparatively small. Therefore, the conditions for vacancy accumulation and thus the formation and growth of gas bubbles are the most favorable here. If a metal of high atomic mass is bombarded by  $He^+$  of comparatively low energy ( $E = 30$  keV), the depth distribution for the radiation defects has a gently falling rear part, and the maximum values occur immediately under the surface. Correspondingly, vacancy accumulation, gas-bubble growth, and blistering occur at a depth exceeding the mean ion range. In a metal of low atomic mass, the defect distribution [9, 12] has a gently sloping leading edge but a steep rear one, and therefore the blisters are formed at a depth less than the mean range.

Our results on the implantation of  $He^+$  in molybdenum at 300°K are in good agreement with published data [2], but for aluminum there is a substantial difference from [3]. In that study, the  $\eta(N)$  curves did not have a plateau, while the implantation coefficient at 78°K was 0.1, which is much less than our value.

The plateau on the  $\eta(N)$  curve indicates that the filling of the metal with helium is in a certain sense analogous to that with hydrogen on bombardment with  $H^+$  at 78°K [9, 13]. The helium ions penetrating into the metal are retarded mainly in a certain layer  $\Delta L$  at a depth of  $\lambda_m$ . While this layer has reasonably many unfilled traps for the helium, there is very little diffusion of helium from this layer, although the activation energy is fairly low (e.g., 0.25 eV for tungsten [14]). As the bombardment continues, the  $\Delta L$  layer becomes filled (when all the traps in the layer are full) and the helium diffuses freely within this layer to the boundaries. Therefore, this  $\Delta L$  layer with the limiting helium concentration expands towards

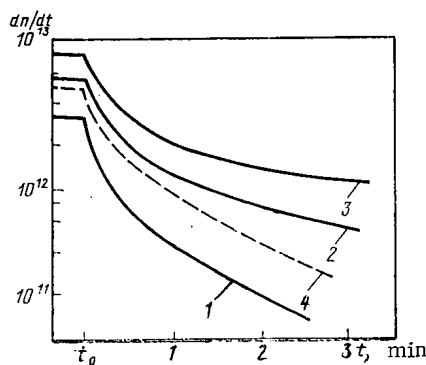


Fig. 3. Change in rate of spontaneous desorption with time ( $N \approx 1 \cdot 10^{17} \text{ cm}^{-2}$ ): 1, 2) W(100) and W(110), correspondingly,  $T = 78^\circ\text{K}$ ; 3) W(110),  $T = 300^\circ\text{K}$ ; 4) Al (111),  $T = 78^\circ\text{K}$ ;  $T_0$  is instant when irradiation stopped.

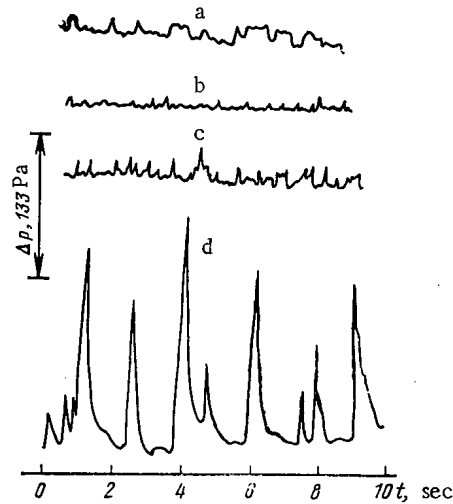


Fig. 4 Fluctuations in helium pressure: a, b) W(100) and W(110), correspondingly, in firmly activated desorption,  $\Delta p = 1.3 \cdot 10^{-6}$  Pa; c, d) Al (111) during irradiation at 78 and 300°K, correspondingly,  $\Delta p = 1.3 \cdot 10^{-5}$  Pa.

the surface and into the target. A marked fall in  $\eta$  at  $N = N_0$  indicates that the front representing the limiting concentration has attained the surface and the helium is beginning to dissolve freely into the vacuum. Therefore, a plateau can occur in two cases: if the material has a sufficiently high concentration of helium traps, and if the traps are evenly distributed in the surface layer. Only in these cases will the diffusion flux to the surface be constant for  $N < N_0$ , and consequently so will  $\eta$ .

Figure 3 shows results on the desorption of helium from tungsten and aluminum. At 78°K, the values of  $dn/dt$  and the total amount of released helium during and after the irradiation are less than those at 300°K and are dependent on the crystallographic orientation. The diffusion coefficients calculated from the slopes of the curves are correspondingly as follows for the  $\langle 100 \rangle$  and  $\langle 110 \rangle$  crystallographic directions:  $D_1 = 6 \cdot 10^{-13}$  cm<sup>2</sup>·sec<sup>-1</sup>,  $D_2 = 2.6 \cdot 10^{-13}$  cm<sup>2</sup>·sec<sup>-1</sup>, i.e., the diffusion coefficient is higher in the direction with more dense atomic packing. Such high diffusion coefficients at 78°K and helium concentrations  $N < N_0$  are difficult to explain in terms of classical diffusion of helium atoms between interstitial sites, for which the activation energy can scarcely be less than 0.25 eV. It is likely that here, as in the case of low-temperature release of implanted hydrogen [10], the minor release of helium during the radiation and the spontaneous desorption for  $N < N_0$  are due to diffusion to the surface in the form of complexes consisting of displaced metal atoms and helium ones. The mobility of such a complex may be fairly high, as may that of a single displaced atom.

The desorption during and after irradiation at  $N \geq N_0$  is accompanied by fluctuations in the helium pressure (Fig. 4) associated with helium release from the failed blisters. The amplitude and frequency of the fluctuations are dependent on the temperature, the nature of the material, and the crystallographic orientation of the irradiated surface. The amplitude of the fluctuations and the dimensions of the layers of failed blisters increase with temperature; this is particularly prominent for aluminum. In single-crystal tungsten targets with (111), (100), (110) crystallographic planes at the surfaces, the critical dose, the size of the blisters, and the amplitude of the pressure fluctuation increase with the packing density of the atoms in the direction of incidence, i.e., as the channeling conditions improve (one can take the concentration  $N_0$  at which the blisters are formed). With aluminum, the amplitude of the fluctuations is 50 times that found with tungsten; correspondingly, the size of the blisters in tungsten is  $< 2$   $\mu$ m, while blistering in aluminum is characterized by extensive surface exfoliation (Fig. 5). The surface relief under the exfoliation indicates that there has previously been fusion of gas bubbles of size  $< 1$   $\mu$ m.

Some of the implanted helium is released when the target is heated from 78 to 300°K. The proportion  $\alpha$  of the helium released is dependent on the target material, (e.g., about 10% for

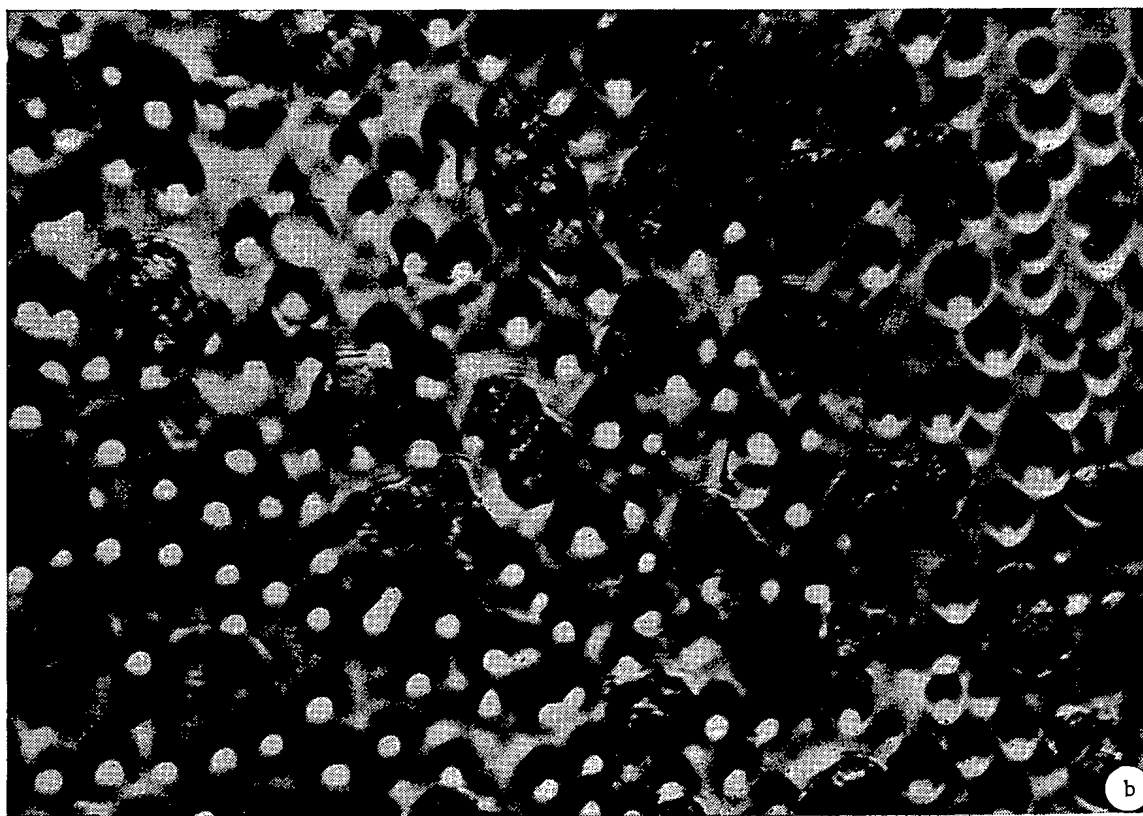
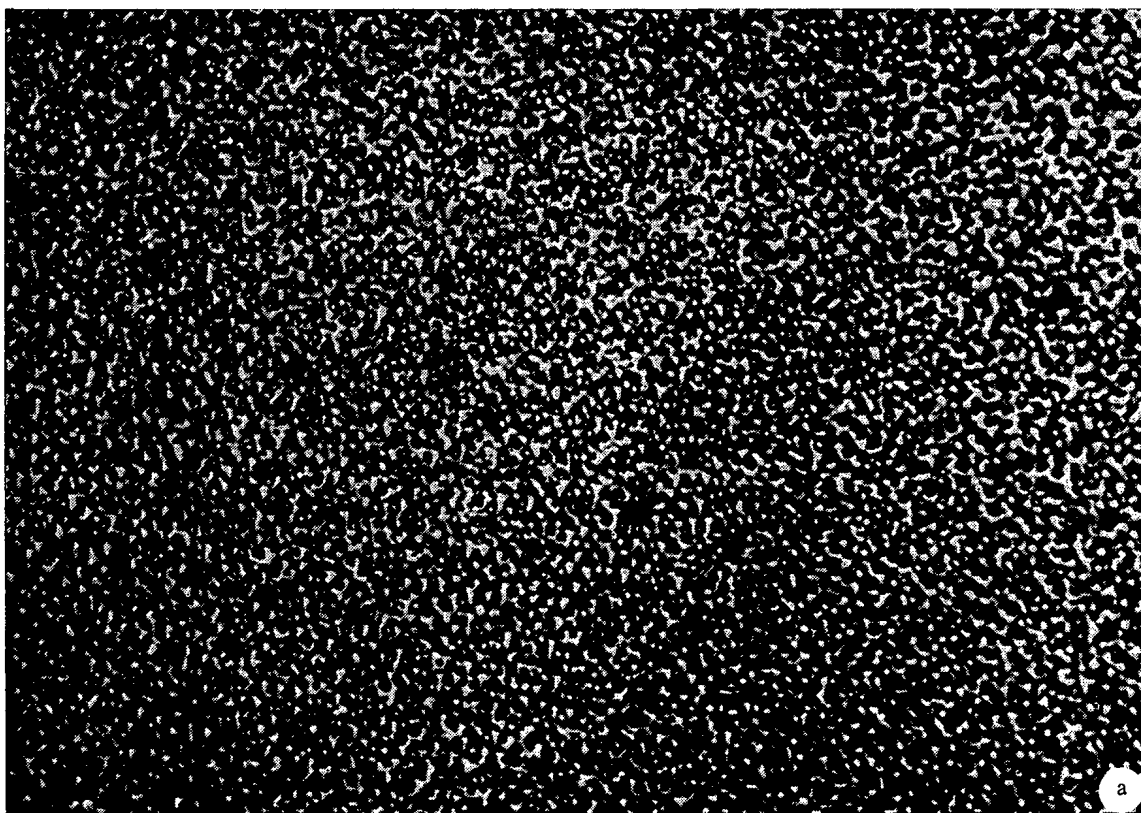


Fig. 5. Photomicrographs of irradiated surfaces of doses of  $N \approx 1 \cdot 10^{18} \text{ cm}^{-2}$ ; a) W(100),  $T = 78^\circ\text{K}$  ( $\times 2000$ ); b, c) Al (111),  $T = 78$  and  $300^\circ\text{K}$ , correspondingly ( $\times 2000$ ).



Fig. 5 (continued)

tungsten or 20% for aluminum), as well as on the crystallographic orientation. The value of  $\alpha$  increases with the packing density in the irradiation direction. For example, for tungsten the values of  $\alpha$  for the (111), (100), and (110) planes are 10, 9.5, and 7.5%, correspondingly. Polycrystalline tungsten shows the least release (7%). It is likely that at this low temperature the helium is derived mainly from interstitial sites and certain traps that are unstable in this temperature range. This is confirmed by the following: If a target, e.g., of polycrystalline tungsten, is first irradiated at 300°K to nearly complete saturation (when all the stable traps are filled and  $\eta = 0$ ) and is then cooled to 78°K and again irradiated with various doses, then on heating from 78 to 300°K all the helium implanted at 78°K is released. Calculations show that this amount of helium is equal to that released from targets that have not undergone preliminary bombardment at 300°K, i.e., it corresponds to  $\alpha = 7\%$ . Therefore, bombardment of tungsten at 78°K causes about 7% of the implanted helium to be trapped by interstitial sites and radiation defects that are unstable in the range 78–300°K; the rest of the implanted helium is taken up by more stable traps, which also determine the trapping at 300°K. These traps may be dislocations, grain boundaries, or vacancies. However, the trapping of the helium by dislocations and grain boundaries is evidently not decisive, since the values of  $N_0$  and  $\eta$  for single crystals are even higher than those for polycrystalline materials. It is very likely that vacancy defects of radiation origin are the helium traps at this temperature. Estimates [15] show that 10 or more vacancies may be formed when a  ${}^4\text{He}^+$  ion of energy 30 keV is stopped in a metal. Around each vacancy defect there is evidently a fairly extensive zone within which the activation energy for diffusion of helium atoms is much lower than elsewhere. The dimensions of this zone and the performance in helium atoms trapped by vacancy defects increases. Correspondingly, for  $N \gg N_0$  the implantation coefficient for  ${}^4\text{He}^+$  attains the stable value (from 0 to 0.5) dependent on the atomic mass of the metal and the irradiation temperature. The desorption during irradiation and the brief spontaneous desorption afterwards under these conditions are related to diffusion of the free helium atoms, evidently along with some mobile complexes. At very high temperatures, the values of  $\eta$  and  $N_0$  are substantially determined by thermal vacancies.

## LITERATURE CITED

1. A. T. Budnikov and N. P. Katrich, in: Single-Crystal Production and Examination [in Russian], VNII Monokristallov, Kharkov (1978), p. 40.

2. S. Erents and G. McCracken, *Radiat. Eff.*, 18, 191 (1973).
3. K. Wilson and G. Thomas, *J. Nucl. Mater.*, 63, 266 (1976).
4. N. P. Katrich and G. T. Adonkin, in: *Proceedings of the Sixth All-Union Conference on the Physics of Interactions between Charged Particles and Single Crystals* [in Russian], Moscow State Univ., (1975), p. 496.
5. E. S. Borovik, N. P. Katrich, and G. T. Nikolaev, *At. Energ.*, 18, No. 2, 91 (1965).
6. N. P. Katrich and G. T. Adonkin, in: *Single Crystals and Scintillators* [in Russian], VNII Monokristallov, Kharkov (1977), p. 34.
7. N. P. Katrich and A. T. Budnikov, in: *Proceedings of the Seventh International Conference on Atomic Collisions in Solids* [in Russian], Vol. 2, Moscow State Univ., (1980), p. 323.
8. N. P. Katrich and A. T. Budnikov, [6], p. 40.
9. N. P. Katrich and A. T. Budnikov, in: *Proceedings of the Sixth All-Union Conference on the Interaction of Atomic Particles with Solids* [in Russian], Minsk. Radiotekh. Inst., (1981), p. 143.
10. A. T. Budnikov and N. P. Katrich, in: *Proceedings of the Ninth All-Union Conference on the Physics of the Interactions of Charged Particles with Crystals* [in Russian], Moscow State Univ., (1979), p. 309.
11. A. T. Budnikov and N. P. Katrich, in: *Single Crystals and Their Applications* [in Russian], VNII Monokristallov, Kharkov (1979), p. 39.
12. A. T. Budnikov and N. P. Katrich, in: *Proceedings of the Tenth All-Union Conference on the Physics of the Interactions of Charged Particles with Crystals* [in Russian], Moscow State Univ., (1981), p. 443.
13. N. P. Katrich, *At. Energ.*, 25, No. 3, 217 (1968).
14. A. Veen and L. Caspers, *Delft. Prog. Rept.*, Al, No. 5, 160 (1976).
15. M. W. Thompson, *Defects and Radiation Damage in Metals*, Cambridge Univ. Press, (1969).

## THERMORADIATION DECOMPOSITION OF CARBON DIOXIDE

B. G. Dzantiev, A. N. Ermakov,  
V. M. Zhitomirskii, and V. N. Popov

UDC 541.15

The cycle of experiments conducted by the authors to study the mechanism and optimization of the thermoradiation decomposition of water vapor (TRDW) into hydrogen [1-6] allowed the conclusion to be drawn that the efficiency  $\eta$  of conversion of the radiation energy into  $H_2$ , is determined by the competition of elementary reactions, with the participation of active H and OH centers, and is a complex function of the temperature  $T$ , dose intensity  $\delta$ , and the irradiation time  $\tau$ . In optimum conditions (at a high temperature and a small time of contact, and with the exclusion of reverse oxidation reactions of  $H_2$ ), the radiation yield of hydrogen  $G(H_2) = 8$ , which corresponds to  $\eta = 20\%$ . The energy index achieved allows TRDW to be considered on a par with thermomechanical, electrochemical, and plasma methods of decomposition of water.

At the same time, taking account of the relatively low energy utilization factor  $\epsilon$  of the fission products (for systems with fixed fuel  $\epsilon < 0.3$ ), it is advantageous to continue the search for promising radiation processes having higher radiation yields. In a number of papers [7, 8] the use of radiation for the decomposition of carbon dioxide was proposed:



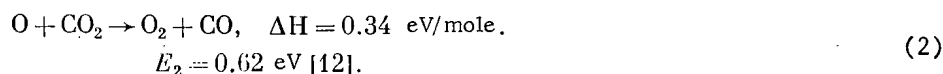
There is contradictory information in the literature [9-11] about the efficiency of reaction (1). Despite the quite considerable number of experiments and the diversity of experimental conditions (different types of radiation ( $\gamma$ , e, n, p,  $\alpha$ , and ff), different pressures, and the addition of acceptors), the mechanism of the radiolysis of  $CO_2$  has not been established unambiguously, and the value of  $G(CO)$  varies within the limits of 0.1-8 mole/100 eV. The results of [9] are the most reliable:  $G(CO) = 7.8$ . A slightly higher value of  $G(CO) = 8-10$

Translated from *Atomnaya Énergiya*, Vol. 53, No. 5, pp. 314-317, November, 1982. Original article submitted January 15, 1982.

was obtained in [8], where, as the authors assume, vibrationally excited molecules of  $\text{CO}_2$  make a definite contribution. A consideration of the kinetics of vibrational processes during the pulsed irradiation of  $\text{CO}_2$  [8], in the opinion of the authors, opens up the possibility of further increasing  $G(\text{CO})$  right up to 16-20 for an energy injection of  $d \approx 3-10 \text{ J/cm}^3$ . It is important for this that the stated values of  $d$  should be achieved during a time  $\tau$  of the order of or less than the time of vibrational relaxation ( $10^{-4}-10^{-5} \text{ sec}$ , with  $P \approx 10^5 \text{ Pa}$ ), which corresponds to an energy potential of  $10^2-10^3 \text{ kW/liter}$ . It is obvious that the achievement of these conditions is an exceptionally complicated problem.

In [9, 10], the mechanism of the radiolysis of  $\text{CO}_2$  was investigated using kinetic spectroscopy and the technique of radical and electron acceptors. The data obtained allowed the authors of these papers, independently from the author of [11], to formulate the primary stages of decomposition of  $\text{CO}_2$  and to distinguish the contribution of ionic processes and dissociation processes of electron-excited molecules. An analysis of the data allows the maximum possible radiation yield of the decomposition of  $\text{CO}_2$  for low values of  $d$  to be estimated, i.e., in the absence of a contribution of vibrationally excited molecules to the decomposition of  $\text{CO}_2$ . This consideration leads to  $G^0(\text{CO}) = G^0(\text{O}) = 7.6$  (the sign "0" denotes the primary yield). An independent estimate of  $G^0(\text{CO})$  follows from data about the yield of ozone by the irradiation of  $\text{CO}_2\text{-O}_2$  mixtures [10]; in this case  $G^0(\text{CO}) \approx 7$ .

At a high temperature, the atoms of oxygen formed during the radiolysis of  $\text{CO}_2$  can enter into a detachment reaction:



In the limit this gives  $G_{\text{max}}(\text{CO}) \approx 2G^0(\text{CO}) \approx 14-15$ . Estimates show that reaction (2) predominates over the recombination reaction of atomic hydrogen for

$$T \geq \frac{E_2}{R} \left[ \ln \left( \frac{A_2}{K_p [\text{O}]} \right) \right]^{-1}. \quad (3)$$

Here  $E_2$  and  $A_2$  are the energy of activation and the preexponent of reaction (2);  $K_p$  and  $[\text{O}]$  are, respectively, the recombination constant and the stationary concentration of oxygen atoms. Substituting, in Eq.(3),  $E_2 = 0.62 \text{ eV}$ ,  $A_2 = 2 \cdot 10^{13} \text{ cm}^3/(\text{mole} \cdot \text{sec})$  and  $K_p = 2 \cdot 10^{16} \text{ cm}^6/(\text{mole}^2 \cdot \text{sec})$  [12], we find that for  $[\text{O}] \leq 10^{-10} \text{ mole/cm}^3$ ,  $T \approx 500^\circ \text{K}$ . Thus, in the case of the radiation decomposition of  $\text{CO}_2$ , a regime of irradiation is possible for which, in conditions of a relatively low degree of ionization, a low energy injection ( $\sim 10^{-2} \text{ J/cm}^3$ ), and  $T \geq 500^\circ \text{K}$ , a high radiation breakdown efficiency of  $\text{CO}_2$  can be expected:  $G_{\text{max}}(\text{CO}) = 14-15 \text{ mole/100 eV}$

and  $\eta_m = \frac{G_{\text{max}}}{G_{\text{theor}}} = \frac{G_{\text{max}}}{100 / \Delta H_1 [\text{eV/mole}]} \approx \frac{2.9 \text{ eV}}{7 \text{ eV}} \approx 0.4 \text{ (40\%)}$ . A similar path, with the participation of excited  $\text{CO}_2$  molecules in reaction (2), was proposed in [9]: According to these estimates, reaction (2) predominates over the recombination reactions of atomic hydrogen with  $\frac{n_e}{n_0} \approx 10^{-3}$ , which imposes rigorous conditions on the energy potential (intensity  $\delta \geq 10^{25} \text{ eV}/(\text{cm}^3 \cdot \text{sec})$ ).

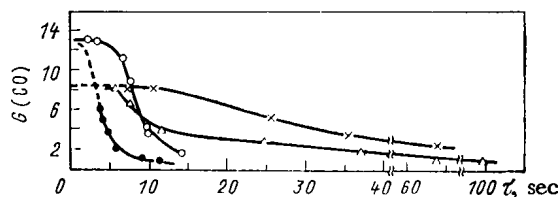


Fig. 1. Dependence of the radiation yield of CO on the duration of irradiation for a different dose intensity,  $\text{eV}/(\text{cm}^3 \cdot \text{sec})$ :  $\circ$   $5 \cdot 10^{16}$  ( $T = 500^\circ \text{C}$ );  $\times$   $\sim 6 \cdot 10^{16}$  ( $T = 20^\circ \text{C}$ );  $\Delta$   $\sim 1.2 \cdot 10^{17}$  ( $T = 20^\circ \text{C}$ )  $\bullet$   $\sim 4 \cdot 10^{16}$  ( $T = 700^\circ \text{C}$ ).

In the present paper, the results are given of an experimental investigation of the high-temperature radiolysis of carbon dioxide. For comparison and quantitative agreement of these results with the literature data of [9-11], the radiation yield of carbon monoxide  $G(\text{CO})$  at room temperature was also measured.

The experiments were conducted on a U-12 accelerator, using a metallic-flow facility. The  $\text{CO}_2$  source was gas in steel cylinders, without preliminary purification. The special features of construction and operation of the facility and also the dosimetry were described earlier in [3]. Depending on the temperature conditions of irradiation of the  $\text{CO}_2$ , both a reactor with electrical heating and also a reactor cooled by running water were used. For the heated reactor, the temperature field in the reactor was determined beforehand as a function of the feed velocity of the gas. The  $\text{CO}_2$  flow rate was monitored by the readings of a rheometer and a rotameter. In contrast from [3], the radiolysis products in the present experiments were concentrated by absorption of the  $\text{CO}_2$  with alkali. In order to monitor the  $\text{CO}_2$  absorption process, a reference gas ( $\text{N}_2$ ) with a known flow rate was added to the mixture at the exit from the irradiated volume. From the ratio of the chromatographic peaks of nitrogen in experiments with and without absorption of  $\text{CO}_2$ , the amount of  $\text{CO}_2$  that reacted with the alkali and the concentration of CO were assessed.

Figure 1 shows the dependence of the radiation yield of CO on the time of irradiation of  $\text{CO}_2$  for three temperature values (20, 500, and  $700^\circ\text{C}$ ) and a dose intensity of  $\sim 4 \cdot 10^{16} - 1.2 \cdot 10^{17} \text{ eV}/(\text{cm}^3 \cdot \text{sec})$ . It can be seen that the curve  $G(\text{CO}) = f(\tau)$ , corresponding to  $20^\circ\text{C}$ , reaches a plateau  $G(\text{CO}) = 8$  for  $\tau \leq 15 \text{ sec}$ . The value obtained for the radiation yield coincides well with the data of the experiment in [9], performed with  $\delta = 10^{24} \text{ eV}/(\text{cm}^3 \cdot \text{sec})$  [ $G(\text{CO}) = 7.8$ ]. This indicates, additionally, that the formation of CO is related with ion-molecular processes which are independent of the dose intensity, with dissociative ionization processes, and with dissociations of electron-excited molecules. With a large duration of irradiation (low flow rate of  $\text{CO}_2$ ), a reduction of  $G(\text{CO})$  is observed, due to reverse oxidation reactions of CO to  $\text{CO}_2$  in interaction processes with active centers present in the irradiation zone. For example, as a result of the oxidation of CO in reactions with atomic oxygen



The characteristic reaction time of Eq. (4) is  $\tau_4 \approx \frac{1}{K_4 [\text{O}] [\text{CO}_2]}$ . With  $[\text{O}] \approx 10^{-10} \text{ mole}/\text{cm}^3$ ,  $\tau_4 \approx 20 \text{ sec}$ , which is close to that observed in the experiment. In the limit, with  $\tau \gg \tau_4$ , a stationary concentration of  $[\text{CO}]_\infty \approx 0.1\%$  is established, independent of the dose intensity (Fig. 2). Similar values of  $[\text{CO}]_\infty$  with significantly higher values of  $\delta \approx 10^{24} \text{ eV}/(\text{cm}^3 \cdot \text{sec})$  were observed also, earlier in [9], i.e., at a low temperature the stationary concentration of CO during the radiation decomposition of  $\text{CO}_2$  is independent of the radiation intensity in the range  $10^{16} - 10^{24} \text{ eV}/(\text{cm}^3 \cdot \text{sec})$ .

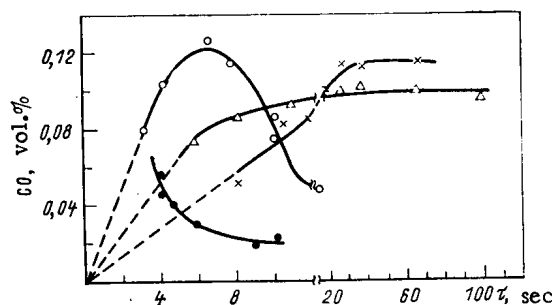


Fig. 2. Dependence of the concentration of CO on the duration of irradiation for a different dose intensity,  $\text{eV}/(\text{cm}^3 \cdot \text{sec})$ :  
 ○)  $\sim 5 \cdot 10^{16}$ ; ×)  $\sim 6 \cdot 10^{16}$ ; Δ)  $\sim 1.2 \cdot 10^{17}$ ;  
 ●)  $\sim 4 \cdot 10^{16}$ ; temperature values are the same as in Fig. 1.

the concentration  $[CO] \approx 0.1\%$  for  $T = 500^\circ C$  is achieved for a significantly shorter duration of  $\sim 5$  sec (see Fig. 2). The value of  $G(CO) = 13 \pm 1$  (see Fig. 1), corresponding to this concentration and temperature, confirms that the concentration  $[CO] \approx 1\%$  is also close to the stationary concentration for irradiation at  $T = 500^\circ C$ . The value found for  $G(CO)$  corresponds to a 35% conversion of radiation energy into CO energy; this exceeds the same index for the thermoradiation decomposition of water vapor by almost a factor of two. It should be emphasized that the yields of CO attained are obtained with specific energy injections of  $\sim 10^{-2} \text{ J/cm}^3$  and small degrees of ionization ( $\leq 10^{-7}$ ). In these conditions, the role of vibrationally excited molecules of  $CO_2$  in its decomposition processes is negligibly small [8].

We also note the absence of a plateau ( $CO_\infty$ ) for the kinetic curves of the formation of CO (see Fig. 2) at high temperature ( $500, 700^\circ C$ ). This, obviously, is due to interaction reactions of CO with the heated wall of the reactor and, possibly, also with the ozone formed during radiolysis. For this reason, because of the increase of the speed of the surface oxidation process with reduction of temperature, in order to achieve the value of  $G(CO) = 13-14$  at  $T \approx 700^\circ C$ , an irradiation duration of  $\sim 1$  sec is necessary, which for the reactor investigated presumes a flow rate of  $CO_2 \approx 10^3$  liter/h. For a flow rate of  $CO_2 \approx 400$  liter/h ( $\tau \approx 4$  sec),  $G = 6$ .

The results obtained are a record for large-scale energy processes and allow the process of thermoradiation decomposition of carbon dioxide to be considered as a promising and economical path for the transformation of radiation energy into carrier energy.

#### LITERATURE CITED

1. B. G. Dzantiev, A. N. Ermakov, and V. N. Popov, *At. Énerg.*, **46**, No. 5, 359 (1979).
2. B. G. Dzantiev, A. N. Ermakov, and V. N. Popov, *Problems of Nuclear Science and Technology. Ser. Atomic-Hydrogen Power Generation*, **1**(5), 86 (1979).
3. V. N. Popov et al., *At. Energ.*, **52**, No. 1, 64 (1982).
4. B. G. Dzantiev et al., *Khim. Vys. Energ.*, **16**, No. 1, 93 (1982).
5. B. G. Dzantiev et al., *Problems of Nuclear Science and Technology. Ser. Atomic-Hydrogen Power Generation*, **1**(8), 53 (1981).
6. B. G. Dzantiev et al., *Khim. Vys. Energ.*, **16**, No. 4, 373 (1982).
7. V. A. Legasov, *Priroda*, No. 3, 3 (1977).
8. I. G. Belousov et al., *Problems of Nuclear Science and Technology*, **1**(5), 43 (1979).
9. C. Willis, A. Boyd, and P. Binder, *Can. J. Chem.*, **48**, 1951 (1970).
10. G. Meaburn et al., *J. Phys. Chem.*, **72**, 3920 (1968).
11. R. Kummer et al., *J. Phys. Chem.*, **181**, No. 25, 2451 (1977).
12. V. N. Kondrat'ev, *Velocity Constants of Gas-Phase Reactions. Handbook [in Russian]*, Moscow (1970).

# INCREASE OF THE ELECTRON-BEAM IRRADIATION EFFICIENCY OF CYLINDRICAL OBJECTS BY MEANS OF MAGNETIC SYSTEMS

L. L. Akrachkova, N. K. Kuksanov, R. A. Salimov,  
Yu. N. Timko, and E. E. Finkel'

UDC 621.384.6

At the present time, electron accelerators are widely used in the industrial technology of the radiation modification of polymer insulation for cable products and electroinsulation tubes. Of the direct action domestic accelerators, type ÉLV accelerators [1] are the most suitable for this process, owing to the quite powerful beam (20 kW), the possibility of regulating the electron energies within wide limits (0.5–1.5 MeV) without altering the power, the quite high reliability, and the relatively simple maintenance and operation. This ensures high technicoeconomic radiation technology indices for the output of electroinsulation and cable production. At the same time, when analyzing the technological indexes of the radiation modification lines for the insulation of conductors, cables, and heat-shrunk tubes for different methods of shaping the radiation zone (Fig. 1), it was established that there is a considerable reserve for increasing production capacity and for expansion of the catalog of irradiation for cable components on ÉLV-type accelerators. It is important to note that a large catalog of cable components, in practice, excludes the possibility of modifying the polyethylene insulation of cable components by a single technological scheme.

Long uniform components themselves are an element of the conveying equipment for their movement in the zone of the electron beam, independently of the one-sided or two-sided method of forming the irradiation zone (see Fig. 1). In the present paper we shall confine ourselves to considering only two technological indices: the beam-current utilization index,

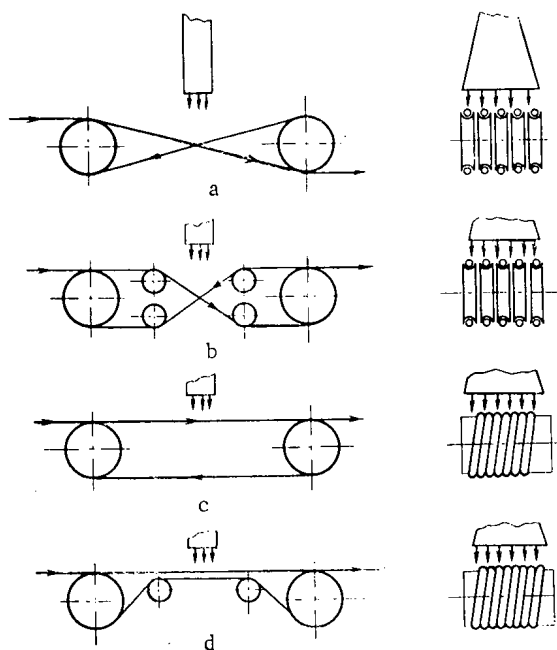


Fig. 1. Conveyance of cables in the irradiation zone, using reversible rollers (a), reversible and intermediate rollers (b), a reciprocating drum (c), and a reciprocating drum and intermediate rollers (d).

Translated from *Atomnaya Énergiya*, Vol. 53, No. 5, pp. 317–319, November, 1982. Original article submitted December 21, 1981.

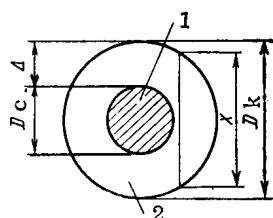


Fig. 2

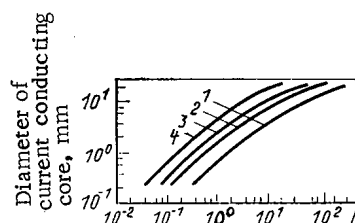


Fig. 3

Fig. 2. Geometrical parameters of the cable: 1) current-conducting core; 2) insulation.

Fig. 3. Dependence of the coefficient K on the core diameter for electron energies of 0.5 (1), 0.75 (2), 1 (3), and 1.5 (4) MeV.

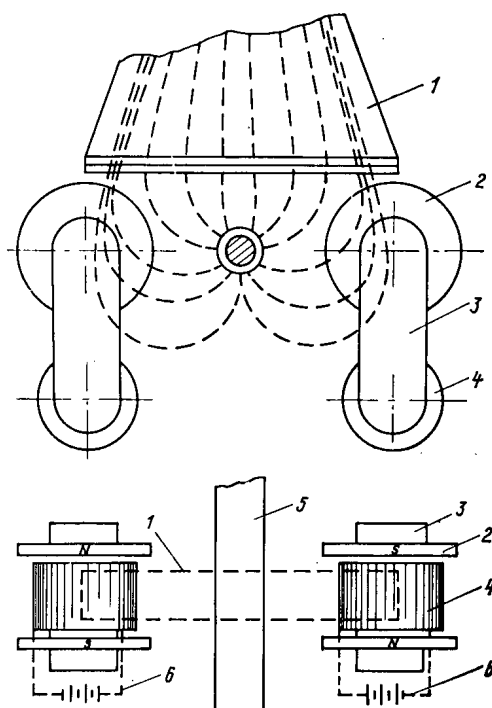


Fig. 4. Schematic diagram of the magnetic system with all-around scanning: 1) funnel; 2) magnet pole; 3) magnetic core; 4) magnet coil; 5) cable to be irradiated; 6) power-supply unit.

taking account of losses due to incomplete overlapping of the beam cross-section by the component being irradiated, and the electron-energy utilization index, taking account of losses due to absorption in the current-conducting core and incomplete absorption of part of the electrons by the polymer insulator.

For lines  $\alpha$  and  $b$  of the conventional roller system (see Fig. 1) and with two-sided irradiation, the beam-current and energy utilization indexes for conductors with a diameter of 0.2-2 mm vary from 0.4 to 0.9 and 0.8 to 0.6, respectively. For lines  $c$  and  $d$ , for which the working principle is based on the passage around a cylindrical surface by the conductor (cable) and its subsequent movement along the cylinder axis — "reciprocating drum" [2], the beam-current utilization index is equal to 0.9 for the whole catalog of cable components, but the values of  $K_e$  are the same as for lines  $\alpha$  and  $b$ .

The considerable power losses of the electron beam (the energy utilization index varies from 0.8 to 0.6 for all methods of forming a one-sided or two-sided irradiation zone) are due to the different thicknesses of the polymer material in the direction of incidence of the electron beam because of the cylindrical shape of the item (Fig. 2). This feature, in conjunction with the presence of the metal current-carrying core screening part of the material from the incident electron beam, makes it extremely difficult to achieve an acceptable distribution of the absorbed dose and a high-intensity utilization efficiency of the electron beam.

In the case of two-sided irradiation of cylindrical items on lines  $\alpha$ -d (see Fig. 1), the nonuniformity of the absorbed dose in the insulation with a thickness of 0.2-3 mm amounts to  $\pm 25\%$  (within the established limits) for cables with a diameter of 2-11 mm. However, for cables with a diameter in excess of 11 mm and with this same thickness of insulator, an acceptable uniformity of the absorbed dose cannot be achieved from irradiation on  $\dot{E}$ LV-type accelerators. This is because in order to ensure the required uniformity of the absorbed dose in the case of two-sided irradiation, the choice of the electron energy is determined by the maximum thickness of the insulation  $X$  (see Fig. 2):

$$X = \sqrt{D_k^2 - D_c^2} = \sqrt{(D_c + 2\Delta)^2 - D_c^2}, \quad (1)$$

where  $D_k$  and  $D_c$  are the diameter of the cable and current-conducting core, respectively;  $\Delta$  is the radial thickness of the insulator. The value of  $X$  with constant radial thickness increases with increase of the cross section of the current-conducting core of the cable.

Thus, the most important geometrical parameter of the cable, defining the choice of the necessary electron energy, is  $X$ . Then as the characteristic parameter when determining the technicoeconomic indices of the process, it is convenient to assume the parameter  $K = D_c/\Delta$ , so that

$$X = 2\Delta \sqrt{K+1}. \quad (2)$$

The curves given in Fig. 3 show with what dimensions of insulation, with a density of  $1 \text{ g/cm}^3$ , and with what core diameters, an irradiation nonuniformity of less than 25% can be ensured in the case of two-sided irradiation with electron of given energy. It is obvious that for comparable values of  $D_c$  and  $\Delta$ , and their absolute values of more than 15 mm, the necessity arises for a significant increase of energy of the electrons.

The uniformity of the absorbed dose in the insulation and the efficiency of utilization of the electron beam intensity in type- $\dot{E}$ LV accelerators can be improved considerably by ensuring normal incidence of the electrons on the cylindrical surface. In this case, the catalog of these components is simultaneously extended with respect to the overall dimensions. A promising course for the solution of this important problem is the use of magnetic systems, shaping the electron trajectories in the required way.

In the present paper, the results are given of investigations on the irradiation of cable blanks with an external diameter of 25 to 50 mm and an insulation thickness of 2.5 to 10 mm on the  $\dot{E}$ LV-2 accelerator, equipped with the magnetic system described for the first time in [3]. The system (Fig. 4) consists of two C-shaped magnets, generating nonuniform and oppositely directed magnetic fields below the outlet window of the funnel of the scanning device. The electrons of the scanning beam, emerging into the atmosphere through the foil of the outlet window, are diverted in the magnetic field at different angles and are directed onto the item, almost perpendicular to its surface. With an electron energy of 1.5 MeV, the nonuniform magnetic field provides a focused electron beam on a cylindrical object with a diameter of up to 100 mm, with a nonuniformity of the electron density over the circumference of the object of not more than  $\pm 10\%$ .

For comparison, cable blanks of different construction (see Table 1) were irradiated "in a single pass" in the circular radiation field created by the magnetic system, and also by the conventional scheme of two-sided irradiation (with rotation of the object by  $180^\circ$ ).

The determination of the angular (sectors I-VIII) and depth (layers 1-6) distribution of the absorbed dose in the cable insulation was conducted according to the scheme shown in Fig. 5. The content of the gel-fraction in the irradiated polyethylene (determined by an extraction method) was used as the dose factor. The results of the investigation of the absorbed dose distribution over the perimeter of the cable blank insulation, when irradiated

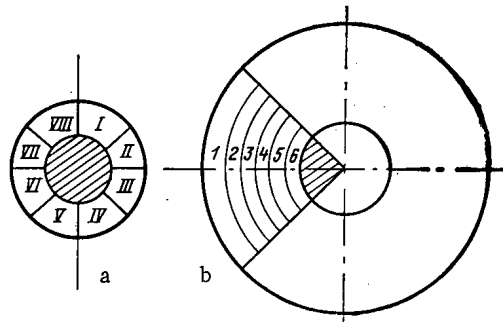


Fig. 5. Section of cable, irradiated on the ELV-2 accelerator using all-round scanning, with angular (a) and depth (b) distribution of the absorbed dose.

TABLE 1. Absorbed Dose Distribution in the Insulation of High-Voltage Cables

Cable diameter, mm	Insulation thickness, mm	Nonuniformity of absorbed dose over the perimeter of the insulation, ±%	
		irradiation in circular radiation field	two-sided irradiation
50	10	10,6	94
45	10	7,3	70
40	10	4,6	50
40	5	4,6	45
35	5	3,1	38
35	2,5	3,1	33
30	5	2,7	33
25	2,5	2,2	30

with electrons with an energy of 1.5 MeV, are shown in Table 1. It can be seen that as a result of irradiation in the circular radiation field, the nonuniformity of the absorbed dose over the periphery of the insulation is decreased from 10.6% for cables with a diameter of 50 mm to 2.2% for cables with a diameter of 25 mm. The thickness of the irradiated layer of insulation corresponds to the classical ionization curve for one-sided irradiation of a flat polyethylene sample with electrons with an energy of 1.5 MeV. For all the irradiated cables shown in Table 1, the depth of the layer of insulation in which the nonuniformity of the absorbed dose did not exceed  $\pm 25\%$  amounts to  $\sim 4$  mm for an energy of 1.5 MeV.

Thus, the quality of irradiation of the insulation using the circular radiation field depends only slightly on the cross section of the current-conducting core, and is determined by the energy of the electrons and the thickness of the insulation being irradiated. On analyzing the data about the distribution of the absorbed dose field in the plane of the cross section of high-voltage cable insulation, the permissible nonuniformity of the absorbed dose over the perimeter of the insulation was established for two-sided irradiation. The irradiation nonuniformity depends to a large degree on the parameter K, which with a given maximum electron energy significantly limits the range of dimensions of cable components irradiated on the existing electron accelerators.

The circular radiation field ensures a high quality of irradiation of the insulation over a wide range of cross sections of current-conducting cores. In the case of two-sided irradiation by the conventional method, i.e., in the absence of the magnetic field, the catalog of cable units which can be irradiated on the accelerator with a given maximum electron energy is limited by both the cross sections of the current-conducting core and by the thickness of the insulation. The results obtained are of important value for the further improvement of technological systems and plant designs, for the purpose of increasing the irradiation efficiency of electroinsulated and cable components.

LITERATURE CITED

1. G. I. Budker, in: Report of the Second All-Union Conference on the Application of Charged Particle Accelerators in the National Economy [in Russian], Vol. 1, Scientific-Research Institute of Electrophysical Equipment, Leningrad (1975), p. 51.
2. E. E. Finkel et al., USA Patent No. 3,860,159 (1975).
3. V. L. Auslender et al., in: Report of the Third All-Union Conference on the Application of Charged Particle Accelerators in the National Economy [in Russian], Vol. 1, Scientific-Research Institute of Electrophysical Equipment, Leningrad (1979), p. 126.

# DISTRIBUTION OF GAS IN A REACTOR WITH SPHERICAL FUEL ELEMENTS

A. S. Pushnov, I. I. Gel'perin,  
and A. M. Kagan

UDC 66.023:661.566:533.608

A uniform distribution of gas in reactors with spherical fuel elements can be ensured in two ways: first, by artificially increasing the hydraulic resistance near the reactor walls to values approximating the resistance of the whole layer (this can be achieved by replacing some or all of the large spheres by small ones [1]); second, by using converging and diverging headers [2]. However, the aerodynamics of such headers has not been studied sufficiently to permit a simpler technical design with reduced hydraulic resistance.

We report on the determination of the optimum angles of inclination  $\alpha$  of the baffles forming the diverging and converging headers for ensuring uniformity of the gas distribution over the length of an assembly of spheres. The experiments were performed under isothermal conditions. The gas moved through the apparatus in a Z-shaped path. Seven different-sized spherical shot with diameters from 3 to 5 mm were used. The equivalent diameter of the layer of spheres  $d_e = 1.99 \times 10^{-3}$  m, the void fraction in the assembly  $\epsilon = 0.53$ ,  $\alpha$  was varied from 0 to 6°, the height of the layer  $H = 95$  mm, and the assembly of spheres was 580 mm long and 300 mm wide. The upper and lower parts of the gas-permeable assembly were made of wire gauze.

The experiments on the layer of spheres were performed at velocities from 0.18 to 0.8 m/sec. During the experiments the velocity distribution was monitored in six equally spaced cross sections, and the pressure drop  $\Delta p$  in the layer was measured. In Fig. 1 the insert is a schematic diagram of the experimental apparatus, and the points show the test cross sections. In each cross section the local velocity was measured every 10 mm with a constant-temperature thermoanemometer.\* The pressure drop was monitored with an inclined micromanom-

\*A. A. Shishimarov and A. N. Gavrilov helped with the experiments.

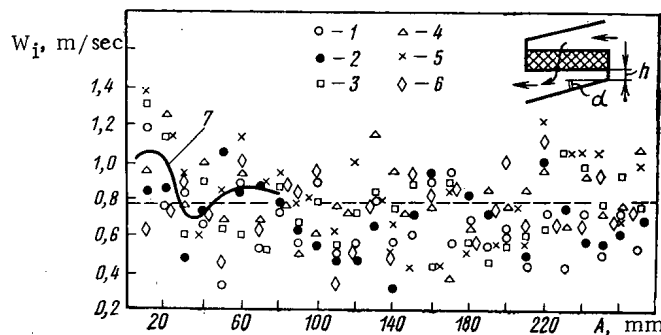


Fig. 1. Distribution of local velocity  $W_i$  over width of assembly of spheres as a function of distance  $A$  from wall for  $h = 0$  mm,  $\alpha = 4^\circ$ ,  $\bar{W}_{ap} = 0.789$  m/sec: 1-6) different directions of displacement of transducer within layer of spheres (test cross sections); 7) distribution of local velocity  $\bar{W}_i$  near wall, averaged for each distance  $A$  from wall; ---) average velocity of gas through apparatus  $\bar{W}_{ap}$ .

Translated from *Atomnaya Énergiya*, Vol. 53, No. 5, pp. 320-321, November, 1982. Original article submitted October 10, 1980; revision submitted February 22, 1982.

eter. Repeated calibration of the thermoanemometer transducer after the experiments were completed showed good reproducibility of the calibration curve. The maximum deviation did not exceed  $\pm 1.5\%$ .

A typical velocity distribution in the layer of pellets is shown in Fig. 1. From the results in [1, 3-5], one might expect that the velocity of the gas would be higher near the wall than in the central part of the assembly. Experiments in [5] with identical spheres showed that the maximum velocity should be found at  $\sim 2$  sphere diameters from the wall. Figure 1 shows that the flow velocity varies from 0.5 to 1 m/sec in the central part of the assembly of spheres, and from 0.6 to 1.4 m/sec near the wall. The increase in the local velocity  $W_i$  as the wall is approached is pronounced for test sections 1, 3, and 5, but is less noticeable for cross sections 2 and 4. In cross section 6 the velocity decreases. This is clearly due to the random orientation of the thermoanemometer transducer with respect to a sphere. In order to recognize the laws of the gas distribution, the local velocity  $W_i$  must be averaged over all six cross sections for each distance  $A$  from the wall (curve 7 on Fig. 1). The average velocity  $\bar{W}_i$  increases with decreasing distance  $A$  from the wall. Thus, while far from the wall, where  $A = 40$  mm,  $\bar{W}_i = 0.77$  m/sec, at  $A = 10$  mm (the nearest approach of the transducer to the wall)  $\bar{W}_i = 1.06$  m/sec. This effect is accounted for by the increase in the local void fraction  $\epsilon$  with decreasing distance from the wall for a fixed layer of spheres [6].

A statistical analysis of the measured values was performed with the program described in [7]. The total degree of irregularity of the gas distribution in the layer of spheres was estimated with the relation [7]

$$\psi = \left\{ \frac{\sum_{i=1}^{mn} |W_{ij} - \bar{W}_{ap}|}{mn\bar{W}_{ap}} \right\} 100\%,$$

which characterizes the average scatter. Here  $m$  is the number of test cross sections;  $n$ , number of test points in a given cross section;  $W_{ij}$ , local velocity at the  $i$ -th point of the  $j$ -th cross section; and  $\bar{W}_{ap}$ , average velocity of the gas through the apparatus.

It might be expected that the function  $\psi = f(\alpha)$  for  $\bar{W}_{ap} = \text{const}$  should have a minimum corresponding to the optimum value of  $\alpha$  of the baffles forming the diverging and converging headers.

Measurements of the velocity distribution showed that over the whole range of velocities tested, the largest deviations of the  $\bar{W}_j$  values of  $\bar{W}_j$ , the average velocity over the  $j$ -th cross section, from  $\bar{W}_{ap}$  occurred in the first and last cross sections of the assembly traversed by the gas.

The measured velocity distributions can also be used to estimate the nonuniformity of the temperature distribution in the reactor. Possible overheating of the spheres can be estimated as the ratio of the minimum flow rate of the gas in the assembly to the average over the apparatus:  $\bar{W}_{i,\min}/\bar{W}_{ap}$ , where  $\bar{W}_{i,\min}$  is the arithmetic mean of the local velocities which are lower than  $\bar{W}_{ap}$ . Figure 2 shows that this ratio is minimum for  $\alpha = 4^\circ$ . We note that as  $\bar{W}_{ap}$  is increased, the ratio  $\bar{W}_{i,\min}/\bar{W}_{ap}$  decreases somewhat. An increase of  $\alpha$  from 1 to  $4^\circ$  with identical flow rates leads to a certain decrease in the ratio  $\bar{W}_j/\bar{W}_{ap}$ .

The effect of the height  $h$  of the dead end, located at the end of the converging and the beginning of the diverging headers, on the gas distribution within the assembly as  $\alpha \rightarrow 0$  was

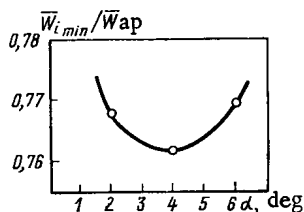


Fig. 2. Effect of  $\alpha$  on the ratio  $\bar{W}_{i,\min}/\bar{W}_{ap}$ .

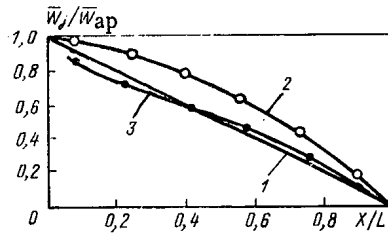


Fig. 3. Comparison of our results with data of [8]: 1) ideal gas distribution; 2) curve from [8] for width of diverging and collecting headers  $h = 40$  mm and  $\alpha = 0^\circ$ ; spheres were shot 2-2.5 mm in diameter,  $\epsilon = 0.34-0.35$ ; 3) our results for  $h = 0$ ,  $\alpha = 4^\circ$ , scaled to a diverging header;  $L$ , length of assembly;  $X$ , running distance from end of assembly to  $j$ -th cross section.

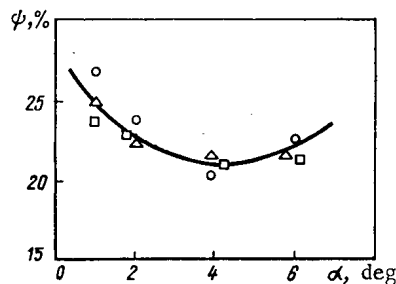


Fig. 4

Fig. 4.  $\psi$  as a function of  $\alpha$  for  $h = 0$  mm:  $\circ, \Delta, \square$ )  $\bar{w}_{ap} = 0.78, 0.36$ , and  $0.17$  m/sec, respectively.

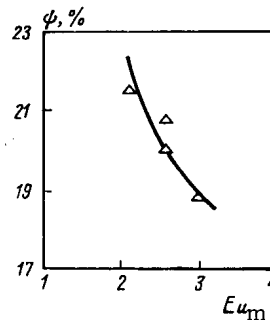


Fig. 5

Fig. 5.  $\psi$  as a function of the Euler number  $Eu_m$  for experimental apparatus with spherical packing and  $\alpha = 4^\circ$ .

insignificant in the range tested, where  $h/L = 0.025-0.105$ . When  $\alpha$  was increased from  $1$  to  $4^\circ$  at identical flow rates, the deleterious effect of the dead end increased somewhat, and an increase in  $h$  from  $15$  to  $53$  mm for a constant angle  $\alpha = 4^\circ$  led to an increase in  $\psi$  over the whole cross section of the assembly by  $\sim 20\%$ .

We compared the results in [8], where the gas distribution was studied in a reactor with spheres of approximately the same size, and also for a Z-shaped path of the gas through the apparatus but without a converging header, with our results, scaled to a diverging header, i.e., to the conditions in [8]. The comparison showed that our construction with a converging header with  $\alpha = 4^\circ$  and  $h = 0$  is preferable (curves 2 and 3 of Fig. 3).

In processing the experimental data on  $\psi$  as a function of  $\alpha$  for various values of  $\bar{w}_{ap}$ , it was established that all the experimental points are correlated by the single curve of Fig. 4, and consequently the velocity  $\bar{w}_{ap}$  has practically no effect on  $\psi$ . Figure 4 also shows that the optimum value of  $\alpha$  for spheres is  $4^\circ$ , since at this value  $\psi$  has a minimum over the whole range of velocities tested. This conclusion agrees with that drawn above on the basis of other criteria.

The dependence of  $\psi$  on the Euler number  $Eu_m$  (Fig. 5) can be established from the measured values of the head loss, where  $Eu_m = \Delta p \epsilon^2 / HS_g \rho W_0^2$ ;  $W_0$  is the gas velocity in the calculation at an empty cross section of the assembly;  $\rho$ , density of the gas in  $\text{kg} \cdot \text{sec}^2/\text{m}^4$ ; and  $S_g$ , specific surface of the spheres in  $\text{m}^2/\text{m}^3$ .

The results of the investigation can be used to develop computational procedures. It is necessary to take account of the fact that the maximum increase in the velocity of the gas flow, and therefore the greatest heat removal from spherical fuel elements, is most probable near the assembly walls, and that the greatest overheating of the spheres occurs in the central part of the assembly, where there is the largest number of points at which the local velocity is below the average velocity of the gas through the apparatus. The experimental apparatus for  $\alpha = 4^\circ$  ensures the best gas distribution in a layer of spheres as compared with similar reactor assemblies, but without tapering headers, of the type described in [8].

## LITERATURE CITED

1. E. K. Popov, "Investigation of aerodynamic nonuniformities in reactors with a fixed layer of catalyst," Dissertation, Scientific-Research Institute of Synthetic Rubber Monomers, Yaroslavl' (1980).
2. R. G. Bogoyavlenskii, Hydrodynamics and Heat Transfer in High-Temperature Nuclear Reactors with Spherical Fuel Elements [in Russian], Atomizdat, Moscow (1978).
3. V. Staněk and V. Eckert, Chem. Eng. Sci., 34, 933 (1979).
4. J. Marivoet, P. Teodoroiu, and S. Wajc, Chem. Eng. Sci., 29, 1836 (1974).
5. A. S. Puschnow (Pushnov), A. M. Kagan, and I. I. Gel'perin, Khim. Promst, No. 10, 39 (1980).
6. A. Puschnow, Ideen des exakten Wissens, No. 10, 620 (1973).
7. A. S. Puschnow (Pushnov) et al., in: Proc. State Univ. of the Nitrogen Industry No. 57 [in Russian], (1980), p. 130.
8. G. K. Kvashilava et al., "Problems of atomic science and technology," Ser. Atomno-Vodorodnaya Energetika i Tekhnologiya, No. 2 (7), 136 (1980).

# A NONDESTRUCTIVE METHOD OF DETERMINING THE Pu/U RATIO IN FAST REACTOR FUEL ELEMENTS, BASED ON X-RAY SPECTROMETRY

A. V. Bushuev, V. I. Galkov, A. V. Zbonarev,  
A. F. Zolotov, A. A. Kutuzov,  
N. A. Mel'nichenko, V. N. Ozerkov,  
and V. V. Chachin

UDC 621.039.516.22

The bulk analysis of the element composition of spent fuel in the conditions existing at nuclear power stations is possible only on the basis of simple low labor-consuming methods, which provide acceptable accuracy for small time intervals. From this point of view, the methods of  $\gamma$ - and x-ray spectrometry are promising, the advantages of which increase in proportion with the improvement of detectors and analyzing equipment.

In the present paper, the problems for determining the ratio of Pu/U in fast reactor spent fuel elements are considered by recording the x radiation excited by fission product radiation. After a preliminary analysis, it was established that the  $K_{\alpha_1}$  lines of uranium ( $E = 98.43$  keV) and plutonium ( $E = 103$  and  $7$  keV) are the most promising [1]. A spectrometric system is necessary for their observation, with an energy resolution in the stated energy range of not more than 600-700 eV.

X-ray semiconductor spectrometers satisfy these requirements. Ge (Li) spectrometers were used for the measurements, with a beryllium inlet window and with a cooled first cascade of the preamplifier. The experiments were conducted with spent fuel elements from a fast reactor core. The fuel was uranium dioxide and the cladding was stainless steel with a thickness of 0.15 mm. The fuel elements were placed on a carriage, which moved by means of an automated system. The radiation from the fuel element entered the detector through a collimating system.

When measuring the radiation spectra of the fuel elements in the energy range 90-140 keV, it was established that the lines of the characteristic x radiation of uranium and pluto-

Translated from Atomnaya Energiya, Vol. 53, No. 5, pp. 322-323, November, 1982. Original article submitted April 27, 1981.

Declassified and Approved For Release 2013/03/04 : CIA-RDP10-02196R000300010005-6  
 nium can be distinguished in the total spectrum. The sources of excitation of the x radiation are the fission product  $\gamma$  quanta. The contribution of other sources, as estimates show, can be neglected [2]. The number of x-ray quanta of the  $i$ -th element  $I_i$  is related with the content of this element in the sample  $N_i$ , the K-radiation functions  $W_i^K$ , and its yield  $w_i^K$ , by the following relation:

$$I_i = N_i W_i^K w_i^K.$$

The excitation function can be written in the form of the product of the photoeffect cross section in the K shell  $\sigma_\Phi(E)$  and the  $\gamma$ -quanta flux  $\Phi_\gamma(E)$  ( $E_K^1$  is the photoeffect threshold)

$$W_i^K = \int_{E_K^1}^{\infty} \sigma_\Phi^i(E) \Phi_\gamma(E) dE.$$

Taking account of the dependence of the photoeffect cross section on the  $\gamma$ -quanta energy, we finally obtain

$$\frac{N_{Pu}}{N_U} = \frac{I_{Pu}}{I_U} \left( \frac{Z_U}{Z_{Pu}} \right)^5 \left[ 1 + \frac{\int_{E_K^U}^{E_K^{Pu}} [\Phi_\gamma(E)/E^3] dE}{\int_{E_K^{Pu}}^{\infty} [\Phi_\gamma(E)/E^3] dE} \right] \frac{w_U^K}{w_{Pu}^K}.$$

In order to evaluate the ratio of the integrals, it is necessary to know the  $\gamma$ -emission spectrum of the fission products  $N_\gamma(E_\gamma)$  in the region of high values of  $E_K^U$ . In order to construct the actual spectrum  $N'_\gamma(E_\gamma)$  from the measured spectrum, it is necessary to introduce a correction for the self-absorption of the  $\gamma$  radiation, and to take account of the change of efficiency in recording the quanta as a function of their energy. By using the corrected spectrum  $N'_\gamma(E_\gamma)$  and the summed values of  $N'_\gamma(E)/E^3$  in the range up to 300 keV, the following value was obtained for the ratio  $W_U/W_{Pu}$  for the samples investigated:

$$\frac{W_U}{W_{Pu}} = \left( \frac{Z_U}{Z_{Pu}} \right)^5 [1 + (0.040 \pm 0.004)].$$

The following factors can influence the measurement results:

1. Inadequate distribution of uranium and plutonium along the radius of the fuel element. This effect depends on the neutron spectrum in the reactor and the diameter of the fuel element. In consequence of the low effective cross section of the  $^{238}\text{U}(n, \gamma)$  reaction in the core of the fast reactor, and the small diameter of the fuel element, the plutonium is distributed uniformly along the radius of the fuel elements from the reactor core.

2. The different absorption coefficients of the  $K_{\alpha_1}$  x-ray quanta of uranium and plutonium are the reason for the slight difference in the probability of their absorption within the fuel elements and in the efficiency of recording these quanta with the detector. The total influence of these effects on the result of measuring the relative intensity of the  $K_{\alpha_1}$  and  $K_{\alpha_2}$  x-ray lines of uranium was investigated. The value obtained experimentally differed from the theoretical value by 0.5%, for an energy difference of 3.8 keV. As the energy differences of the  $K_{\alpha_1}$  lines of uranium and plutonium is equal to 5.2 keV, it can be expected that the correction does not exceed 1%. The reason for such a low value is the mutual compensation of these effects, as both the self-absorption and recording efficiency are reduced with increase of the radiation energy.

The proposed method was tested practically by carrying out a number of experiments with fast reactor fuel elements. The values of the Pu/U ratio obtained, averaged over the height of the fuel elements, coincided within the limits of the measurement error with the data of gravimetric determinations.

Thus, the possibility is shown for discriminating the x-ray emission lines of plutonium and uranium in the emission spectrum of spent fuel elements by means of a Ge (Li) spectrom-

Declassified and Approved For Release 2013/03/04 : CIA-RDP10-02196R000300010005-6

eter. The accuracy in determining the Pu/U ratio by the method of recording the x-ray emission is estimated. With a deep fuel burnup of  $\sim 4\%$ , the accuracy of the analysis can attain 3%. The time expenditure for this amounts to 5-10 h. The analysis time can be shortened by a factor of 5-10 with the increase of the transmission power of the measurement circuit (in the experiments described, the total loading did not exceed 2 kHz, and it is possible to increase it to 10 kHz) and an increase of the energy resolution (for the best Soviet spectrometers it attains 450-500 eV for  $E_\gamma = 122$  keV). The reliability of the data is confirmed by comparison with the results of gravimetric determination. The procedure for the nondestructive determination of plutonium buildup in fast reactor fuel elements has been developed and tested.

#### LITERATURE CITED

1. Kh. Bote et al., in: Proceedings of the Fourth COMECON Symposium "Investigations in the Field of Spent Fuel Reprocessing," Report KV 77/A9 [in Russian], Czechoslovakia (1977).
2. T. Vol'dset, Applied X-ray Spectrometry [in Russian], Atomizdat, Moscow (1977).

#### CALCULATION OF ENERGY LIBERATION IN THE LOOP CHANNELS BY THE MONTE CARLO METHOD

V. A. Antonov, F. M. Arinkin,  
G. A. Batyrbekov, A. A. Blyskavka,  
V. V. Sinyavskii, and Yu. A. Sobolev

UDC 621.039.134

In testing the loop channels (LC) in experimental reactors, it is important to know the absolute value of the heat liberation in the fuel composition of the LC. This question becomes especially critical in testing fuel elements in a reactor, where several independent experiments are being performed at once and the power level of the reactor cannot be established arbitrarily. In this case, the LC construction must be developed so that at a given power level the required heat liberation in the LC is ensured.

Calculation of the heat liberation is associated with certain difficulties. The presence in the LC structure of absorbing screens, moderators, and fissile materials, and also the clearly expressed heterogeneity over the radius and height of the channel, necessitates the neutron-physics calculation of a reactor with LC in three-dimensional geometry, with precise separation of its basic elements and the use of a sufficiently high approximation of the transport equation. These requirements may be most completely satisfied using the Monte Carlo method. At present, a library of modules for reactor calculation by the Monte Carlo method has been developed [1], allowing a program for the calculation of the given reactor composition to be assembled, by special programming means, from individual modules [2]. In particular, the library includes modules by means of which a program for the calculation of a reactor with "cylinder-in-cylinder" geometry (a geometric structure of the reactor consisting of a set of parallel cylinders of identical height, enclosed by a cylinder of larger radius) may be obtained. The volume of each cylinder, after the removal of the cylinders which it contains, may be filled by a material which is inhomogeneous over the height. The boundaries of the homogeneous volumes are planar and are parallel to the end-plane of the cylinder.

The neutron trajectories in this geometry are modeled in a multigroup transport approximation using the BNAB system of constants [3]. It is assumed that the elastic scattering on all nuclei except hydrogen is isotropic in the laboratory coordinate system, but the cross section of such scattering is replaced by the "corrected transport" cross section [3]. The elastic cross section for hydrogen is accurately modeled within the framework of the group approximation. Inelastic scattering is assumed to be isotropic in the laboratory coordinate system.

---

Translated from Atomnaya Énergiya, Vol. 53, No. 5, pp. 323-324, November, 1982. Original article submitted July 14, 1981; revision submitted January 25, 1982.

Reactor characteristics such as  $K_{ef}$ , the mean value of the sources of secondary fission neutrons, and the group-mean neutron fluxes in individual regions of the reactor are also calculated. Because of the small volume of the operative memory of the computer, the statistical error is only calculated for  $K_{ef}$  (for the results below,  $\Delta K_{ef} = 0.03$ ). The parameters of the neutrons from the source are chosen by the generation method.

To calculate the heat liberation, the value of the source functional of the secondary fission neutrons is used, with the analytic expression

$$Q_l = \int_{V_l} \int \int v_f(E) \Sigma_f(r, E) \Phi(r, E, \Omega) dr dE d\Omega, \quad (1)$$

where all the notation is conventional, and integration is taken over the volume  $V_l$ . To calculate this functional in the program, estimation from the collision density is used

$$Q_l = \frac{1}{nT} \sum_j \sum_{i=1}^T \sum_m \left( \frac{\bar{v}_f \Sigma_f}{\Sigma_t} \right)_{j,i,m}. \quad (2)$$

Here  $n$  is the number of generations;  $T$ , number of neutrons in the generations;  $j$ , running number of the  $n$ -th generation;  $i$ , running number of neutrons in the  $j$ -th generation;  $m$ , running number of neutron collisions; and  $\Sigma_t \Sigma_f$ , group-mean total cross section of interaction and fission. The summation is taken within the limits of the  $l$ -th homogeneous zone. The normalization of the mean values of the fission-neutron sources takes the form

$$C_l = \frac{Q_l/V_l}{\sum_{a,z} Q_l/V_{a,z}}. \quad (3)$$

Multiplying and dividing Eq. (3) by  $k\bar{v}_f^{a,z}$  an expression expedient for calculating the specific energy liberation is obtained

$$C_l = \frac{Q_l/V_l k\bar{v}_f^{a,z}}{\sum_{a,z} Q_l/V_{a,z} k\bar{v}_f^{a,z}} = \frac{q_V^{(l)}}{A_0}, \quad (4)$$

where  $k$  is the number of fissions corresponding to a 1-W thermal power of the reactor;  $V_{a,z}$ , volume of all the zones containing fissile material;  $\bar{v}^{a,z}$ , mean yield of secondary neutrons in one fission event over all the zones containing fissile material;  $q_V^{(l)}$ , mean specific heat liberation in the volume  $V_l$ ;  $A_0$ , mean specific heat liberation for all zones containing material with a 1-MW reactor power. In water-water reactors, the main contribution to the heat liberation in fissile zones is that of neutrons of thermal and intermediate energy. The contribution to the heat liberation from fissile  $^{235}\text{U}$  nuclei is very small, and therefore the value of  $\bar{v}_f^{a,z}$  is known sufficiently accurately.

The heat liberation was calculated per 1 MW of thermal power of the reactor, i.e.,  $\Sigma Q_l / k\bar{v}_f^{a,z} = 10^6$  W. As a result, the specific energy liberation in the  $l$ -th zone is calculated as follows:

$$A_0 C = q_V, \text{ W}/(\text{cm}^3 \cdot \text{MW}),$$

where

$$A_0 = 10^6 / V_{a,z}, \text{ W}/\text{cm}^3.$$

Calculations of the heat liberation by the given method allow the contribution to the total heat liberation coming only from the reaction  $(n, f)$  to be determined; the contribution from neutron moderation and  $\gamma$  quanta is not taken into account. In the neutron-physics calculation, neutron thermalization is also not taken into account. The calculations are performed for two loop channels. The following mean values of  $q_V$  over the whole sample are obtained:

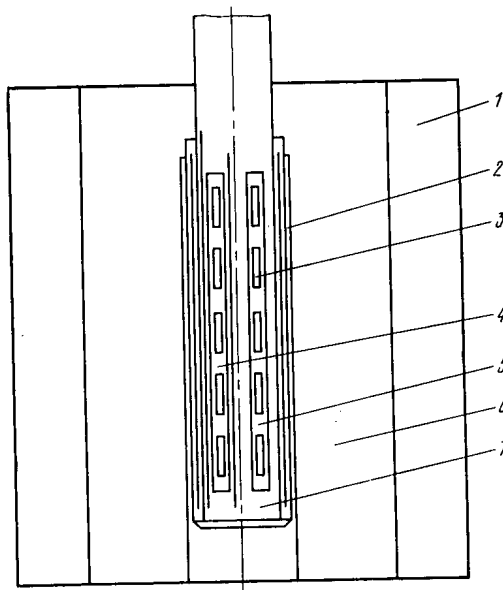


Fig. 1. Diagram of the mock-up position in the active zone: 1) Lateral reflector of the reactor; 2) external absorbing screen of boron carbide; 3) calorimetric detectors; 4) internal absorbing screen; 5) ampul with samples; 6) active zone of the reactor; 7) physical model.

In the case of ampuls with an outer screen, 45.0 (calculation) and 58.3 (experiment); for ampuls with an inner and outer screen, 29.5 (calculation) and 34.8 (experiment). Up to 100,000 histories are considered in order to obtain sufficient accuracy; the length of the mean history (depending on the geometric dimensions of the calculated ensemble and its composition) in this case is 0.31 sec, and the number of generations is 200.

Investigations with two physical mock-ups of the LC were performed for experimental verification of the effectiveness of the mathematical model. Energy liberation in the samples was measured by thermodivergator-calorimeters [4]. A diagram of the positioning of the mock-up in the active zone of a VVR-K reactor is shown in Fig. 1.

An external absorbing screen containing boron carbide with a natural isotopic mixture is attached to the body of the mock-up. At the center of the mock-up, ampuls with samples of fuel composition (uranium dioxide of 90% enrichment) are placed; an additional internal screen of boron anhydride is placed in one of the ampuls. The samples are placed at 68-mm intervals over the height of the ampuls, symmetrically with respect to the center of the active zone.

As is known, the heat liberation from the  $(n, f)$  reaction and the  $\gamma$  component of the reactor radiation are determined by the calorimeter. For comparison with the results of the calculation, it is necessary to isolate the component of the  $\gamma$  radiation, which is calculated by the method described in [5], in the physical measurements.

The basic contribution to the discrepancy of the calculation from the experimental data comes from the error in the experimental data, the statistical error in the results of the calculation, and the error due to neglecting neutron thermalization in the calculation. How the influence of neutron thermalization is taken into account may be verified by specifying the macroscopic constants of the thermal group obtained by particular methods.

Comparison of the calculated and experimental values of  $q_\gamma$  shows that they are in satisfactory agreement, and the method of calculation may be recommended for determining the heat liberation in experimental reactor devices having high gradients of the neutron field in the case of heterogeneity of the construction. The total heat liberation in the fuel composition of the LC may be obtained on the basis of the results of calculated and experimental values of the spectral parameter of the reactor  $\gamma$  radiation.

## LITERATURE CITED

1. V. G. Zolotukhin et al., in: Collection of Papers on Programs and Methods of Calculation of Fast Reactors [in Russian], Dmitrovgrad (1975), p. 255.
2. A. A. Blyskavka, Preprint FEI-79 [in Russian], Obninsk (1976).
3. L. P. Abagyan et al., Group Constants for Nuclear-Reactor Calculation [in Russian], Atomizdat, Moscow (1964).
4. Yu. A. Tsoglin et al., in: Proceedings of the Second Coordinational Conference on High-Dose Dosimetry [in Russian], Fan, Tashkent (1966). p. 70.
5. Yu. L. Tsoglin and S. S. Ogorodnik, At. Energ., 38, No. 2, 96 (1975).

INVESTIGATION OF THE STRUCTURE OF Kh18N10T  
STAINLESS STEEL, IRRADIATED WITH FAST NEUTRONS  
AT A TEMPERATURE OF 300°C

Sh. Sh. Ibragimov, V. F. Reutov,  
S. P. Vagin, and B. D. Utkelbaev

UDC 621.039.531

From experiments on prolonged annealing, it is well-known that stainless austenitic steels are metastable at a quite high temperature [1]. The action of neutron irradiation also leads to the appearance of new phases which are absent after normal heat treatment [2, 3]. As a result of this, the main bulk of experimental results has been obtained at an irradiation temperature exceeding 400°C [4, 5]. However, there is a definite interest in the results of a study of the structure of austenitic steels subjected to irradiation by neutrons up to high fluence values ( $\sim 10^{26}$  neutrons/m<sup>2</sup>) at a lower irradiation temperature.

For this purpose, an electron-microscopic investigation of the structure of Kh18N10T stainless austenitic steel, irradiated with fast neutrons up to a fluence of  $5.8 \cdot 10^{26}$  neutrons/m<sup>2</sup> ( $E > 0.1$  MeV) at a temperature of  $\sim 300^\circ\text{C}$ , was carried out. The corresponding level of damage amounted to 33 displacements/atom. Samples of Kh18N10T steel were used as the subjects for the investigation, austenitically treated at 1500°C during 30 min, from which regular sheaths were prepared for the fuel elements of the BN-350 reactor. For comparison, unirradiated samples were also studied, together with the irradiated samples, and were subjected to the same thermochemical treatment.

During the investigation of the structure of the unirradiated samples, the presence of irregular buildups of dissociations and also of packing defects of small concentration, and

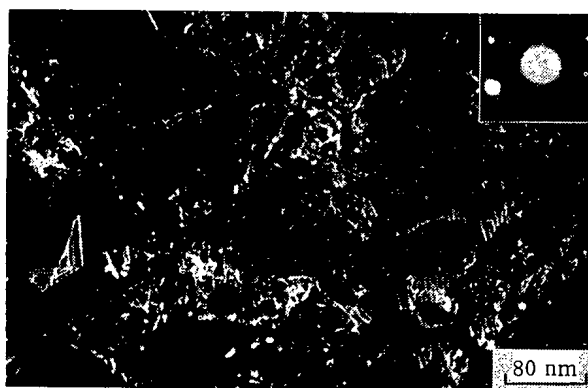


Fig. 1. Dark-field image of the original structure of Kh18N10T austenitic stainless steel with  $\bar{g} = (131)$ .

Translated from Atomnaya Énergiya, Vol. 53, pp. 324-325, November, 1982. Original article submitted September 25, 1981.

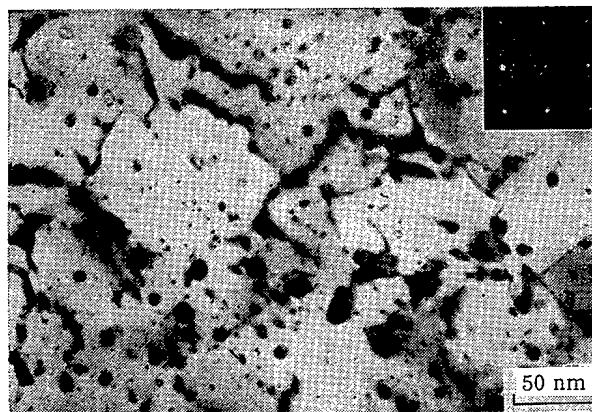


Fig. 2. Light-field image of the structure of Kh18N10T austenitic stainless steel, irradiated by fast neutrons up to a fluence of  $5.8 \cdot 10^{26}$  neutrons/m<sup>2</sup> ( $E > 0.1$  MeV) at a temperature of  $\sim 300^\circ\text{C}$  (axis of zone [001]).

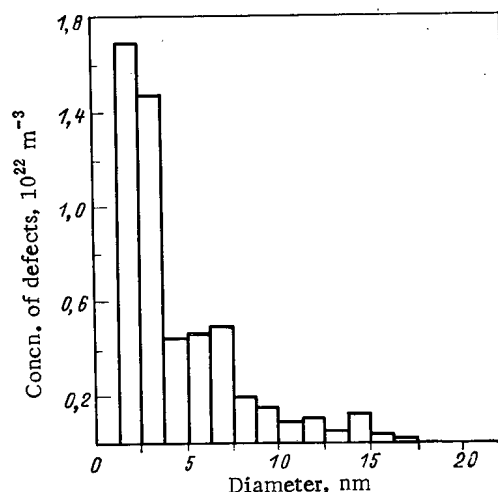


Fig. 3. Histogram of the distribution of finely dispersed formations in Kh18N10T austenitic stainless steel, irradiated with fast neutrons up to a fluence of  $5.8 \cdot 10^{26}$  neutrons/m<sup>2</sup> ( $E > 0.1$  MeV) at a temperature of  $\sim 300^\circ\text{C}$ .

of segregations of different size from those usually present in steels of this type, was revealed in them (Fig. 1).

The irradiated steel samples are characterized by an increased (in relation to the original sample) dislocation structure, forming a "dislocation forest." In addition to this, a high concentration ( $6 \cdot 10^{22} \text{ m}^{-3}$ ) of finely dispersed formations is observed, with sizes from 1 to 17.5 nm, uniformly distributed throughout the body of the grain (Fig. 2). From the histogram of the distribution of these formations with respect to size (Fig. 3), it can be seen that their size is mainly  $< 4$  nm. As a result of this, the accumulation of similar defects does not create additional reflections on the electronogram (see Fig. 2). When studying the nature of the images of the formations being investigated in different diffraction conditions, it was established that, firstly, they all have a moiré striated contrast; secondly, in the twin-beam dynamic conditions, they do not form a black-white contrast, which is characteristic for the buildup of these radiation defects. This allows the conclusion that the observed finely dispersed formations represent segregations. In this connection, by means of the D-2-1/2 procedure [6], the presence among them of phases of the types "injection" and "subtraction" was established.

After annealing the samples in the range 500-700°C, it was found that the concentrations and sizes of the finely dispersed segregations were markedly reduced with increase of the annealing temperature and, primarily, the segregations with a size of up to 4 nm disappeared. This disappearance of the segregations without the formation of dislocation loops or the accumulations of dislocations confirms once again that these segregations cannot be considered as accumulations of radiation defects.

## LITERATURE CITED

1. B. Weis and R. Stikler, *Met. Trans.*, 3, 851 (1972).
2. H. Branger and J. Straalsund, *J. Nucl. Mater.*, 46, 134.
3. E. Bloom and J. Sriegler, *ASTM-STR-529*, p. 360 (1973).
4. H. Branger and F. Garner, *J. Nucl. Mater.*, 73, No. 1, 9 (1978).
5. E. Lee, A. Rowcliffe, and E. Kenik, *J. Nucl. Mater.*, 83, No. 1, 79 (1979).
6. W. Bell, *J. Appl. Phys.*, 47, 1677 (1976).

# NEW CLASS OF BOUNDARY INTEGRAL EQUATIONS OF NEUTRON-TRANSPORT THEORY

B. D. Abramov

UDC 519.9:621.039.51.12

The solution of boundary problems for integrodifferential equations of neutron transport in media with piecewise-constant (with respect to the spatial coordinate) cross sections, as is known [1, 2], may be reduced to the solution of linear boundary integral equations (BIE), with subsequent recovery of the neutron flux density with the given homogeneous zones according to any analytic formula. This is the essence of the BIE method.

At present, two main classes of linear BIE are known: integral equations of Fredholm type, the core of which consists of fundamental solutions (Green's functions) of the corresponding transport equations, and singular integral equations. In the present work, the existence of a new class of BIE, which are also integral equations of Fredholm type but have cores of a simpler structure, is established. For example, for problems consisting in the solution of the equation

$$\Omega \nabla \psi + \psi = \frac{c}{4\pi} \int d\Omega' \psi(x, \Omega') \quad (1)$$

in the convex region  $G \subset R_3$ , bounded by a piecewise-smooth surface  $\Gamma$  of class  $C^{(1)}$ , with a boundary condition on  $\Gamma$

$$\psi(x, \Omega) = f(x, \Omega), \quad \Omega n(x) < 0, \quad x \in \Gamma, \quad (2)$$

the corresponding new BIE may be written in the form

$$\int_{\Gamma} d\gamma' \Omega n(x') \psi(x', \Omega) D(x - x', \Omega) = \frac{c}{4\pi} \int d\Omega' \int_{\Gamma} d\gamma' \times \\ \times [\Omega n(x') \psi(x', \Omega) - \Omega' n(x') \psi(x', \Omega')] \int_0^{\infty} dt e^{-t} D(x - x' - \Omega' t, \Omega), \quad (3)$$

where  $D(x, \Omega) = e^{-(\Omega, x)} \delta(\alpha, x) \delta(\beta, x)$ ;  $\Omega, \alpha, \beta$  are mutually orthogonal unit vectors;  $n(x')$ , unit vector of the external normal to  $\Gamma$ ;  $f$ , known functions;  $\Omega n(x')$ ;  $(\Omega, x)$ ;  $(\alpha, x)$ ;  $(\beta, x)$ , scalar products of the corresponding vectors in  $R_3$ ;  $\delta(\alpha, x)$ ,  $\delta(\beta, x)$ , Dirac delta functions of the given scalar products; and  $\int_{\Gamma} d\gamma' \dots$ , integral over the surface  $\Gamma$ .

Translated from *Atomnaya Énergiya*, Vol. 53, No. 5, pp. 325-327, November, 1982. Original article submitted December 15, 1981.

Since at almost all  $x_0 \in \pi_\Omega$  and  $x \in \Gamma$  such that  $\Omega n(x) > 0$

$$\int_{\Gamma} d\gamma' \Omega n(x') \psi(x', \Omega) D(x-x', \Omega) = \\ = \psi(x_0 + \Omega t_0, \Omega) - f(x_0 + \Omega t_0, \Omega) e^{-(t^0 - t_0)}, \quad (4)$$

where  $\pi_\Omega, x_0$  are orthogonal projections of the region  $G$  and the vector  $x$  on the plane  $(\Omega, x) = 0$ , and, at given  $x_0 \in \pi_\Omega$  the points  $t^0, t_0, t^0 > t_0$  are points of intersection of  $\Gamma$  with the straight line  $x_0 + \Omega t, -\infty < t < \infty$ , then, rewriting the right-hand side of Eq. (3) in the form

$$\frac{c}{4\pi} \int_{\Gamma} d\gamma' \int_{-\infty}^{\infty} dp \frac{\exp(-p - |x-x'-\Omega p|)}{|x-x'-\Omega p|^2} \times \\ \times [\Omega n(x') \psi(x', \Omega) - \omega n(x') \psi(x', \omega)], \quad (5)$$

where  $\omega = (x - x' - \Omega p) / |x - x' - \Omega p|$ , it may be shown that the BIE in Eqs. (3) and (2) is an integral equation of the second kind for the functions  $\psi(x, \Omega), \Omega n(x) > 0, x \in \Gamma$ .

Explicit solution of Eq. (1) from a sufficiently broad class of functions including the solution of the initial boundary problem in Eqs. (1) and (2), evidently satisfies Eq. (3). This follows, in particular, from the relation

$$\int_{\Gamma} d\gamma' \Omega n(x') \psi(x', \Omega) D(x-x', \Omega) = \int_G dx' [\Omega \nabla \psi(x', \Omega) + \psi(x', \Omega)] D(x-x', \Omega); \\ \int d\Omega' \int_{\Gamma} d\gamma' \Omega' n(x') \psi(x', \Omega') \int_0^{\infty} dt e^{-t} D(x-x'-\Omega' t, \Omega) = \\ = - \int d\Omega' \int_G dx' \psi(x', \Omega') D(x-x', \Omega) + \\ + \int d\Omega' \int_G dx' [\Omega' \nabla \psi(x', \Omega') + \psi(x', \Omega')] \int_0^{\infty} dt e^{-t} D(x-x'-\Omega' t, \Omega); \\ \int d\Omega' \int_{\Gamma} d\gamma' \Omega' n(x') \psi(x', \Omega') \int_0^{\infty} dt e^{-t} D(x-x'-\Omega' t, \Omega) = \\ = \int d\Omega' \int_G dx' [\Omega' \nabla \psi(x', \Omega') + \psi(x', \Omega')] \int_0^{\infty} dt e^{-t} D(x-x'-\Omega' t, \Omega), \quad (6)$$

which is a generalization of the Ostrogradskii-Gauss formula, taking account of equations of the type  $\Omega \nabla \delta(\alpha, x) = (\Omega, \alpha) \delta^{(1)}(\alpha, x) = 0$  for  $(\Omega, \alpha) = 0$ , and the identity

$$\delta(\alpha, x-x'-\Omega' t) \delta(\beta, x-x'-\Omega' t) = \\ = \int_{-\infty}^{\infty} dp \delta[t - (\Omega', x-x'-\Omega p)] \delta(\alpha', x-x'-\Omega p) \delta(\beta', x-x'-\Omega p), \quad (7)$$

where  $\alpha', \beta'$  are such that  $(\Omega', \alpha') = (\Omega', \beta') = (\alpha', \beta') = 0, |\alpha'| = |\beta'| = 1$ .

It may be shown, further, in the class of functions written in the following form for  $x \in \Gamma, \Omega n(x) > 0$

$$\psi(x, \Omega) = \int_G dx' \mathcal{E}(x-x', \Omega) Q(x') - \int_{\Gamma} d\gamma' \Omega n(x') f(x', \Omega) \mathcal{E}(x-x', \Omega), \quad (8)$$

where  $Q$  is some function summed in  $G$ ;  $\mathcal{E}(x, \Omega) = e^{-(\Omega, x)} \theta(\Omega, x) \delta(\alpha, x) \delta(\beta, x)$ , solution of the equation  $\Omega \nabla \mathcal{E} + \mathcal{E} = \delta(x)$ ; and  $\theta$  unit Heaviside step function; that the BIE in Eqs. (3) and (2) does not have a solution differing from the corresponding limiting values of the solution of the problem in Eqs. (1) and (2) on the surface  $\Gamma$ .

In fact, noting that if  $Q$  is the solution of the Peierls equation

$$P[Q](x) \equiv Q(x) - \frac{c}{4\pi} \int_G d\Omega \int dx' \mathcal{E}(x-x', \Omega) Q(x') + \int_G d\Omega \int_{\Gamma} d\gamma' \Omega_n(x') f(x', \Omega) \mathcal{E}(x-x', \Omega) = 0, \quad (9)$$

then  $Q(x) = (c/4\pi) \int d\Omega \psi(x, \Omega)$ , while Eq. (8) is the solution of the problem in Eqs. (1) and (2),

Eq. (8) is substituted into Eq. (3), taking account of Eq. (6). The result is  $\int_G dx' D(x-x', \Omega)$

$$P[Q](x') = 0. \text{ Since for } x \in \Gamma, \text{ such that } \Omega_n(x) > 0, \int_G dx' D(x-x', \Omega), P[Q](x') = \int_G dx' \mathcal{E}(x-x', \Omega) P[Q](x'),$$

it is readily evident that all the solutions of the subsequent equation differing from the Peierls equations are equal to zero on substitution into Eq. (8) for  $\psi(x, \Omega), \Omega_n(x) > 0, x \in \Gamma$ , which is what was required.

Note that in the spaces  $L_p(\Gamma)$  the functions  $\psi$  with the norm  $\|\psi\|_p = \left\{ \int_G d\Omega \int_{\Gamma} d\gamma \Omega_n(x) |\Omega_n(x)| |\psi(x, \Omega)|^p \right\}^{1/p}$ ,  $1 \leq p < \infty$ , the BIE in Eqs. (3) and (2) are uniquely solvable if, say,  $2cde' < 1$ , where  $d$  is the diameter of region  $G$ .

The BIE in Eqs. (3) and (2) and analogous BIE for more complex problems may be derived, e.g., from the corresponding equations of [2]. In particular, the BIE in Eqs. (3) and (2) are equivalent to Eq. (3) with the conditions in Eqs. (2a) and (2b) of [2]. They allow the neutron flux at the boundaries of the homogeneous zones and at the external surface to be determined without solving the corresponding transport equations inside the given zones, and may be used to construct new numerical schemes of the BIE method.

#### LITERATURE CITED

1. Yu. I. Ershov and S. B. Shikhov, Methods of Solving Boundary Problems of Transport Theory [in Russian], Atomizdat, Moscow (1977).
2. B. D. Abramov, At. Energ., 41, No. 3, 198 (1976).

#### INFLUENCE OF RADIATION HISTORY ON THE SWELLING OF STEEL

N. A. Demin and Yu. V. Konobeev

UDC 621.039.548.34

The large scatter observed in data on the radiational swelling of austenitic stainless steels may be associated with the radiation history, together with the influence of other factors, e.g., variations in composition, thermomechanical treatment, and the dependence of the swelling on neutron flux density. The final swelling of the steel in a fast reactor may depend especially strongly on the preliminary irradiation at reduced temperature up to small fluxes, at which a high concentration of sinks for point defects in the form of small pores and dislocational loops appears in the material. This is indicated by the reactor data of [1], and also by imitational experiments on the irradiation of stainless steel by electrons in a high-voltage microscope. According to these experiments, the temperature curve of swelling is shifted toward lower temperatures as a result of "seeding" the pores in preliminary irradiation up to a small flux at low temperature [2]. There are interesting results on the modeling of preliminary low-temperature irradiation on the basis of a theoretical model allowing the kinetics of pore formation in austenitic stainless steel irradiated in a fast reactor up to 72 shifts/atom to be satisfactorily described [3]. Calculations were performed for a rate of damage creation  $K = 10^{-6}$  shifts/atom·sec. Two sets of irradiation conditions were considered, as follows:

- 1) "Seeding" the pores at temperatures of 400 and 500°C by irradiation to 5 shifts/atom, with subsequent irradiation at a temperature of 400-700°C to a total damage of 70 shifts/atom;

Translated from Atomnaya Energiya, Vol. 53, No. 5, pp. 327-328, November, 1982. Original article submitted January 11, 1982.

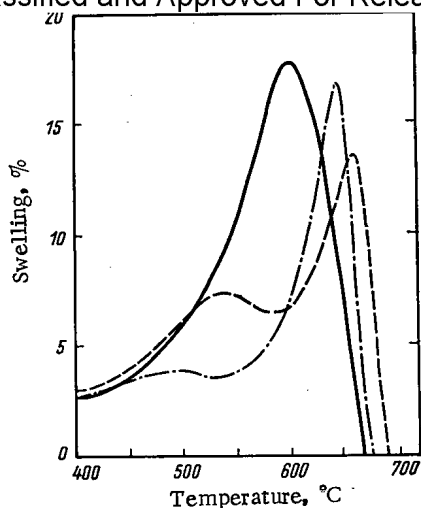


Fig. 1

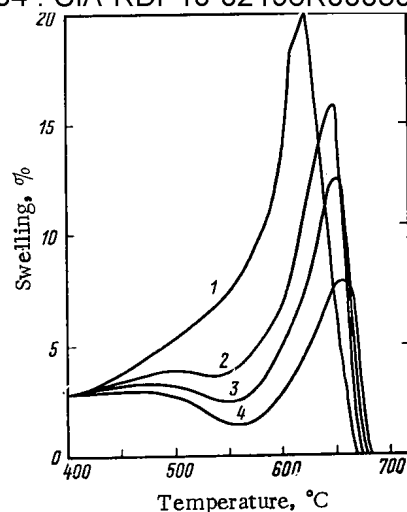


Fig. 2

Fig. 1. Temperature dependence of the swelling of austenitic stainless steel in the initial annealed state according to the predictions of the theoretical model. The total defect-forming dose was 70 shifts/atom; the solid curve corresponds to irradiation in constant conditions and the dash-dot and dashed curves to preliminary irradiation by a dose of 5 shifts/atom at 400 and 500°C, respectively.

Fig. 2. Calculated temperature dependence of the swelling of austenitic stainless steel at a total dose of 70 shifts/atom, of which doses of 1, 5, 10, and 30 shifts/atom are accumulated by preliminary irradiation.

2) irradiation at 400°C to 1, 5, 10, and 20 shifts/atom, and then at temperatures of 400–700°C up to a total damage of 70 shifts/atom.

A total damage of 70 shifts/atom was chosen for two reasons — with a view to comparing the results of calculation with experimental data [4] on the swelling of steel 316 in the annealed state, and because the process of pore coagulation plays no significant part at a damage of 70 shifts/atom. (This process was ignored in [3].) The results of calculating the temperature curves of swelling for conditions 1 and 2 are shown in Figs. 1 and 2.

It is evident from Fig. 1 that "seeding" the pores at low temperature leads to a shift in the temperature curve of swelling toward higher temperatures. The swelling is reduced in the range 500–600°C and the temperature dependence is "smoothed," which may facilitate the stability of the geometric dimensions and form of parts of the fast-reactor active region. This is explained in that the vacancy pores formed as a result of low-temperature "seeding" partially dissolve during the subsequent irradiation at higher temperature. The effect is especially clearly expressed in the case of "seeding" of pores at 400°C. The optimal dose of preliminary irradiation at 400°C was found by calculations for the second set of irradiation conditions (Fig. 2). It may be seen that there appears a minimum on the swelling curve in the region of ~550°C after preliminary irradiation to 5 shifts/atom; the depth of the minimum increases with a rise in preliminary dose. Since it is desirable to use material with a weak temperature dependence of swelling in order to avoid bending of the fuel-element casings in fast reactors, irradiation to 5 shifts/atom is optimum.

Thus, the theoretical model developed [3] predicts a fairly strong influence of preliminary low-temperature irradiation on the swelling of the stainless steel in the fast reactor. This permits the conclusion that the scatter of reactor data on the swelling of steels is partially explained by the different radiation history of samples in a fast reactor.

#### LITERATURE CITED

1. V. I. Shcherbak et al., *At. Énerg.*, **46**, No. 2, 91 (1979).
2. M. Makin, G. Walters, and A. Foreman, *J. Nucl. Mat.*, **95**, 155 (1980).

3. N. A. Demin and Yu. V. Konobeev, At. Energ., 48, No. 1, 20 (1980).
4. T. Kenfield, W. Appleby, and H. Busboom, J. Nucl. Mat., 75, 85 (1978).

# DETERMINING THE RELAXATION LENGTH OF A FLUX OF MODERATED AND THERMAL NEUTRONS ON THE BASIS OF THE $P_2$ APPROXIMATION

I. A. Kozachok and V. V. Kulik

UDC 621.039:5:53;  
550.832.53

In order to describe the spatial distribution of neutrons in protective materials and in geological and other media using the relaxation length, it is desirable to have analytical relations between this parameter and the neutron age, the diffusion length, and the asymptotic relaxation length. The corresponding calculation formulas for moderated (subthermal) and thermal neutrons may be obtained using the theory of the retardation and diffusion of neutrons based on the  $P_2$  approximation of the spherical harmonic method [1-4].

Consider a plane, isotropic, monoenergetic source in an infinite homogeneous medium. The expression for the retardation density of the neutrons in the given approximation takes the form [2]

$$q(z) = BK_0\left(\frac{R}{\Lambda_{as}}\right), \quad R = \sqrt{z^2 + R_0^2}, \quad B = \frac{1}{\pi\Lambda_{as}} e^{R_0/\Lambda_{as}}, \quad (1)$$

where  $K_0(x)$  is a Bessel function of imaginary argument;  $R_0 = 2\tau/\Lambda_{as}$ ;  $\tau = L_s^2 - \Lambda_{as}^2/2$ , variable of the type of the neutron age; and  $L_s$ , retardation length. As follows from the asymptotic form of the expression [1], the parameter  $\Lambda_{as}$  may be regarded as an asymptotic relaxation length of the moderated neutrons.

To calculate  $\Lambda_{as}$  and  $L_s$ , use is made of expressions obtained on the basis of the  $P_2$  approximation [3]

$$L_s^2 = \theta(u_0, u_1) + \frac{1}{2}[a(u_0)l_s^2(u_0) + a(u_1)l_s^2(u_1)]; \quad (2)$$

$$\Lambda_{as}^2 = 2[b(u_0)l_s^2(u_0) + b(u_1)l_s^2(u_1)]. \quad (3)$$

Here:  $\theta(u_0, u_1)$  is the Fermi age;  $u_0$  and  $u_1$ , initial and final lethargies;  $l_s(u)$ , free path length of the neutrons; and

$$a = \frac{1}{3\xi(1-\bar{\mu})} \left( \frac{\bar{\xi}^2}{\xi} - \frac{\Delta u \bar{\mu}}{1-\bar{\mu}} \right), \quad b = \frac{1}{3\xi(1-\bar{\mu})} \left( \frac{\bar{\xi}^2}{2\xi} - \frac{\Delta u \bar{\mu}}{1-\bar{\mu}} + \frac{8}{15} \frac{\xi}{1-\bar{\mu}^2} \right),$$

where  $\xi$  and  $\bar{\xi}^2$  are the mean change and mean square change in lethargy in one collision;  $\bar{\mu}$  and  $\bar{\mu}^2$ , mean cosine and mean square cosine of the scattering angle in the laboratory coordinate system; and  $\Delta u \bar{\mu}$ , mean value of the product of the change in lethargy and the cosine of the scattering angle.

The parameter  $b(u)$  depends relatively weakly on the composition of the medium and the neutron energy and is approximately equal to unity. Therefore, as follows from Eq. (3), a numerical estimate of  $\Lambda_{as}$  when  $l_s^2(u_1) \ll l_s^2(u_0)$  (which is usually the case for hydrogen-containing media) may be obtained from the expression

$$\Lambda_{as} \approx \sqrt{2} l_s(u_0). \quad (3a)$$

The result obtained using the  $P_2$  approximation for the distribution of thermal neutrons forming in the retardation of fast neutrons [2, 4] for the given source may be written in the form

Translated from Atomnaya Energiya, Vol. 53, No. 5, pp. 328-330, November, 1982. Original article submitted January 15, 1982.

$$\Phi_T(z) = \frac{1}{1+p_2} \left\{ \frac{1}{2\Sigma_a L} \int_{-\infty}^{\infty} e^{-\frac{|z-z'|}{L}} [1+\varepsilon(z')] q(z') dz' + \frac{p_2}{\Sigma_a} q(z) \right\}, \quad (4)$$

where

$$\varepsilon(z) = 2\Sigma_a L^2 \frac{\overline{\Delta u \mu l_s}}{(1-\mu) \xi \Lambda_{as}^2} \left[ 1 - \frac{R_0}{R} \frac{K_1(R/\Lambda_{as})}{K_0(R/\Lambda_{as})} \right];$$

$$p_2 = \frac{4}{5} \frac{\Sigma_a}{\Sigma_a + \frac{3}{2} (1-\mu^2) \Sigma_s};$$

$$L^2 = \frac{1+p_2}{3\Sigma_a \Sigma_{tr}}; \Sigma_{tr} = \Sigma_a + (1-\mu) \Sigma_s;$$

$L$  is the diffusion length of the neutrons;  $\Sigma_{tr}$ ,  $\Sigma_a$ , and  $\Sigma_s$  are macroscopic cross sections (transport, absorption, and scattering) of the thermal neutrons. The parameters of the moderated neutrons are taken at the "junction" energy  $E^*$  of the spectra of the moderated and thermal neutrons or, practically without loss in accuracy, at a value of the mean thermal neutron energy  $E = 0.025$  eV.

Analysis of Eq. (4) shows that the corrections introduced in the given approximation in the elementary theory of thermal neutron diffusion are usually small [2, 4]. The main influence on the accuracy of calculating the thermal neutron flux in the  $P_2$  approximation is exerted through the zero harmonic of the retardation density in Eq. (1), which plays the role of the thermal neutron source function in Eq. (4) at  $\varepsilon = p_2 = 0$ .

Setting the corrections  $\varepsilon$  and  $p_2$  equal to zero, the expression for  $\Phi_T(z)$  is written in the form

$$\Phi_T(z) = \frac{1}{2\Sigma_a L} \left\{ e^{-z/L} \int_0^{\infty} e^{z'/L} q(z') dz' + 2 \int_z^{\infty} \text{sh} \frac{z-z'}{L} q(z') dz' \right\}, \quad z \geq 0. \quad (5)$$

Depending on the characteristic dimensionless parameter  $\beta = L/\Lambda_{as}$ , it is easy to find asymptotic expressions that are expedient for analysis and calculation from Eq. (5)

$$\Phi_T(z) = \frac{B}{2\Sigma_a} \sqrt{\frac{\pi \Lambda_{as}}{2z}} e^{-\frac{z}{\Lambda_{as}}} \left[ 1 + \beta^2 \left( 1 + \frac{\Lambda_{as}}{z} + \frac{\Lambda_{as}^2}{2z^2} \right) \right]; \quad \beta^2 \ll 1; \quad z^2 \gg R_0^2; \quad (6)$$

$$\Phi_T(z) = \frac{BC}{2\Sigma_a} e^{-z/L} \left[ 1 - e^{-\frac{\beta-1}{L} z} F(\beta, z) \right]; \quad \beta > 1; \quad z^2 \gg R_0^2. \quad (7)$$

Here

$$C = \int_0^{\infty} e^{y^2} K_0 \left( \beta \sqrt{y^2 + \frac{R_0^2}{L^2}} \right) dy;$$

$$F(\beta, z) = \frac{\pi}{C \sqrt{2\beta}} \left[ \frac{f\left(\sqrt{\frac{\beta-1}{L}} z\right)}{\sqrt{\beta-1}} - \frac{f\left(\sqrt{\frac{\beta+1}{L}} z\right)}{\sqrt{\beta+1}} \right],$$

where  $f(x) = \sum_{n=1}^N a_n (1+px)^{-n}$  is an auxiliary function used in approximating the probability integral ( $a_n$ ,  $p$  are numerical values) [5].

Equations (6) and (7) have a clear physical meaning. The first is a particular case of the asymptotic expansion of  $\Phi_T$  in powers of  $\beta^2$

$$\Phi_T(z) = \frac{1}{\Sigma_a} q(z) \left\{ 1 + \beta^2 \left[ \frac{z^2}{R^2} \frac{K_2(R/\Lambda_{as})}{K_0(R/\Lambda_{as})} - \frac{\Lambda_{as}}{R} \frac{K_1(R/\Lambda_{as})}{K_0(R/\Lambda_{as})} \right] + \dots \right\}, \quad \beta < 1. \quad (8)$$

It shows that, when  $L < \Lambda_{as}$ , the attenuation of the thermal neutron flux is mainly determined by the distribution function in Eq. (1) for the moderated neutrons; as  $\beta \rightarrow 0$ , the distribution of thermal and moderated neutrons coincides, apart from the constants. It follows from Eq. (7) that when  $L > \Lambda_{as}$  the distribution function of neutrons from a purely thermal source plays the main role at large distances from the source; with increase in  $\beta$ , the relative contribution of the correction term determined by the distribution of moderated neutrons rapidly decreases.

The relaxation length of the neutron flux is determined, within the limits of a layer of thickness  $\Delta z = z_2 - z_1$ , by means of the measured or calculated neutron flux at the points  $z_1$  and  $z_2$ , in accordance with the formula [6]

$$\frac{1}{\lambda(z_1, z_2)} = \frac{1}{\Delta z} [\ln \Phi(z_1) - \ln \Phi(z_2)]. \quad (9)$$

Using Eq. (1), in which the function  $K_0(R/\Lambda_{as})$  is replaced by its asymptotic value  $\sqrt{\pi \Lambda_{as}/(2R)} e^{-R/\Lambda_{as}}$  (when  $R \gg 2\Lambda_{as}$ , the relative error of this substitution  $\delta \leq 4.2\%$ ) the following expression is obtained for the relaxation length of the moderated neutron flux

$$\frac{1}{\lambda_3(z_1, z_2)} = \frac{1}{\Delta z} \left( \frac{R_2 - R_1}{\Lambda_{as}} + \frac{1}{2} \ln \frac{R_2}{R_1} \right), \quad R_i = \sqrt{z_i^2 + R_0^2} \gg 2\Lambda_{as}. \quad (10)$$

When  $z_i^2 \gg R_0^2$ , Eq. (10) simplifies to give

$$\frac{1}{\lambda_3(z_1, z_2)} = \frac{1}{\Lambda_{as}} + \frac{1}{2\Delta z} \ln \frac{z_2}{z_1} \quad (11)$$

or

$$\frac{1}{\lambda_3(z)} = \frac{1}{\Lambda_{as}} + \frac{1}{2z}, \quad \frac{\Delta z}{z} \ll 1, \quad z \approx z_1.$$

It follows from Eq. (11) that, when  $z^2 \gg R_0^2$  and  $z \gg \Lambda_{as}/2$ , the relaxation length becomes independent of the distance to the source and represents the relaxation length  $\Lambda_{as}$ . According to Eq. (3), the latter is determined solely by the neutron properties of the moderator and the initial and final neutron energies. At a smaller distance from the source, as is evident from Eq. (10), the relaxation length depends also on  $z_1$ ,  $\Delta z$ , and the neutron age.

For the relaxation length of the thermal neutron flux when  $\beta < 1$  Eqs. (8) and (9) lead to the expression

$$\frac{1}{\lambda_T(z_1, z_2)} = \frac{1}{\lambda^*(z_1, z_2)} + \Delta_1(\beta, z_1, z_2), \quad (12)$$

where  $\lambda^*(z_1, z_2) \equiv \lambda_3(z_1, z_2)$  where  $u_1 = u(E^*)$ .

In Eq. (12), the relaxation length  $\lambda^*$  is determined by one of Eqs. (10) and (11), and the transverse dimension  $\Delta_1(\beta, z_1, z_2)$  by the corresponding value obtained from Eq. (8). For example, when  $R \gg 2\Lambda_{as}$ ,  $z^2 \gg R_0^2$ , and  $\beta^4 \ll 1$ , the relaxation length  $\lambda^*(z_1, z_2)$  is determined by the first formula in Eq. (11) and  $\Delta_1(\beta, z_1, z_2)$  by the expression

$$\Delta_1(\beta, z_1, z_2) = \frac{1}{\Delta z} \ln \frac{1 + \beta^2 \left( 1 + \frac{\Lambda_{as}}{z_1} + \frac{\Lambda_{as}^2}{2z_1^2} \right)}{1 + \beta^2 \left( 1 + \frac{\Lambda_{as}}{z_2} + \frac{\Lambda_{as}^2}{2z_2^2} \right)}. \quad (13)$$

When the condition  $\beta > 1$  is satisfied, the approximate expression for the relaxation length of the thermal neutron flux follows from Eqs. (7) and (9) and is different in character from Eq. (12):

$$\frac{1}{\lambda_T(z_1, z_2)} = \frac{1}{L} - \Delta_2(\beta, z_1, z_2), \quad (14)$$

where

TABLE 1. Relaxation Length of the Thermal Neutron Flux from a Planar Source in Water, cm

$E_0$ , MeV	$z_1, z_2$ , cm	Calculation from Eq.			Experimental value
		(12), (13)	(14), (15)	(5), (9)	
0.92	{ 20; 30	3,35	—	3,57	3,4
	{ 25; 35	3,37	—	3,50	3,4
1,0	{ 20; 30	—	3,44	3,16	3,0
	{ 25; 35	—	3,15	3,07	2,9

$$\Delta_2(\beta, z_1, z_2) = \frac{1}{\Delta z} \ln \frac{1 - e^{-\frac{\beta-1}{L} z_2} F(\beta, z_2)}{1 - e^{-\frac{\beta-1}{L} z_1} F(\beta, z_1)}. \quad (15)$$

Equations (12) and (14) show that when  $\beta < 1$ , the relaxation length of the thermal neutron flux tends asymptotically to its limiting value  $\Lambda_{as}$ , and when  $\beta > 1$ , to the value  $L$ .

As an illustration, Table 1 shows the theoretical and experimental values of the relaxation length of the thermal neutron flux in water, from planar approximately monoenergetic sources of initial energy  $E_0 = 0.92$  and  $1.0$  MeV [7, 8]. The parameters  $L_s^2$  and  $\Lambda_{as}$  calculated from Eqs. (2) and (3) when  $E_1 = 0.025$  eV and  $E_0 = 0.92$  MeV are  $15.6 \text{ cm}^2$  and  $3.53 \text{ cm}$ , respectively; when  $E_0 = 1.0$  MeV, they are  $14.5 \text{ cm}^2$  and  $2.73 \text{ cm}$ , respectively. An anomalous decrease in these parameters with rise in initial energy is explained by the resonant scattering cross section at the oxygen nucleus. The same anomalous effect is also noted for the relaxation length of thermal neutrons, the calculated values of which agree satisfactorily, as is evident from Table 1, with the experimental data.

#### LITERATURE CITED

1. I. A. Kozachok and V. V. Kulik, *At. Énerg.*, **32**, No. 4, 307 (1972).
2. I. A. Kozachok, V. V. Kulik, and V. I. Pirogov, *At. Énerg.*, **38**, No. 3, 167 (1975).
3. I. A. Kozachok, *Geofiz. Zh.*, No. 1, 13 (1980).
4. I. A. Kozachuk and V. V. Kulik, *Dokl. Akad. Nauk Ukr. SSR, Ser. B*, No. 2, 23 (1981).
5. Handbook on Special Functions [in Russian], Nauka, Moscow (1979).
6. Experimental Investigation of the Fields of Gamma Rays and Neutrons [in Russian], Atomizdat, Moscow (1974).
7. V. I. Kukhtevich and B. I. Sinitsyn, *At. Énerg.*, **10**, No. 5, 511 (1961).
8. K. Shure and P. Roys. *Nucl. Sci. Eng.*, **2**, No. 2, 170 (1957).

# ACCOMMODATION LENGTH OF HELIUM IN THE GAP BETWEEN THE FUEL AND THE SHELL

Yu. M. Golovchenko, V. M. Makhin,  
V. A. Neverov, B. V. Samsonov, A. P. Sych,  
V. A. Tsykanov, and V. P. Sheshunov

UDC 621.039.546

The accuracy of calculations in determining the temperature of various points of nuclear reactors depends to a considerable extent on knowledge of the thermal characteristics of the materials and the heat liberation from the mixed reactor radiation in the structural elements. Refinement of the experimental data used in the calculations is of practical interest.

With the presence of gas layers in the heat-stressed structural elements, correct account must be taken of the effect of thermal accommodation of the gas molecules [1], leading to an additional temperature difference in the boundary layer between the gas and the solid. This effect is especially considerable [2] for powdery materials with a sharp difference in the molecular weights of such components as the charge of uranium-carbide or uranium-dioxide particles in the helium. In the calculational methods of [1, 2], to obtain the real temperature difference, the given phenomenon is taken into account by the introduction of the so-called accommodation length  $l_{ac}$ , equivalent to the increase in thickness of the gas layer.

Table 1 shows the literature data on  $l_{ac}$  reduced to the helium pressure  $P_0 = 0.098$  MPa and obtained by analysis of the results of measuring the contact heat conductivity of the two surfaces at various pressures and compositions of the filler gas. The scatter observed in the values of  $l_{ac}$  is due to methodological errors of the measurements and the difference in experimental conditions. In [10, 11], the possibility of varying the properties of gases in conditions of reactor irradiation was indicated. This may lead to indeterminacy in the calculational thermal characteristics of thin gas layers.

In the present work, results of investigations in the thermally insulated loop channel of the SM-2 reactor, with the aim of refining the thermal conductivity of the gap between the ends of the fuel rods of surface-oxidized aluminum and the stainless-steel shell of diameter  $6.9 \cdot 10^{-3}$  m and thickness  $0.35 \cdot 10^{-3}$  m at various pressures of the gas filling the fuel element (helium), are given.

The method of measuring was considered in detail in [12]. The thermal conductivity of the gap ( $\alpha_k$ ) was determined from measurements of the thermal power of the fuel element and the temperature at the center of the fuel rod, and also from the calculated of the internal shell surface.

The power of the fuel element was found by a calorimetric method [12] according to the heating of a coolant using a calibrated electric heater with the fuel element introduced in the active region or removed. For relative measurements of the fuel-element power, a neutron-flux sensor ("direct charge") was used. The relative error of determining the absolute value of the fuel-element power is  $\sim 6\%$ . The stability of maintaining the fuel-element power in the course of the experiments with different helium pressures in the fuel element was no worse than 1%.

A thermoelectric thermometer of type XA in a molybdenum protective square of outer diameter  $\sim 3 \cdot 10^{-3}$  m was placed at the center of the fuel rod. Close contact of the thermometer with the rod was ensured by closely placed wire coils of silver between the rod and the thermometer. As shown by calculations using programs realizing the method of integral equations [13], the possible radial shift of the rod relative to the shell does not lead to significant change in the thermometer reading.

It is known [1] that  $\alpha_k$  is determined from the formula

---

Translated from Atomnaya Energiya, Vol. 53, No. 5, pp. 330-331, November, 1982. Original article submitted January 18, 1982.

TABLE 1. Experimental Data on the Accommodation Length for Helium Molecules

Contact pair	$l_{ac}$ 10 <sup>-6</sup> m	Measure- ment tempera- ture, °K	Experimental conditions	Liter- ature
12Kh18N9T stain- less steel-ura- nium	13	~ 300	Laboratory	[3]
Aluminum-ura- nium	16	~ 300	"	[3]
12Kh18N9T-	10	~ 300	"	[3]
12Kh18N9T	6	—	"	[4]
Magnox-uranium	7	~ 560	"	[5]
Magnox-uranium	13-15	300-500	"	[6]
Aluminum- uranium	15	640 *	In-reactor	[7]
Stainless steel- uranium dioxide	15	640 *	In-reactor	[7]
Zircalloy-ura- nium	11	640 *	The same	[7, 8]
Stainless steel- uranium dioxide	25	370 - 700	"	[9]

\*In [7, 8], the temperature distribution is taken in the form  $l_{ac}(P, T) = l_{ac}(\frac{P_0}{P}) (\frac{T}{273})^{1.221}$ .

$$\alpha_h = \frac{q_s}{\Delta T} \quad (1)$$

and depends on the properties of the filler gas, the dimensions of the gap, and the conditions of surface contact

$$\alpha_h = \alpha_{hT} + \frac{\lambda_g(T)}{\delta(T) + l_{ac}(T) \frac{P_0}{P}} \quad (2)$$

Here  $q_s$  is the specific heat flux from the rod surface, W/m<sup>2</sup>;  $\Delta T$ , temperature difference of the rod surface and the shell, °K;  $\alpha_{hT}$ , component of  $\alpha_k$  due to the heat transfer through the "contact spot" of the surfaces, W/m<sup>2</sup>·°K;  $\lambda_g$ , thermal conductivity of the filler gas at a mean gap temperature  $\bar{T}$ , W/m·°K;  $\delta(T)$ , gap between the contacting surfaces, m; and  $P$ , filler-gas pressure ( $P_0 = 0.098$  MPa), MPa.

Analysis of Eqs. (1) and (2) shows that it is more correct to determine  $l_{ac}$  at constant fuel-element power and unchanged conditions of shell cooling. In this case, the temperature change at the center of the rod with variation in helium pressure will be due mainly to the accommodation effect and less (by a factor of 3-5) to the thermal expansion of the rod. When the condition  $\alpha_{hT} \ll \alpha_k$  is satisfied,  $l_{ac}$  is proportional, in the first approximation, to the derivative of the function  $T = f(1/P)$ , where  $T$  is the temperature at the center of the fuel element and  $1/P$  is the inverse value of the helium pressure.

To realize the given conditions, the test was performed at the nominal reactor power with a practically constant fuel-element power and the following basic parameters:

Shell temperature	453-458°K;
Temperature at center of the rod	709-840°K;
Gas pressure in fuel element	0.026-0.780 MPa;
Linear thermal load	24.3- 25.0 kW/m;
Mean gas temperature in gap	578-702°K.

As a result of analysis of the experimental data obtained, the thermal conductivity of the gap between the rod and the shell was determined (Fig. 1) with various helium pressures in the fuel element. Taking account of these data, the thermal conductivity of helium [14], and the coefficient of thermal expansion of uranium [15], the value of the equivalent gap (Fig. 2) was calculated from the formula

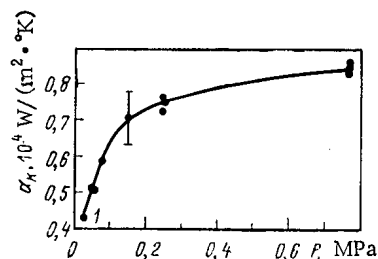


Fig. 1

Fig. 1. Experimental values of  $\alpha_k$  as a function of the helium pressure in the fuel element: 1)  $\alpha_k$  at a helium pressure of 0.026 MPa; approximate value  $\alpha_{kT} < 0.04 \cdot 10^{-4} \text{ W/m}^2 \cdot ^\circ\text{K}$ .

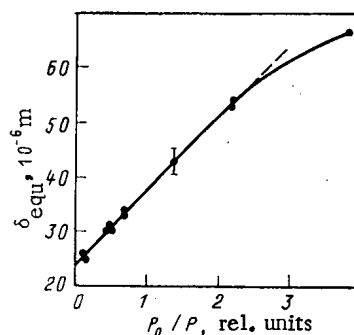


Fig. 2

Fig. 2. Experimental values of  $\delta_{\text{equ}}$  as a function of the inverse helium pressure in the fuel element ( $P_0/P$ ).

$$\delta_{\text{equ}} = \frac{\lambda_g(T)}{\alpha_k} + R_r \alpha(T_R) (T_R - 754), \quad (3)$$

where  $R_r$  is the radius of the outer rod surface, m;  $\alpha$ , thermal expansion coefficient of uranium,  $^\circ\text{K}^{-1}$ ; and  $T_R$ , mean rod temperature,  $^\circ\text{K}$ .

The thermal expansion of the rod was taken into account with respect to  $T_{R1} = 754^\circ\text{K}$  (the mean rod temperature at a helium pressure in the fuel element of 0.071 MPa).

According to Eqs. (2) and (3), when the condition  $\alpha_{kT} \ll \alpha_k$

$$\delta_{\text{equ}} = l_{\text{ac}} \frac{P_0}{P} + \delta(T_{R1}). \quad (4)$$

Thus, the value of  $l_{\text{ac}}$  is determined as the tangent of the angle of slope of the straight line  $\delta_{\text{equ}} = l_{\text{ac}} \frac{P_0}{P} + \delta$  and is  $(13 \pm 2) \cdot 10^{-6} \text{ m}$ . It agrees with the results of most works [5-8, 16], and may be recommended for use in calculation methods (the coefficient of linear correlation here is  $K_r = 0.998$ ).

#### LITERATURE CITED

1. A. A. Sholokhov et al., Determining the Temperature in Nuclear-Reactor Fuel Elements [in Russian], Atomizdat, Moscow (1978).
2. G. N. Dul'nev and Yu. P. Zarichnyak, Thermal Conductivity of Mixtures and Composite Materials [in Russian], Énergiya, Leningrad (1974).
3. V. S. Sandakov and A. S. Pokrovskii, Vopr. At. Nauki Tekh., Ser. Rad. Materialov., Method. Tekh. Obluch., No. 5, 7 (1975).
4. V. M. Popov, Heat Transfer in the Contact Region of Separable and Inseparable Compounds [in Russian], Énergiya, Moscow (1971).
5. R. Skipper and J. Wootton, in: Proceedings of the Second International Geneva Conference, Rep. R/87 UK (1958).
6. Yu. P. Shlykov and E. A. Ganin, Contact Heat Transfer [in Russian], Gosénergoizdat, Moscow-Leningrad (1963).
7. F. Campbell et al., AECL-5400 (1977).
8. J. Ainscough and W. Hobbs, The Effect of Gas Composition and Pressure on the Thermal Conductance of  $\text{UO}_2$ -Zircalloy Interfaces under Irradiation, IAEA-SM-233/13, Vienna (1979).
9. Yu. G. Spiridonov et al., Vopr. At. Nauki Tekh., Ser. Rad. Materialov., Method. Tekh. Obluch., No. 6, 25 (1975).
10. J. Christensen, Supplementary Modes of Energy Transport across the Fuel Cladding Gap, BNWL-SA-5721, UNCLAS (1975).
11. F. Berger and V. Stach, Jad. Energ., 4, No. 9, 251 (1958).
12. V. A. Tsykanov et al., Vopr. At. Nauki Tekh., Ser. Rad. Materialov., Method. Tekh. Obluch., No. 5, 14 (1975).

13. A. I. Okhrimenko and Yu. N. Polyakov, Temperature Field in the Transverse Cross Section of a Multizone Fuel Element of Complex Profile [in Russian], Preprint PIAR P-28(322), Dimitrovgrad (1977).
14. V. S. Chirkin, Thermophysical Properties of Nuclear-Engineering Materials [in Russian], Atomizdat, Moscow (1968).
15. V. S. Emel'yanov and L. I. Evstyukhin, Metallurgy of Nuclear Fuel [in Russian], Atomizdat, Moscow (1968).
16. V. S. Yamnikov and L. L. Malanchenko, At. Tekh. Rubezhom, No. 2, 21 (1969).

# A SCINTILLATION GAMMA SPECTROMETER FOR THE INVESTIGATION OF ULTRA-DEEP BOREHOLES

E. M. Arm, A. A. Il'inskii, B. É. Metzger,  
and V. I. Pyatakhin

UDC 539.1.074.3

A study of the spatial distribution of concentrations of natural radioactive elements (NRE) *in situ* by the  $\gamma$ -radiation spectrometry method has important value for the solution of a number of geological-geophysical problems arising from the investigation of crystalline rocks of the abyssal zones of the earth's crust and revealed by ultra-deep boreholes.

In 1980, in the All-Union Scientific-Research Institute of Nuclear Geophysics and Geology, a scintillation gamma spectrometer was developed for operating in an environment characteristic for investigations of deep and ultra-deep boreholes (temperature up to 180°C and pressure up to 170 MPa).

The spectrometer provides measurements in the energy range 50 keV-3MeV and can be reconstructed in the range 200 keV-10 MeV. The main error in measuring the energy of the  $\gamma$  quanta does not exceed 3%. The relative energy resolution of the spectrometer with respect to the  $^{137}\text{Cs}$  line (661 keV) is not more than 15%, even including a temperature of the environment of up to 180°C and a maximum total loading of  $10^4$  pulses/sec. The total nonlinearity of the energy scale of the spectrometer is not higher than 3%, and the instability is not more than 1%. The equipment allows continuous measurements along the shaft of a borehole to be simultaneously carried out in four differential channels, and also, in the case of point measurements, it allows differential spectral histograms to be obtained by means of consecutive measurements, with a number of discrete levels of not more than 100. In addition, a connection for a AI-256-6 pulse analyzer is provided for the same purpose, which makes it possible to measure the histograms in parallel over 256 channels.

Autostabilization of the energy scale with respect to the characteristic line in the radiation spectrum being investigated or with respect to the line in the spectrum of a reference isotopic source installed in the collimator is provided in the equipment, the design of which allows the intensity of the reference source to be adjusted.

The spectrometer represents a borehole logging-measurement system, constructed on the basis of an optimum linear telemetry channel (OLTC). Figure 1 shows the structural diagram of the circuit of a working borehole gamma-spectrometer [2].

The OLTC also includes in its communication line (armored logging cable KK of the type KGZ-100-120 or KGZ-92-180), with a length of up to 12 km, a surface optimizing equipment OE, providing the frequency characteristics of the OLTC attenuation, coinciding with the characteristics of the Wiener-Kolmogorov filter [3]. This design of the OLTC minimizes the mean square error, in the reproduction of the shape of the data signals from the scintillation detection unit, from the presence on the cable of external interference, for which the spectral strength density was previously experimentally investigated [4].

The use of this channel allowed the electronic circuit of the borehole instrument to be simplified considerably; it consists of a pulsed spectrometric amplifier (PSA) with a low amplification factor and a scintillation detector unit (SDU). The amplifier was made of

---

Translated from Atomnaya Énergiya, Vol. 53, No. 5, pp. 332-333, November, 1982. Original article submitted February 5, 1982.

Depth, m	Range $E = 1$ MeV	$^{40}\text{K}$ $E = 1.3-1.6$ MeV	$^{40}\text{Ca}$ $E = 1.66-1.9$ MeV	$^{232}\text{Th}$ $E = 2.35-2.9$ MeV
	pulses/min	pulses/min	pulses/min	pulses/min
750				
770				
790				
810				
830				

metal-ceramic tubes of the "nuvistor" type. The SDU was equipped with a high-voltage transformer (HVT) for the power supply of the photomultiplier (FÉU). The detector unit was made in the form of a thermostable (up to 180°C) scintillation unit, based on a monocrystal of sodium iodide, activated with thallium (diameter 50 × 150 mm), and a specially prepared thermostable FÉU-151 [5].

The guard casing of the borehole instrument, with a diameter of  $89 \times 1800$  mm, is made of 35KhGSA steel. The surface recording panel of the spectrometer is assembled from two field amplitude analyzers SGSL-2, with detached counting error correction systems. One of the analyzers is used in the active regime (amplifier and autostabilization system with variable channel amplification). In the other analyzer, the main amplifier is disconnected, and the differential channels are connected in parallel with the channels of the active analyzer. The power supply of the equipment is effected from a universal UPI-K logging source.

Declassified and Approved For Release 2013/03/04 : CIA-RDP10-02196R000300010005-6

of 1 MeV, and by three differential "windows" in energy ranges corresponding to the characteristic maxima in the  $\gamma$  emission spectra of the natural radioactive elements (NRE):  $^{40}\text{K}$  (1.3-1.6 MeV), RaC (1.66-1.9 MeV) and ThC" (2.35-2.9 MeV). Figure 2 shows fragments of the tracings obtained. The recording of the traces was repeated, and the discrepancy between the first and repeated recording did not exceed 3%.

From December 1980 to January 1981,  $\gamma$ -spectrometric investigations were conducted in the Kol'sk ultra-deep borehole. For the first time in world practice, a recording was made of the traces from the spectrometric- $\gamma$ -logging equipment (SGL) at a depth of 6763-10,630 m, with a temperature of the surrounding medium (drilling mud) of up to 180°C and a hydrostatic pressure of up to 130 MPa. The recording was effected by raising the borehole equipment at a rate of 100-125 m/h in a depth scale of 1:200 with a NO-15U4 photorecorder (PR). The operating conditions of the surface part of the equipment were the same as for testing. Logging cables of type KGZ-92-180 with a length of 11.8 and 11.9 km were used.

The characteristics of the spectrometer developed and the results of the measurements in the Kol'sk ultra-deep borehole permit this spectrometer to be recommended for conducting  $\gamma$ -spectrometric investigations of the natural radioactive elements in deep and ultra-deep boreholes, including the exploration and development of petroleum and gas deposits in thermal boreholes.

#### LITERATURE CITED

1. F. A. Alekseev et al., Nuclear Geophysics in the Investigation of Petroleum Deposits [in Russian], Nedra, Moscow (1978).
2. A. A. Il'inskii, B. É. Metzger, and V. I. Pyatakhin, Inventor's Certificate No. 817649, Byull. Izobret., No. 12 (1981).
3. M. Krauss and E. Voshin, Measurement Data Systems [Russian translation], Mir, Moscow (1975).
4. B. É. Metzger and V. I. Pyatakhin, in: Borehole Nuclear-Geophysical Equipment with Controllable Radiation Sources [in Russian], United Scientific and Technical Presses, All-Union Scientific-Research Institute of Nuclear Geophysics and Geochemistry, Moscow, (1978), p. 89.
5. E. M. Arm et al., At. Énerg., 51, No. 6, 395 (1981).

# REMOTE CONTROL MEASUREMENTS OF IONIZING RADIATION FIELDS IN BOREHOLES, BASED ON A FIBER-OPTICS CABLE

V. A. Andronov, V. I. Balaev, E. M. Dianov,  
A. A. Il'inskii, E. V. Karus,  
O. L. Kuznetsov, E. V. Mishin, L. G. Petrosyan,  
A. M. Prokhorov, and V. I. Pyatakhin

UDC 550.3:535.23.08:621.315.2

The efficiency of nuclear-physics methods for investigating the physicomachanical properties and element composition of rocks is universally accepted. At the present time, a combination of procedures and equipment have been developed to a satisfactory degree for investigations in laboratory conditions.

However, the results obtained in this way do not give a sufficiently complete representation of the properties of rocks in their natural occurrence. The reason is that when sampling and extracting a core sample, sludge, and fluid, the properties of the rock and the liquid saturating it are changing, part of the samples during drilling-out is destroyed and is not carried out to the surface. At the same time, drilling with core sampling is more complex and is more expensive than coreless drilling.

One of the routes for increasing the efficiency of geological prospecting operations is the remote-controlled and high-speed determination of the properties and composition of rocks in their natural occurrence, i.e., directly in the boreholes, with depths amounting to 5-10 km or more, by nuclear geophysical methods [1]. For prospecting mineral deposits, first and foremost petroleum and gas, and for actively monitoring the exploitation of the deposits, methods are used based on measurements in the boreholes of the parameters of ionizing radiation fields, steady and nonsteady neutron fields, the  $\gamma$  emission of natural radioactivity, inelastic scattering of fast neutrons, radiative capture of thermal neutrons, induced activity, and scattered  $\gamma$  radiation. Gamma spectrometry, directed at the quantitative determination of the content of natural-radioactive and principal-petrogenic elements, is of particular importance.

The success in interpreting the results obtained depends on both the degree to which the effect of the borehole conditions is considered and on the degree to which the borehole measurements approximate the laboratory measurements. One of the problems of this approximation is the operative transmission of the measurement results, with minimum distortion and losses, from the detectors located in the borehole equipment to the surface recording equipment. For this it is necessary to remove the incompatibility between the volume of signals received and the transmitting capacity of the available borehole telemetry channels, in consequence of the extremely low pass bands of the communication lines — the logging cables. For example, when recording the  $\gamma$  emission of radiative capture in the case of the use of a neutron generator with an output of  $10^7$  neutrons/sec and a frequency generation of 400 Hz at recording time delays of  $0 \leq t \leq 200$   $\mu$ sec, pulsed integral loads for a  $\gamma$  quanta energy of more than 100 keV amount to not less than  $10^5$  pulses/sec, which requires a cable pass band of 1-2 MHz for scintillation spectrometry. The pass band for a 3-km cable with a fluoroplast insulator amounts, in all, to about 10 kHz. The problem mentioned is very urgent for borehole geophysical instrument design, in view of the improvement of individual methods of measuring the fractions of ionizing radiations, and in view of the combination of these measurements with measurements from elastic oscillation, electromagnetism, and other fields, with a constantly increasing depth of the boreholes being investigated.

It can be shown [2] that in the construction of borehole telemetry channels possessing the required transmission capacity, it is most advantageous to be directed to the use of linear telemetry channels using fiber light guides as the guiding structures for the electromagnetic signals.

---

Translated from *Atomnaya Énergiya*, Vol. 53, No. 5, pp. 333-335, November, 1982. Original article submitted March 12, 1982.

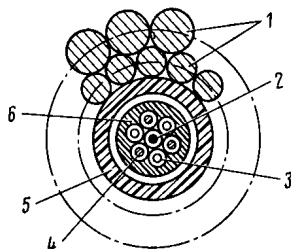


Fig. 1. Cross section of a fiber-optic geophysical cable: 1) steel armor; 2) strong element; 3) light guide; 4) current-carrying core; 5) sheath; 6) polyethylene covering.

By comparison with other types of guiding structures (dual-conductor lines, coaxial lines, and waveguide lines of a surface wave), fiber-optic transmission lines have a number of irrefutable advantages: a wide frequency pass band (from 20 to 2000 MHz/km, depending on the type of light guide) with a low attenuation (10-0.2 dB/km); closure of the relative effect of extraneous electromagnetic fields of noise and induction; potentially low cost (absence of expensive materials with the current tendency for improvement of manufacturing technology); small dimensions (diameter 0.1-0.6 mm); high thermal stability (base of light guide - quartz glass with alloying additives); etc. The available domestic element base - modulated light sources (semiconductor light diodes and lasers) and photocells (photodiodes, phototriodes) - allow telemetry channels to be constructed for transmitting data on a wavelength of 0.85 and 1.05  $\mu\text{m}$ . A specific experience has been built up in the exploitation of these channels with fiber-optic communication lines with a length of several kilometers, designed for analog transmission of signals with a dynamic range of up to 60 dB.

The telemetry channels, including the light diode, waveguide, and photodiode, have been tested as part of a laboratory scintillation system for measuring  $\gamma$  radiation energy spectra. The total nonlinearity of the energy scale of the system in the range of  $\gamma$ -quanta energies of 0.122-4.43 MeV did not exceed 3%, and its energy resolution practically coincided with the inherent resolution of the detector (13% with respect to  $^{137}\text{Cs}$ ) for an integrated loading of up to  $10^5$  pulses/sec (at the level of 50 eV) and a total attenuation in the light guide of 30 dB.

In order to achieve these advantages in using fiber light guides in borehole geophysical data-measuring systems, it is essential to shield the fiber light guides in an appropriate way in the construction of the load-carrying cable. It is well known that a geophysical cable, when operating in a borehole, is subjected to the action of tensile loads, caused by the mass of the borehole instrument and the clamps in the borehole. When the cable passes through the roller pulley-balance at the head of the borehole and is stacked in rows on the drum of the winch hoist, loads originate which cause its deformation in the radial direction. The cable is operated in conditions of high hydrostatic pressure of the liquid in the borehole (up to 100-200 MPa at the face) and at a temperature of up to 300°C. The tensile loads and the elevated temperature lead to elastic stretching of the cable by 1.5%. These special features, and also the existing manufacturing technology of geophysical cables, first and foremost the cable armoring process, impose specific demands on the tensile characteristics of the light guide.

It was shown [3] that for a domestic fiber light guide with stepwise refractive index over the cross section, an increase of the diameter of the light guide up to 180  $\mu\text{m}$  and the choice of a polyamide covering with a diameter of 0.8 mm leads to an increase of the breaking strength of the light guide of up to 3 kg (initially 0.9 kg). It was established by testing these light guides in a high pressure vessel that the action of a hydrostatic pressure of up to 50 MPa increases the light transmission losses in them by not more than 2 dB/km. Stretching to breakdown of the light guides amounts to 0.5-1%. Designs of a fiber-optic geophysical cable and the manufacturing technology have been developed so as to ensure their completeness. Figure 1 shows a cross section of a cable with a length of 1000 m, with three light guides and current carrying copper cores twisted around a strong element in the form of a steel wire.

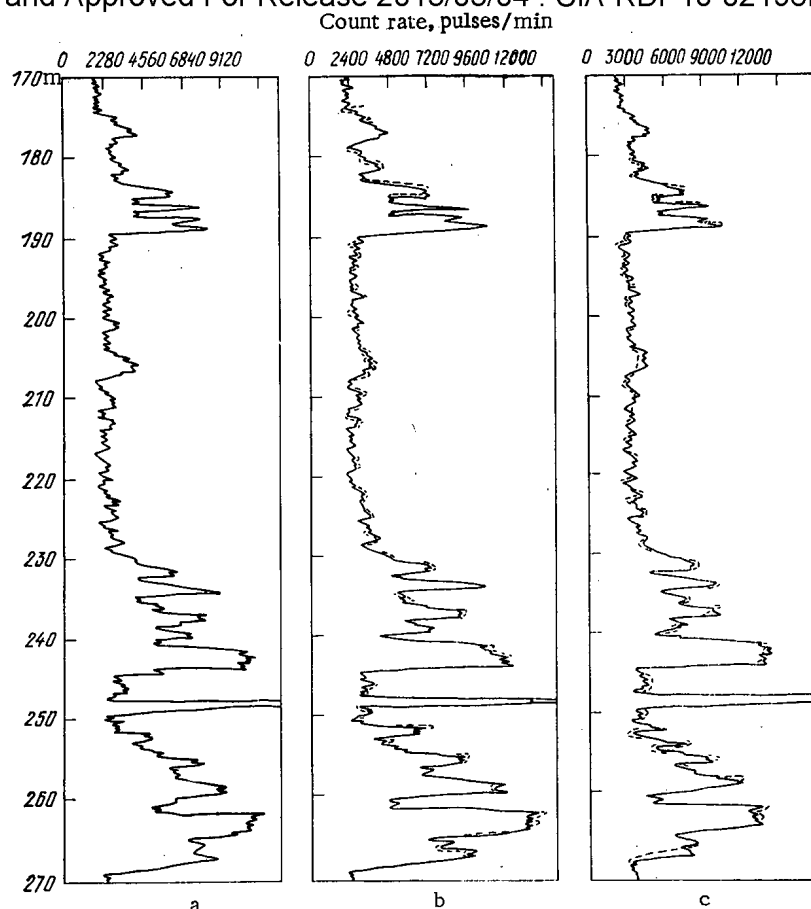


Fig. 2. Results of a  $\gamma$  log of a reference borehole: a-c) NaI(Tl) crystal with size  $30 \times 70$ ,  $50 \times 100$ , and  $50 \times 100$  mm, respectively; calibration rate 1200, 1200, and 1500 pulses/(min·cm);  $\tau = 3.0$  sec for all cases (in b and c,  $V = 350$  and 210 m/h, respectively).

The bunched conductor so formed is covered with a layer of polyethylene at low pressure and an armoring polymer sheath. The load-carrying armor of the cable is made from two counter-wound swathes of steel wire.

It was established during measurements that secondary attenuation in light guides with this construction of the cable did not exceed 2 dB/km for a breaking strength of the cable of up to 58.8 kN and with a minimum radius of curvature of 0.15 m. The cable remains capable of operation at least with a hydrostatic pressure of 78 MPa and a temperature of 100°C.

A treated experimental sample of a fiber-optic geophysical cable was tested in actual borehole conditions, incorporated in a constructed data-measurement system for determining the exposure dose intensity of natural  $\gamma$  radiation — a borehole scintillation gamma radiometer. The structure of the borehole measurement system and its principal characteristics were similar to those considered above. A scintillation detector SP-2 with an NaI(Tl) crystal with a diameter of 50 mm and a height of 100 mm was used in it. The system also included a junction unit for the hermetic insertion of fiber light guides in the cavity of the borehole instrument, calculated at a pressure of 100 atm (1 atm = 101.325 kPa), and a unit for taking off the optical signals from the cable ("optical collector"), providing continuity of measurements with movement of the instrument along the borehole.

During the borehole tests, the spectra of the natural  $\gamma$  radiation at a depth of 130–290 m were recorded continuously, with a rate of movement upwards through the borehole of 350 and 210 m/h. Figure 2 shows a trace made by means of a standard RUR-1 radiometric equipment (a), and also the primary (—) and duplicate (---) record of the measurements, made by means of the equipment in the optical geophysical cable (b, c). The error of the duplicate record is comparable with the statistical measurement error, and the corresponding measurement instability amounted to 1.2%.

Thus, the actual feasibility has been shown for constructing modern data-measurement systems, based on fiber-optic communication lines, for remote-controlled nuclear-physics investigations of boreholes and for measurement of them in other physical fields.

## LITERATURE CITED

1. E. M. Filippov, Nuclear Geophysics [in Russian], Nedra, Novosibirsk, Vol. 1 (1973).
2. E. M. Arm, V. I. Balaev, and V. I. Pyatakhin, The Feasibility of Constructing a Telemetry Channel based on a Fiber-Optic Light-Guide System [in Russian] (manuscript deposited in the All-Union Institute of Scientific and Technical Information, February 14, 1978, No. 511-78), Moscow.
3. Kh. R. Alimov et al., Kvantovaya Elektron., 6 No. 12, 2658 (1979).

# APPLYING SUMMATOR OPERATORS TO THE COMPUTER SOLUTION OF THE INTEGRODIFFERENTIAL EQUATION OF RADIATION TRANSFER

V. I. Bilenko

UDC 519.6.621.039.51

Consider the boundary problem of radiation transfer in a plane layer

$$\mu \frac{\partial \psi(x, \mu)}{\partial x} + \psi(x, \mu) = \frac{\lambda}{2} \int_{-1}^1 \psi(x, t) dt + f(x) \quad (1)$$

with boundary conditions  $\psi(0, \mu) = 0$  when  $\mu > 0$  and  $\psi(h, \mu) = 0$  when  $\mu < 0$ , where  $\mu \in [-1, 1]$ ;  $\lambda \in [0, 1]$ ;  $x \in [0, h]$ ;  $h = \text{const} < \infty$ ;  $f \in C_{[0, h]}$  and  $\psi$  is the desired radiation intensity; the physical meaning of the other quantities in Eq. (1) is well known in transfer theory [1-4].

In the present work, on the basis of the results of [3, 5-7], a simple numerical-analytical algorithm to find approximate solutions of Eq. (1) is outlined. This algorithm, to a certain extent, complements the investigation into the solution of the given problem outlined in [1-4, 8-11]. The simplicity of its computer realization, the theoretical well-foundedness, and comparison of the results of computer solution for a numerical example with the results of calculations by other algorithms [8, 9] indicate that solution of Eq. (1) by the proposed algorithm is expedient.

Algorithm. The scheme for constructing the approximate radiation-intensity function is as follows:

1. By the substitution

$$\varphi(x) = f(x) + \frac{\lambda}{2} \int_{-1}^1 \psi(x, t) dt \quad (2)$$

the initial problem in Eq. (1) is reduced to the integral equation

$$\varphi(x) = f(x) + \frac{\lambda}{2} \int_0^h E(|x-t|) \varphi(t) dt, \quad (3)$$

where  $E(\cdot)$  is the integral exponent [3].

2. Approximating  $E(\cdot)$  by means of any quadrature formula that is accurate for a constant function [3, 8, 10, 11], i.e., setting  $E(\cdot) \approx E_m(\cdot)$ , where  $m$  is the number of quadrature points, Eq. (1) is transformed, giving the equation

---

Translated from Atomnaya Énergiya, Vol. 53, No. 5, pp. 335-337, November, 1982. Original article submitted February 18, 1982.

$$\varphi_m(x) = f(x) + \frac{\lambda}{2} \int_0^x E_m(|x-t|) \varphi_m(t) dt. \quad (3a)$$

3. According to [5-7], Eq. (3) is replaced by the operator equation

$$\varphi_{mn}(x) = U_n(f; x) + \frac{\lambda}{2} U_n \left[ \left\{ \int_0^h E_m(|x_j-t|) \varphi_{mn}(t) dt \right\}_{j=1}^N; x \right], \quad (4)$$

where  $\varphi_{mn}$  is the solution of this equation;  $U_n$  is an arbitrary summator operator [7, 12] defined by the formula

$$U_n(y; x) = \sum_{j=1}^N y(x_j) \pi_j(x) \stackrel{\text{def}}{=} U_n[\{y(x_j)\}_{j=1}^N; x]; \quad \forall y \in C_{[0, h]}, \quad (5)$$

where  $\pi_j(x) = \sum_{h=0}^n a_{jh} \omega_h(x)$  are standard generalized polynomials with respect to the system of linearly independent functions  $\{\omega_h(x)\}_{h=0}^n \subset C_{[0, h]}$ ;  $a_{jh}$  are certain coefficients,  $0 \leq x_1 \leq \dots \leq x_N \leq h$ ,  $N = N(n)$ .

4. The solution  $\varphi_{mn}$  of Eq. (4) is sought in the form of a polynomial

$$\varphi_{mn}(x) = \sum_{h=0}^n c_h \omega_h(x), \quad c_h \stackrel{\text{def}}{=} c_h(m), \quad (6)$$

the unknown coefficients  $\{c_k\}_{k=0}^n$  of which are found from a system of linear algebraic equations of order  $(n+1) \times (n+1)$ , obtained from Eq. (4), according to Eq. (5) [7], by equating the coefficients with linearly independent terms

$$c_k = \sum_{j=1}^N a_{jh} \left[ f(x_j) + \frac{\lambda}{2} \sum_{v=0}^n c_v \left( \int_0^h E_m(|x_j-t|) \omega_v(t) dt \right) \right]; \quad k = \overline{0, n}. \quad (7)$$

5. The approximate solutions  $\psi_{mn}$  of Eq. (1) are obtained from the formula

$$\psi_{mn}(x, \mu) = \begin{cases} \frac{1}{\mu} \int_0^x \varphi_{mn}(t) \exp\left(-\frac{x-t}{\mu}\right) dt & \text{when } \mu > 0; \\ \varphi_{mn}(x) & \text{when } \mu = 0; \\ \frac{1}{|\mu|} \int_x^h \varphi_{mn}(t) \exp\left(-\frac{t-x}{|\mu|}\right) dt & \text{when } \mu < 0. \end{cases} \quad (8)$$

The theoretical basis of algorithm 1-5 follows from the results of [3, 5-7]. Thus, the conditions for the existence and uniqueness of the solution of Eq. (7), and also for its solvability, e.g., by the method of simple iteration, follow from the fact that the integral operators  $T$  and  $T_m$  [3] in Eqs. (3) and (3a), generated, respectively, by the functions (kernels)  $E(|x-t|)$  and  $E_m(|x-t|)$ , and acting in the space  $C_{[0, h]}$ , are totally continuous, and the following inequalities are valid for their norms in a uniform metric [3]:

$$\|T\| < \lambda \leq 1; \quad \|T_m\| < \lambda \leq 1; \quad \forall m \in N. \quad (9)$$

For the error of algorithm 1-5 under the condition that the integrals in Eq. (7) are calculated accurately, in view of Theorem 3.2 from [5] and according to Eqs. (6) and (15) of [3], taking account of Eqs. (8), (3), (4), and (9), the following estimate may readily be obtained for the more important classes of summators [5-7] in a uniform metric:

$$\|\psi(x, \mu) - \varphi_{mn}(x, \mu)\| \leq c \|\varphi_m(x) - U_n(\varphi_m; x)\| + \varepsilon_m, \quad (10)$$

TABLE 1. Approximate Values of the Function  $\varphi(x)$ 

$x$	Data of Minin and Sobolev [8]	Data of Kasti and Kalaba [8]	Data of Pedas [9], $n = 3$	$\varphi_{72}(x)$	$\varphi_{73}(x)$
0	0,083	0,082559	0,082523	0,082516	0,082584
0,1	0,103	0,102958	0,102920	0,102921	0,102973
0,2	0,123	0,122851	0,122789	0,122383	0,122914
0,3	0,141	0,140966	0,140914	0,140901	0,140962

where  $c$  is a constant independent of  $m$  and  $n$ ; and  $\epsilon_m$ , error due to approximation of the integral exponent  $E(\cdot)$  by the approximation  $E_m(\cdot)$  in solving the initial problem in Eq. (1) by the method of discrete ordinates (the Vik-Chandrasekar method (see [1-3], etc.)).

**Remark 1.** Estimates of  $\|y(x) - U_n(y; x)\|$ ,  $\forall y \in \mathcal{K} \subset C_{[0, h]}$  for basic classes of functions  $\mathcal{K}$  and summator operators  $U_n$  are well known in the theory of approximation (see [12, 13, etc.]); the error  $\epsilon_m$  was investigated in sufficient detail in [3, 10, 11].

**Remark 2.** Note that, in contrast to general projection methods (see [14, 15], etc.), the present algorithm does not rest on the projection capability ( $U_n^2 = U_n$ ) of the summator operators employed.

**Numerical Example.** Algorithm 1-5 is realized in the form of computer programs in Analytik and Fortran IV, written, as in [6], on the basis of program 2 of [16]. In this case, the operators  $U_n$  of the form in Eq. (5) are interpolation operators with the nodes  $x_j = \frac{h(1 - \cos j\pi/n)}{2}$ ,  $j = 0, n$ . These operators allow the solution of Eq. (4) to be obtained in the form of an algebraic polynomial

$$\varphi_{mn}(x) = \sum_{k=0}^n c_k(m) (x - h/2)^k, \quad (11)$$

so that the integrals in Eq. (7) are accurately calculated. The function  $E(\cdot)$  is approximated in the programs according to the recommendations of [3] using the Gauss quadrature formula on the segment  $(0, 1]$  with  $m = 3, 7$ .

One example for the verification of the algorithm's efficiency is an equation of the type in Eq. (1) with  $\lambda = 0.5$ ;  $h = 0.3$ ;  $f(x) = \exp(2x - 0.6)/8$  (see [8], and [9], p. 94).

Table 1 gives the results of solving Eq. (3), obtained by Sobolev and Minin by the method of invariant submersion (see [8], p. 94), and by the method of first-order combinations [9], and also gives the values of the polynomial  $\varphi_{72}$  of the form  $\varphi_{72}(x) = 0.1127706 + 0.1946144(x - 0.15) - 0.0472046(x - 0.15)^2$  and of the polynomial  $\varphi_{73}$ . Analyzing the calculated results in Table 1 and also those in Table 2 of [7], where  $m = 6$  and  $n = 3, 6$ , it may be concluded that algorithm 1-5 allows sufficiently high accuracy to be obtained without too large a volume of calculation. An important advantage of the algorithm is that the approximate value of the radiation intensity of the initial problem in Eq. (1) is in simple analytical form.

#### LITERATURE CITED

1. B. Davison, Theory of Neutron Transport [Russian translation], Atomizdat, Moscow (1960).
2. G. I. Marchuk and V. I. Lebedev, Numerical Methods in the Theory of Neutron Transport [in Russian], Atomizdat, Moscow (1981).
3. G. M. Vainikko and A. L. Marshak, Izv. Vyssh. Uchebn. Zaved. Mat., No. 11, 11 (1978).
4. B. D. Abramov and V. A. Korneev, At. Energ., 47, No. 5, 314 (1979).
5. V. K. Dzyadyk, Izv. Akad. Nauk SSSR, Ser. Mat., 34, No. 4, 827 (1970).
6. V. I. Bilenko and P. N. Denisenko, in: Investigations in the Theory of Approximate Functions and Their Applications [in Russian], Mat. Akad. Nauk Ukr. SSR, Kiev (1978), p. 16.
7. V. I. Bilenko, Preprint No. 80.17 of the Institute of Mathematics, Academy of Sciences of the Ukrainian SSR [in Russian], Kiev (1980).
8. D. Kasti and R. Kalaba, Immersion Methods in Applied Mathematics [Russian translation], Mir, Moscow (1976).

9. A. Pedas, Uch. Zap. Tartusk. Gos. Univ., 25, No. 500, 33 (1979).
10. A. L. Marshak, Uch. Zap. Tartusk. Gos. Univ., 25, No. 500, 92 (1979).
11. A. L. Marshak, in: Abstracts of a Conference on Theoretical and Applied Problems of Mathematics [in Russian], Gosuniversiteta, Tartu (1980), p. 99.
12. I. P. Natanson, Constructive Theory of Functions [in Russian], Gostekhteorizdat, Moscow-Leningrad (1949).
13. V. K. Dzyadyk, Introduction to the Theory of Uniform Approximation of Functions by Polynomials [in Russian], Nauka, Moscow (1977).
14. M. A. Krasnosel'skii et al., Approximate Solution of Operator Equations [in Russian], Nauka, Moscow (1969).
15. C. Baker, The Numerical Treatment of Integral Equations, Clarendon Press, Oxford (1977).
16. P. N. Denisenko, in: Mathematical Equipment for a MIR-Series Computer [in Russian], Inst. Kibern. Akad. Nauk Ukr. SSR, Kiev (1974), No. 8, p. 81.

#### DURABILITY OF ZTL PIEZOCERAMIC UNDER THE ACTION OF REACTOR RADIATION

V. M. Baranov, S. P. Martynenko,  
and A. I. Sharapa

UDC 537.228.1:539.125.5.04:549.6

Acoustical methods of analysis and monitoring are extensively used for investigating and monitoring reactors [1, 2]. For this reason it is of practical interest to investigate the change in the properties of piezoelectric transducers used in acoustical monitoring-measuring devices caused by the action of reactor radiation on them. In this work we studied the change in the efficiency of transformation of signals by plates made of ZTL-19 zirconium-titanium-lead piezoceramic with a diameter of 9 mm and thickness 4 mm irradiated in a vertical experimental channel of the IRT (MIFI) reactor. The flux density of thermal neutrons was  $1.9 \cdot 10^{13}$  neutrons/(cm<sup>2</sup>·sec), the flux density of fast neutrons was  $1.2 \cdot 10^{12}$  neutrons/(cm<sup>2</sup>·sec), and the intensity of the dose of  $\gamma$  radiation was 420 W/kg. The temperature of the specimens in the working reactor was 150°C. The irradiation regime was discontinuous, including four cycles of continuous irradiation over five days, with stoppages of the reactor for two, six, and two days between cycles.

For the studies, we prepared a setup based on a rod consisting of a zirconium alloy with 1% niobium with diameter 9.2 mm, length 190 mm, and with two identical piezotransducers fastened to the end faces in order to excite and record resonant oscillations of the rod. The contact between the transducer and the rod is a dry contact, in order to exclude the effect of changes in the properties of the intermediate lubricating layer during the irradiation process. The transducers are pressed to the end faces of the rod with a force of 1 N. We excited the emitter with the help of a generator of high-frequency oscillations, and we amplified the signals from the piezoreceiver and recorded them on an oscillograph screen. As a measure of the working capacity of the transducers we used the electrical signal of the piezoreceiver at resonance, which is valid assuming that the effect of the radiation flux density on the zirconium rod is small.

We performed the measurements at three resonant frequencies, 73, 168, and 227 kHz at 150°C, which remain practically unchanged with time, indicating the insignificant, for this investigation, change in the physicomechanical properties of the rod, piezotransducers, and contact layer.

Figure 1 shows the results of measurements of the relative change in the amplitude of the recorded signal;  $A_0$  is the starting (prior to the beginning of irradiation) value of the amplitude. The quite rapid decrease in the transduction efficiency during the initial period of irradiation, which was approximately the same for all frequencies investigated, is evident. The threefold drop in the efficiency is attained with thermal neutron fluences  $\sim (0.6-0.8) \cdot 10^{19}$  neutron/cm<sup>2</sup> [the corresponding fluence of fast neutrons is  $(0.4-0.5) \cdot 10^{18}$  neutrons/

---

Translated from Atomnaya Énergiya, Vol. 53, No. 5, p. 337, November, 1982. Original article submitted February 22, 1982.

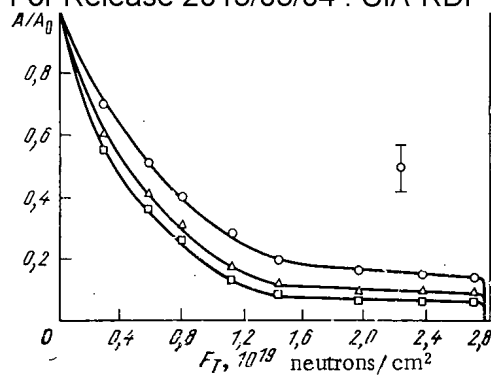


Fig. 1. Relative change in the transduction efficiency of a pair of piezo-elements made of ZTL-19 ceramic during irradiation in an IRT (MIFI) reactor with resonant frequencies 227 ( $\circ$ ); 168 ( $\square$ ); and 73 kHz ( $\triangle$ ).

$\text{cm}^2$ , and the density of the radiation dose obtained was  $(1.4-1.8) \cdot 10^5 \text{ Gy}$ . These results correspond well with the results obtained in the USSR and abroad for piezoceramics of a similar class [3, 4].

Complete breakdown of the piezotransducers occurred after 400 h of irradiation, which corresponds to thermal and fast neutron fluences of  $2.7 \cdot 10^{19}$  and  $1.62 \cdot 10^{18}$  neutrons/ $\text{cm}^2$  and an absorbed density of the  $\gamma$  radiation dose of  $6.1 \cdot 10^5 \text{ Gy}$  ( $6.1 \cdot 10^7 \text{ rad}$ ). The breakdown was accompanied by a sharp drop in the electrical resistance of the piezoemitter circuit to 100-200  $\Omega$ , which made further measurements impossible. The reason for this phenomenon has not been established; it is possible that the fluoroplastic insulation of the electrical lines breaks down. It should be noted that during long-term stoppage of the reactor (up to 6 days) no changes were observed in the signal amplitude, which indicates the actions of the integral characteristics of the irradiation on the piezoelectric properties of the transducers.

It has thus been established that it is possible to reliably use acoustical, in particular, ultrasonic, piezotransducers based on the ZTL piezoceramic with thermal and fast neutron flux densities  $1.9 \cdot 10^{13}$  and  $1.2 \cdot 10^{12}$  neutrons/( $\text{cm}^2 \cdot \text{sec}$ ) up to thermal neutron fluences of  $2.7 \cdot 10^{19}$  and  $1.62 \cdot 10^{18}$  neutrons/ $\text{cm}^2$ , respectively.

#### LITERATURE CITED

1. V. M. Baranov, Ultrasonic Measurements in Nuclear Engineering [in Russian], Atomizdat, Moscow (1975).
2. Acoustical Emission and Its Applications to Nondestructive Testing in Nuclear Energetics [in Russian], Atomizdat, Moscow (1980).
3. V. P. Solov'ev and I. I. Kuz'min, Izv. Akad. Nauk SSSR, Ser. Fiz., 34, No. 12, 2604 (1970).
4. G. Broomfield, J. Nucl. Mater., 91, No. 1, 23 (1980).

# RADIOACTIVE AEROSOLS IN VENTILATION SYSTEMS OF THE CHERNOBYL'SK NUCLEAR POWER PLANT

S. S. Chernyi and V. P. Grigorov

UDC 621.039.58:541.182.2

Information concerning the basic properties of radioactive aerosols (dispersity, mass concentration, etc.) is necessary in order to arrange an efficient system for cleaning air and for estimating the radiation danger from aerosols. There is, however, practically no information on the properties of aerosols in different ventilation systems of existing nuclear power plants. Results of investigations of properties of aerosols at a nuclear power plant with VVER-440 are presented only in [1, 2], and such information for the first and second blocks of the Beloyarsk nuclear power plant is presented in [3].

In this paper we describe results of investigations of the properties of radioactive aerosols in ventilation systems of the first and second blocks of the Chernobyl'sk nuclear power plant in 1978-1979. We collected samples of radioactive aerosols from air ducts of ventilation systems in front of the aerosol filters. In order to determine the dispersity of the radioactive aerosols, we used a six-cascade impactor, and in order to determine the mass concentration and volume activity, we used the analytical AFA filters. After collecting the specimens, we stored them for days.

Table 1 presents the parameters of the logarithmic normal distributions (LND) of the activity and masses of particles according to their aerodynamics dimensions (medium diameter  $d_a$  and  $d_m$ ; standard deviation  $\sigma_a$  and  $\sigma_m$ ), averaged over a large number of experiments.

$^{51}\text{Cr}$ ,  $^{133}\text{I}$ , and  $^{131}\text{I}$ , as well as  $^{64}\text{Cu}$ , made the main contribution to the radioactivity of the aerosols. It was found from an analysis of the experimental data that the short-lived nuclides are related to particles finer ( $d_a < 0.4 \mu\text{m}$ ) than long-lived nuclides, and their radioactivity is determined primarily by  $^{88}\text{Rb}$  and  $^{138}\text{Cs}$ . The mass concentration of aerosols in different ventilation systems was  $2.1 \cdot 10^{-2}$ – $1.5 \cdot 10^{-1} \text{ mg/m}^3$ .

D-23kl aerosol filters are used to remove aerosols from the air at the nuclear power plant [4]. The efficiency of some aerosol filtering systems equipped with these filters was calculated with respect to the volume activity before and after the aerosol filters. The filtration efficiency for VTs-1AB, VTs-2A, and VTs-2A' constituted (for the last ventilation

TABLE 1. Parameters of LND of Aerosols  
According to Aerodynamic Dimensions of Particles

Ventilation system	LND parameters			
	$d_a, \mu\text{m}$	$\sigma_a$	$d_m, \mu\text{m}$	$\sigma_m$
VTs-1AB	0,6	2,4	1,8	3,1
VTs-2A	1,0	2,6	1,5	3,6
VTs-2B	1,1	2,2	—	—
VTs-2A'	0,7	1,8	1,2	2,7
VTs-2VE	0,5	1,7	1,8	2,7
VP-1	1,2	2,3	—	—
VP-2	0,9	2,2	—	—
VP-101	0,9	2,1	—	—
VP-102	0,7	2,2	—	—
VP-8	0,8	2,3	—	—
VP-9	1,3	2,2	—	—
RTs	0,8	1,8	—	—
Vertical ventilation tube	0,8	2,0	—	—

Translated from Atomnaya Énergiya, Vol. 53, No. 5, p. 338, November, 1982. Original article submitted March 4, 1982.

TABLE 2. Inflow of Radioactive Aerosols  
(including aerosol phase of iodine)

Ventilation system	Fraction of inflow, %	Ventilation system	Fraction of inflow, %
VTs-1AB	20,4	VP-101	4,9
VTs-2A	17,4	VP-102	2,5
VTs-2B	4,1	V-8	2,1
VTs-2A'	5,0	V-9	2,7
VTs-2VE	0,1	V-108	0,4
VP-1	15,3	V-109	0,3
VP-2	24,8		

system, including aerosol trapping not only by aerosol filters but also by carbon filters) 99.3, 97.0, and 99.99%, respectively. It should be noted that emission of radioactive aerosols constituted 15-20% of allowable emissions [5, 6].

The inflow of radioactive aerosols into the basic ventilation systems of the first and second blocks was calculated from the experimental data on the volume activity of aerosols for the first half of 1979 (Table 2). It is evident that the largest amount of aerosols (with respect to activity) enters into the VTs-1AB, VTs-2A, VP-1, and VP-2 ventilation systems, while the least amount of aerosols enters the VTs-2VE system.

We thank our colleagues at the Chernobyl'sk nuclear power plant, A. N. Varbants, G. I. Krasnozhen, and V. G. Perminov, for help in conducting the investigations.

## LITERATURE CITED

1. S. S. Chernyi et al., *At. Énerg.*, 42, No. 3, 208 (1977).
2. V. P. Grigorov and S. S. Chernyi, in: *Industrial and Hygienic Cleaning of Gases* [in Russian], TsINTIkhimneftemash, Moscow (1978), No. 1, p. 21.
3. R. I. Pogodin et al., *At. Énerg.*, 51, No. 4, 262 (1981).
4. V. M. Krupchatnikov, *Ventilation in Working with Radioactive Substances* [in Russian], Atomizdat, Moscow (1978).
5. L. A. Buldakov et al., *Radiation Safety in Nuclear Energetics* [in Russian], Atomizdat, Moscow (1981).
6. *Public Health Rules for Designing and Using Nuclear Electrical Power Plants*, SP-AÉS-79, Atomizdat, Moscow (1981).

# How To Comply With The New Copyright Law

*Participation in the Copyright Clearance Center (CCC) assures you of legal photocopying at the moment of need.*

Libraries everywhere have found the easy way to fill photocopy requests legally and instantly, without the need to seek permissions, from more than 3000 key publications in business, science, humanities, and social science. You can:

*Fill requests for multiple copies, interlibrary loan (beyond the CONTU guidelines), and reserve desk without fear of copyright infringement.*

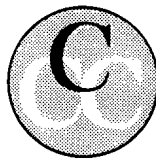
Supply copies from CCC-registered publications simply and easily.

The Copyright Clearance Center is your one-stop place for on-the-spot clearance to photocopy for internal use.

Its flexible reporting system accepts photocopying reports and returns an itemized invoice. You send only one convenient payment. CCC distributes it to the many publishers whose works you need.

And, you need not keep any records, the CCC computer will do it for you. Register now with the CCC and you will never again have to decline a photocopy request or wonder about compliance with the law for any publication participating in the CCC.

To register or for more information, just contact:

		<b>Copyright Clearance Center</b>	
		21 Congress Street Salem, Massachusetts 01970 (617) 744-3350 <small>a not-for-profit corporation</small>	
NAME		TITLE	
ORGANIZATION			
ADDRESS			
CITY		STATE	ZIP
COUNTRY		TELEPHONE	

# CHANGING YOUR ADDRESS?

In order to receive your journal without interruption, please complete this change of address notice and forward to the Publisher, 60 days in advance, if possible.

(Please Print)

Old Address:

name

address

city

state (or country)

zip code

New Address

name

address

city

state (or country)

zip code

date new address effective

name of journal



**233 Spring Street, New York, New York 10013**

**MEASUREMENT TECHNIQUES***Izmeritel'naya Tekhnika*

Vol. 25, 1982 (12 issues) ..... \$400

**MECHANICS OF COMPOSITE MATERIALS***Mekhanika Kompozitnykh Materialov*

Vol. 18, 1982 (6 issues) ..... \$330

**METAL SCIENCE AND HEAT TREATMENT***Metallovedenie i Termicheskaya Obrabotka Metallov*

Vol. 24, 1982 (12 issues) ..... \$420

**METALLURGIST***Metallurg*

Vol. 26, 1982 (12 issues) ..... \$435

**PROBLEMS OF INFORMATION TRANSMISSION***Problemy Peredachi Informatsii*

Vol. 18, 1982 (4 issues) ..... \$320

**PROGRAMMING AND COMPUTER SOFTWARE***Programmirovaniye*

Vol. 8, 1982 (6 issues) ..... \$135

**PROTECTION OF METALS***Zashchita Metallov*

Vol. 18, 1982 (6 issues) ..... \$380

**RADIOPHYSICS AND QUANTUM ELECTRONICS***Izvestiya Vysshikh Uchebnykh Zavedenii, Radiofizika*

Vol. 25, 1982 (12 issues) ..... \$400

**REFRACTORIES***Ogneupory*

Vol. 23, 1982 (12 issues) ..... \$380

**SIBERIAN MATHEMATICAL JOURNAL***Sibirskii Matematicheskii Zhurnal*

Vol. 23, 1982 (6 issues) ..... \$495

**SOIL MECHANICS AND  
FOUNDATION ENGINEERING***Osnovaniya, Fundamenty i Mekhanika Gruntov*

Vol. 19, 1982 (6 issues) ..... \$380

**SOLAR SYSTEM RESEARCH***Astronomicheskii Vestnik*

Vol. 16, 1982 (4 issues) ..... \$275

**SOVIET APPLIED MECHANICS***Prikladnaya Mekhanika*

Vol. 18, 1982 (12 issues) ..... \$400

**SOVIET ATOMIC ENERGY***Atomnaya Energiya*

Vols. 52-53 (12 issues) ..... \$440

**SOVIET JOURNAL OF GLASS PHYSICS  
AND CHEMISTRY***Fizika i Khimiya Stekla*

Vol. 8, 1982 (6 issues) ..... \$175

**SOVIET JOURNAL OF  
NONDESTRUCTIVE TESTING***Defektoskopiya*

Vol. 18, 1982 (12 issues) ..... \$485

**SOVIET MATERIALS SCIENCE***Fiziko-khimicheskaya Mekhanika Materialov*

Vol. 18, 1982 (6 issues) ..... \$345

**SOVIET MICROELECTRONICS***Mikroelektronika*

Vol. 11, 1982 (6 issues) ..... \$195

**SOVIET MINING SCIENCE***Fiziko-tehnicheskie Problemy Razrabotki**Poleznykh Iskopaemykh*

Vol. 18, 1982 (6 issues) ..... \$420

**SOVIET PHYSICS JOURNAL***Izvestiya Vysshikh Uchebnykh Zavedenii, Fizika*

Vol. 25, 1982 (12 issues) ..... \$400

**SOVIET POWDER METALLURGY AND  
METAL CERAMICS***Poroshkovaya Metallurgiya*

Vol. 21, 1982 (12 issues) ..... \$435

**STRENGTH OF MATERIALS***Problemy Prochnosti*

Vol. 14, 1982 (12 issues) ..... \$495

**THEORETICAL AND MATHEMATICAL PHYSICS***Teoreticheskaya i Matematicheskaya Fizika*

Vols. 50-53, 1982 (12 issues) ..... \$380

**UKRAINIAN MATHEMATICAL JOURNAL***Ukrainskii Matematicheskii Zhurnal*

Vol. 34, 1982 (6 issues) ..... \$380

Send for Your Free Examination Copy

Plenum Publishing Corporation, 233 Spring St., New York, N.Y. 10013

In United Kingdom: 88/90 Middlesex St., London E1 7EZ, England

Prices slightly higher outside the U.S. Prices subject to change without notice

# RUSSIAN JOURNALS IN THE PHYSICAL AND MATHEMATICAL SCIENCES

AVAILABLE IN ENGLISH TRANSLATION

## ALGEBRA AND LOGIC

*Algebra i Logika*

Vol. 21, 1982 (6 issues) ..... \$270

## ASTROPHYSICS

*Astrofizika*

Vol. 18, 1982 (4 issues) ..... \$320

## AUTOMATION AND REMOTE CONTROL

*Avtomatika i Telemekhanika*

Vol. 43, 1982 (24 issues) ..... \$495

## COMBUSTION, EXPLOSION, AND SHOCK WAVES

*Fizika Goreniya i Vzryva*

Vol. 18, 1982 (6 issues) ..... \$345

## COSMIC RESEARCH

*Kosmicheskie Issledovaniya*

Vol. 20, 1982 (6 issues) ..... \$425

## CYBERNETICS

*Kibernetika*

Vol. 18, 1982 (6 issues) ..... \$345

## DIFFERENTIAL EQUATIONS

*Differentsial'nye Uravneniya*

Vol. 18, 1982 (12 issues) ..... \$395

## DOKLADY BIOPHYSICS

*Doklady Akademii Nauk SSSR*

Vols. 262-267, 1982 (2 issues) ..... \$145

## FLUID DYNAMICS

*Izvestiya Akademii Nauk SSSR,*

*Mekhanika Zhidkosti i Gaza*

Vol. 17, 1982 (6 issues) ..... \$380

## FUNCTIONAL ANALYSIS AND ITS APPLICATIONS

*Funktsional'nyi Analiz i Ego Prilozheniya*

Vol. 16, 1982 (4 issues) ..... \$320

## GLASS AND CERAMICS

*Steklo i Keramika*

Vol. 39, 1982 (6 issues) ..... \$460

## HIGH TEMPERATURE

OSWR/NED/MTB

## HYDROTECHNICAL CONSTRUCTION

*Gidrotekhnicheskoe Stroitel'stvo*

Vol. 16, 1982 (12 issues) ..... \$305

## INDUSTRIAL LABORATORY

*Zavodskaya Laboratoriya*

Vol. 48, 1982 (12 issues) ..... \$400

## INSTRUMENTS AND EXPERIMENTAL TECHNIQUES

*Pribory i Tekhnika Eksperimenta*

Vol. 25, 1982 (12 issues) ..... \$460

## JOURNAL OF APPLIED MECHANICS AND TECHNICAL PHYSICS

*Zhurnal Prikladnoi Mekhaniki i Tekhnicheskoi Fiziki*

Vol. 23, 1982 (6 issues) ..... \$420

## JOURNAL OF APPLIED SPECTROSCOPY

*Zhurnal Prikladnoi Spektroskopii*

Vols. 36-37 (12 issues) ..... \$420

## JOURNAL OF ENGINEERING PHYSICS

*Inzhenerno-fizicheskii Zhurnal*

Vols. 42-43, 1982 (12 issues) ..... \$420

## JOURNAL OF SOVIET LASER RESEARCH

*A translation of articles based on the best Soviet research in the field of lasers*

Vol. 3, 1982 (4 issues) ..... \$95

## JOURNAL OF SOVIET MATHEMATICS

*A translation of Itogi Nauki i Tekhniki and Zapiski*

*Nauchnykh Seminarov Leningradskogo Otdeleniya*

*Matematicheskogo Instituta im. V. A. Steklova AN SSSR*

Vols. 18-20, 1982 (18 issues) ..... \$680

## LITHOLOGY AND MINERAL RESOURCES

*Litologiya i Poleznye Iskopaemye*

Vol. 17, 1982 (6 issues) ..... \$420

## LITHUANIAN MATHEMATICAL JOURNAL

*Litovskii Matematicheskii Sbornik*

Vol. 22, 1982 (4 issues) ..... \$205

## MAGNETOHYDRODYNAMICS

*Magnitnaya Gidrodinamika*

Vol. 18, 1982 (4 issues) ..... \$325

## MATHEMATICAL NOTES

*Matematicheskie Zametki*

Vols. 31-32, 1982 (12 issues) ..... \$400

continued on inside back cover